Investigating a novel photoactivatable diarylacetylene as an antimicrobial agent against Gram-positive bacteria

RYAN WAITE

Investigating a novel photoactivatable diarylacetylene as an antimicrobial agent against Gram-positive bacteria

Ryan Waite

The emergence of antibiotic resistance is a growing threat to human health, and therefore, alternatives to existing compounds are urgently needed. In this context, a novel fluorescent photoactivatable diarylacetylene has been identified and characterised for its antibacterial activity, which preferentially eliminates Gram-positive over Gram-negative bacteria. This compound effectively eliminates clinically relevant Gram-positive bacteria without the development of tolerance upon repeated subculturing. We noted that bacteria lacking oxidative damage repair pathways exhibited increased sensitivity. Activation of the diarylacetylene led to detectable intracellular oxidative stress and upregulation of reactive oxygen species (ROS) detoxification proteins, suggesting that the mechanism of antibacterial activity is linked to ROS production. Our experiments indicated that the tolerance observed in Gram-negative bacteria is attributed to their lipopolysaccharide-rich outer membrane. Strains with compromised outer membrane integrity demonstrated heightened susceptibility to the compound. Additionally, the removal of accumulated intracellular diarylacetylene is crucial for tolerance; with disruption of the non-specific AcrAB-TolC efflux pump resulting in increased susceptibility. This new diarylacetylene shows promise as an antibacterial agent against Gram-positive bacteria that can be activated *in situ*, potentially for the treatment of skin infections.

Investigating a novel photoactivatable diarylacetylene as an antimicrobial agent against Gram-positive bacteria

Ryan Waite

University of Durham

Department of Bioscience

Ustinov College

A thesis presented in fulfilment of the requirements for the degree of Doctor of Philosophy

October 2024

Table of Contents

Abbreviations

5-ALA - 5-Aminolevulinic acid

8-OxodG - 8-Oxo-7,8-dihydro-2'-deoxyguanine

ABC - ATP binding cassette

AMR - Antimicrobial resistance

AVD - Anti-virulence drug

aPDT - Antimicrobial photodynamic therapy

BER - Base excision repair

CFU - Colony forming units

C=O - Carbonyl group

CTCF - Corrected total cell fluorescence

DEPs - Differentially expressed proteins

DNA - Deoxyribonucleic acid

DNPH - 2,4-dinitrophenylhydrazine

eDNA - Extracellular DNA

EPS - Extracellular polymeric substances

ESBL - Extended spectrum beta lactamase

Fe-S - Iron sulfur

H_2O_2 - Hydrogen peroxide

HE - Hydroethidine

HGF - Horizontal gene transfer

HILIC - Hydrophobic interaction chromatography

HPF - Hydroxyphenyl fluorescein

KDO - 3 Deoxy-α-D-manno-octulosonic acid

KPC - *Klebsiella* producing carbapenems

LC-MS - Liquid chromatography-mass spectrometry

LB - Luria-Bertani

LPS - Lipopolysaccharide

MER - Market entry reward

MDR - Multi drug resistance

MIC - Minimum Inhibitory Concentration

MFS - Major facilitator superfamily

MH - Muller Hinton

MSSA - Methicillin susceptible *S. aureus*

MRSA - Methicillin resistant *S. aureus*

MATE - Multidrug and toxic compound extrusion family

$O_2^{\bullet-}$ - Superoxide

OH· - Hydroxyl radical

PBP - Penicillin binding protein

PDT - Photodynamic therapy

PI - Propidium iodide

PDR - Pan drug resistance

PS - Photosensitiser

RB - Rose Bengal

ROS - Reactive oxygen species

RND - Resistance nodulation cell division superfamily

SEM - Scanning electron microscopy

SNP - Single nucleotide polymorphisms

SMR - Small multidrug resistance family

SPE - Solid phase extraction

STX - Staphyloxanthin

TMP - 5,10,15,20-Tetrakis(1-methyl-pyridino)-21H,23H-porphine, tetra-p-tosylate salt

TAT - Twin-Arginine-Translocation

VRE - Vancomycin resistant *Enterococcus*

VISA - Vancomycin intermediate resistance *S. aureus*

WGS - Whole genome sequencing

Statement of Copyright

Acknowledgements

I would like to express my gratitude to Dr. Adrian Brown for conducting the iTRAQ proteomics used for this project, and to Dr. Wenbin Wei for analysing the whole genome sequencing data. My thanks also go to Dr. Chieko Itakura for her expertise in Scanning Electron Microscopy, and to Candace Adams for her initial training and the foundational experiments upon which this thesis is based. I am grateful to Dr. Joy Paterson and the Sharples lab for their hospitality and support in my work on clinically relevant pathogens, as well as to the members of LightOx for their ongoing assistance throughout my PhD. Finally, I would like to extend my thanks to my supervisors, Professor Carrie Ambler and Dr. Gary Sharples, for their invaluable guidance and support over the past four years.

Dedication

To Socks, Soup and Quinn. For forcing me to take breaks by sitting on my keyboard
For Liv, for making it all worthwhile

Chapter 1. Introduction

1.1 The Rise of Antibiotics and the AMR Crisis

Since the discovery of penicillin in the 1920s, antibiotics have become fundamental in managing infectious diseases, leading to significant public health improvements. Over the following decades, numerous classes of antibiotics were developed, with the last major class emerging in the 1980s (1). However, the lack of new antimicrobials and the increasing prevalence of antibiotic resistance have created what is often termed the "silent pandemic." In 2019 alone, antimicrobial resistance (AMR) was responsible for over 1.3 million deaths worldwide (2).

1.2 Development of Antibiotic Resistance

While the advent of antibiotics has allowed for the effective treatment of bacteria (3), their widespread overuse in healthcare and agriculture has contributed to a significant public health challenge (4). Today, antibiotics are frequently prescribed for common infections and used preventively in livestock, creating an environment of high selection pressure (5). This overuse selects for the emergence of bacterial strains capable of evading the effects of broad-spectrum antibiotics. Bacteria which have acquired resistance can pass genetic material to their offspring, enabling the inheritance of resistance traits via vertical transmission (6). Moreover, resistant traits can be rapidly shared across bacterial populations through horizontal gene transfer, further exacerbating the crisis.

1.3 Horizontal transmission of resistance

Bacteria can acquire resistance genes through horizontal gene transfer (HGT) via three primary mechanisms: transformation, the uptake of free DNA from the environment; transduction, the transfer of DNA mediated by bacteriophages; and conjugation, the direct transfer of plasmids between bacteria via a conjugation pilus. As only competent bacteria, which have a more permeable membrane, can take up DNA through transformation (7), and phage mediated transfer of resistance genes is rare (8), conjugation is the most common mode of genetic transfer, allowing rapid dissemination of resistance traits (9).

1.4 Bacterial Conjugation and resistance dissemination

Conjugation involves the transfer of a plasmid containing the fertility (F) factor from a donor bacterium to a recipient. The F factor encodes the necessary genes for the conjugation process, known as tra (transfer) genes, which govern the assembly of the relaxosome and conjugation pilus, as well as the replication and transfer of the plasmid itself (10).

The conjugation pilus extends from the donor bacterium to establish contact with the recipient, facilitating DNA transfer (11). The relaxosome, a complex including relaxase/helicase, nicks the plasmid at the transfer origin and unwinds it, allowing the transfer strand to move through the conjugation pilus (12). Once the strand is delivered into the recipient, it reforms into a circular structure and is converted into double-stranded DNA (10).

Following the successful conjugation of the plasmid, expression of the genes present then occurs in the recipient, resistance genes present on the conjugation plasmid are also

expressed and therefore the transfer of the conjugation plasmid can lead to the rapid spread of resistance genes between bacterial populations (13).

1.5 Mechanisms of antimicrobial resistance

1.5.1 Altering of the target site

Conventional antibiotics function through tight binding to specific sites on their targets to damage or inhibit them. The target site of an antibiotic varies depending on its class, but a common feature among them is their ability to bind specific targets with high affinity, disrupting essential bacterial processes.

For example, β-lactams irreversibly bind to the active site of penicillin-binding proteins (PBPs), mimicking the D-alanyl-D-alanine chain and rendering them unable to participate in peptidoglycan cross-linking, ultimately weakening the bacterial cell wall(14). Fluoroquinolones target DNA gyrase or topoisomerase, forming stable drug-enzyme-DNA complexes. This interaction induces a conformational change that leads to the accumulation of toxic DNA-drug-enzyme intermediates, ultimately inhibiting DNA replication and leading to bacterial cell death (15). Tetracyclines bind to a specific site on the 30S ribosomal subunit, preventing the association of aminoacyl-tRNA with the ribosome. This inhibition disrupts protein synthesis, halting bacterial growth (16).

While these antibiotics differ in their mechanisms, their effectiveness relies on their ability to bind their respective targets with high affinity, thereby disrupting critical bacterial functions. mutations can occur in these targeted enzymes to reduce the binding affinity of antibiotics (17).

Modifications can occur through changes in the amino acid sequence. For example, in the DNA gyrase GyrA of *K. pneumoniae*, a Ser83Leu mutation induces a structural change that reduces binding affinity for fluoroquinolones (18). Additionally, bacteria can develop mutations or acquire genes through horizontal gene transfer, enabling them to encode modified versions of targeted enzymes. In *S. aureus*, the acquisition of the *mecA* gene enables the production of a modified PBP, known as PBP2a. This modified protein has a significantly lower binding affinity for beta-lactams, allowing the bacteria to continue synthesising peptidoglycan even in their presence (19).

1.5.2 Antibiotic inactivation

Bacteria have developed mechanisms to inactivate antibiotics through direct degradation or chemical modification (9). As shown in *E. coli's* resistance to macrolides, a class of antibiotics that inhibit protein synthesis through interference with the 50s ribosomal subunit (20). *E. coli* employs esterases, *ereA* and *ereB*, to hydrolyse the carbonyl group in the macrolide lactone ring, leading to inactivation of the drug and consequent resistance (21).

In addition to hydrolysis, *E. coli* can also inactivate macrolides by transferring a phosphate group to the hydroxyl residue of the macrolide ring through the enzyme macrolide phosphotransferase (22). This phosphorylated macrolide is unable to interact with the critical residue of its ribosomal target, rendering it ineffective in inhibiting protein synthesis (23).

1.5.3 Efflux of the antibiotic

To prevent the accumulation of toxic substances within their cells, bacteria utilise efflux pumps to export various compounds, including antibiotics (24). There are five well-characterised families of efflux pumps: the Major Facilitator Superfamily (MFS), the ATP-Binding Cassette (ABC) family, the Small Multidrug Resistance (SMR) family, the Resistance-Nodulation-Cell Division (RND) superfamily, and the Multidrug and Toxic Compound Extrusion (MATE) family (25).

These pumps can recognise and export antibiotics, contributing to both natural and acquired resistance. By overexpressing these pumps, bacteria can survive in environments with high concentrations of antibiotics, leading to clinically significant resistance (24). Moreover, efflux pumps can work synergistically with other resistance mechanisms, further enhancing the level of resistance (26).

In Gram-negative bacteria, efflux systems are typically more complex, consisting of multiple subunits that span both the inner and outer membranes, facilitating the transport of substances from the cytoplasm to the extracellular space. A well-studied example is the AcrAB-TolC system, an RND pump known for its high substrate polyspecificity, capable of extruding a wide range of structurally diverse antibiotics (27).

In contrast, Gram-positive bacteria, due to their simpler cellular structure, contain single-compartment systems that span only the cytoplasmic membrane. These pumps generally exhibit higher substrate specificity (28). An example is the macrolide efflux pump system in *S. pyogenes*, an MFS pump that shows a strong affinity for macrolide rings, effectively removing these antibiotics and conferring resistance to this class of drugs (29).

1.5.4 Restricting drug entry or access to the target site

For an antimicrobial to effectively kill or inactivate bacteria, it must be able to reach its target reliably. Bacteria can naturally limit entry of harmful compounds, for example the presence of hydrophilic LPS on Gram-negative outer membranes restricts the entry of hydrophobic molecules, leading to a difference in susceptibility between Gram-positive and Gram-negative bacteria as less of the antibiotic can reach the target site (24).

Through changes in envelope structure, bacteria can reduce the amount of antibiotic that reaches the target. An example is Vancomycin Intermediate Resistant *Staphylococcus aureus* (VISA), which develops a thicker cell wall by increasing nonamidated glutamine residues in the peptidoglycan layer (30). This thicker wall provides moderate resistance to vancomycin, which needs to penetrate the cell wall to reach the target transglucosylase enzyme located on the cell membrane adjacent to the cell wall (9).

In addition, Bacteria in biofilms form a physical barrier that impedes antibiotic penetration. Biofilms are complex communities of single or multi-species bacteria encased in a protective layer of extracellular polymeric substances (EPS), which include polysaccharides, lipids, proteins, and nucleic acids. These substances create a three-dimensional structure that encases the bacterial population (31), reducing the amount of antibiotic that can reach the bacteria.

Biofilms are ubiquitous, as nearly all bacteria have the ability to form them (32). Formation begins when planktonic bacteria adhere to a suitable surface and alter their gene

expression, sometimes resulting in phenotypic changes, which cause them to become irreversibly attached (33). As the bacteria grow, they form a microcolony and produce EPS, which encapsulates them. The maturation of the biofilm allows the EPS to protect the bacteria from antimicrobials and oxidative damage. It also facilitates communication by encapsulating signaling molecules, which attract nearby planktonic cells to join the biofilm (34).

Once established, biofilms show a marked decrease in antibiotic susceptibility, typically by a factor of 10 to 1000 compared to planktonic cells (35). The EPS matrix acts as a physical barrier, preventing or slowing the penetration of antibiotics into the colony. Additionally, the altered microenvironment within the biofilm, along with the presence of sub-populations of bacteria with varying susceptibilities to antibiotics, further contributes to this increased resistance (36).

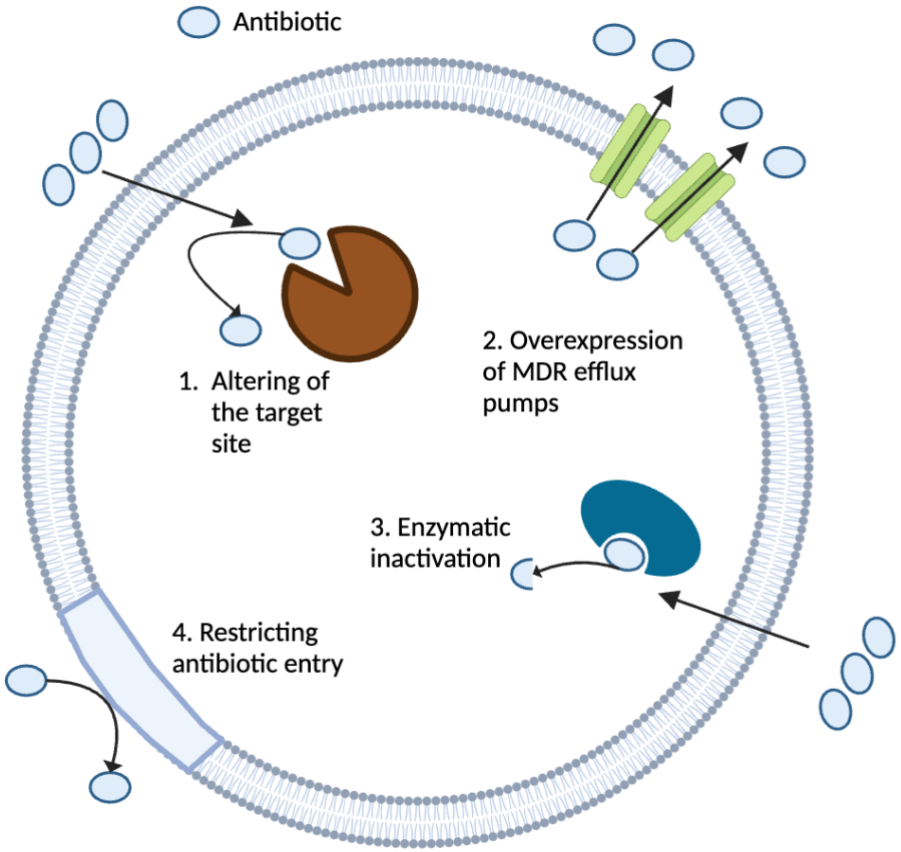

Figure 1. Four mechanisms by which bacteria have displayed resistance to antibiotics, including target site alterations reducing binding affinity; overexpression of MDR efflux pumps to remove antibiotic; destruction or inactivation of the antibiotic and changes in envelope structure to restrict entry of the antibiotic. Created in BioRender.com

1.6 Resistance, tolerance and persistence

In addition to the previously discussed mechanisms of resistance, it is essential to understand the concepts of tolerance and persistence, as they further complicate the treatment of bacterial infections.

Resistance is the ability of bacterial populations to survive and reproduce in the presence of high antibiotic levels due to genetic mutations, often measured by minimal inhibitory concentration (MIC) (37). In contrast, tolerance is the ability of bacterial populations to survive antibiotic exposure without reproducing, by entering a dormant state that makes them less susceptible to antibiotics targeting actively dividing cells, such as those involved in cell wall synthesis (38). A synergistic effect between tolerance and resistance has been observed, with resistance more likely to develop from tolerant strains, as fewer evolutionary steps are needed to transition from tolerance to full resistance (39).

Finally, persistence is a phenomenon where a small subpopulation of bacteria enters a state of slow or arrested growth, allowing them to survive antibiotic treatment and resume growth once the stress is removed, effectively reseeding the population (40). Unlike with tolerance, persistence is not a population-wide trait, as persister cells can spontaneously revert to a susceptible state (41).

1.7 Consequences of resistant infections in hospital settings

As bacteria develop resistance to common antibiotics, the risk of treatment failure and infection relapse increases. Infections caused by resistant strains are associated with twice the number of adverse outcomes compared to those caused by susceptible strains (42) , often resulting in longer hospital stays for patients. The inability to effectively treat these infections

can increase mortality rates, turning previously manageable infections into life-threatening situations.

In many instances, the only available treatments for resistant bacteria are last-resort drugs, such as colistin. These antibiotics tend to be expensive, are not readily accessible in developing countries, and often come with significant side effects (43). Additionally, the rise of resistant infections poses serious risks during surgical procedures, as the effective use of prophylactic antibiotics becomes challenging, leading to an increase in surgical site infections (44). The combined effects of higher mortality rates and prolonged hospitalisations place considerable strain on healthcare systems, resulting in significantly increased costs. In 2019, it was estimated that AMR contributed to an additional $20 billion in healthcare costs and a further $35 billion in lost productivity in the US (45).

Of particular concern are six pathogens highlighted as critical multidrug resistant threats to which new and effective treatments are urgently required, known as the ESKAPE pathogens: *Enterococcus faecium, Staphylococcus aureus, Klebsiella pneumoniae, Acinetobacter baumannii, Pseudomonas aeruginosa* and *Enterobacter* spp. (46).

***Enterococcus faecium*:** This Gram-positive opportunistic pathogen can lead to serious urinary tract infections, bloodstream infections, and infections associated with medical devices. Of particular concern are strains resistant to vancomycin, known as vancomycin-resistant *Enterococcus* (VRE) (47).

***Staphylococcus aureus*:** This Gram-positive cocci colonises the skin or nose in nearly 30% of healthy individuals. However, in immunocompromised patients, it often causes skin infections, pneumonia, and bloodstream infections. Methicillin-resistant *Staphylococcus*

aureus (MRSA) poses a significant threat as it is resistant to methicillin, oxacillin, and related drug classes, including cephalosporins (48).

***Klebsiella pneumoniae*:** This Gram-negative bacterium can cause pneumonia, catheter-associated urinary tract infections, and bloodstream infections. Certain strains of *K. pneumoniae* produce carbapenemases (KPCs), which can inactivate carbapenems and confer resistance to a broad range of antibiotics (49).

***Acinetobacter baumannii*:** A Gram-negative bacterium frequently associated with infections, particularly in intensive care units. Some strains of *A. baumannii* have developed pan-drug resistance (PDR), rendering them resistant to all antibiotics tested except for colistin and tigecycline (50).

***Pseudomonas aeruginosa*:** This Gram-negative opportunistic pathogen is known for causing infections in immunocompromised patients, especially those with cystic fibrosis. *P. aeruginosa* exhibits natural resistance to many antibiotics due to its highly impermeable outer membrane (51), and the presence of multidrug-resistant (MDR) efflux pumps (48).

***Enterobacter spp*.:** *Enterobacter* species are a group of Gram-negative opportunistic pathogens that can cause serious infections, particularly bacteraemia, in immunocompromised patients. The presence of plasmid-encoded extended-spectrum beta-lactamases (ESBLs) and carbapenemases often leads to treatment failures with penicillin derivatives and cephalosporins (52).

The increasing prevalence of pathogens resistant to common antibiotics, along with the emergence of some strains that can withstand even last-resort drugs, has underscored the

urgent need for enhanced monitoring, effective infection control measures, and the development of alternative treatments. These efforts are essential to mitigate the impact of resistant infections on healthcare systems.

1.8 Social changes

While antibiotic resistance is primarily a medical issue, socioeconomic factors significantly drive the progression of AMR. This challenge is exacerbated by insufficient attention to disease prevention, inadequate sanitation, unregulated and unrestricted access to effective antimicrobials (53). The problem is particularly apparent in low-income areas, where a lack of healthcare access can result in inadequate treatment and the overprescribing of inexpensive, broad-spectrum antibiotics, often due to incorrect diagnoses (54). The overuse and misuse of antibiotics, especially for viral infections, add unnecessary selective pressure that drives the development of resistance (55). Although the development of new antibiotics and novel treatments can help combat resistance, improved access to effective healthcare and public education about the threat of AMR and the proper use of antibiotics is crucial (56).

1.9 Development of new antibiotics

To address the lack of development of antibiotics, new incentives have also been established to promote the development of novel antibiotics. A 2017 estimate indicated that developing a new antibiotic can cost around $1.5 billion (57), while the projected annual revenue for an antibiotic is only about $46 million (58). Moreover, the swift emergence of AMR further reduces the financial incentive for developing new antibiotics, as newly introduced drugs quickly become ineffective.

In response to these challenges, governments have implemented both push and pull incentives to facilitate the market entry of new antibiotics (59). Push incentives aim to reduce research and development costs and accelerate the drug development process. For instance, grants serve as push incentives by subsidising development expenses, enabling progress on projects that may not be financially viable (59).

On the other hand, pull incentives reward companies for achieving specific development milestones. One example is the market entry reward (MER), which offers substantial financial compensation to companies that successfully bring antibiotics meeting certain criteria to market, replacing traditional revenue from sales with a fixed payment (59).

Additionally, the United Kingdom's NHS has introduced a subscription system, where companies provide antibiotics for a fixed annual payment, effectively unlinking profit from the volume of antibiotics sold (60). For example, Shionogi's *Cefiderocol* and Pfizer's *ceftazidime-avibactam* have been awarded £10 million annually for 10 years (60). This model is particularly suited for high-value, low-use antibiotics, such as those reserved for treating the ESKAPE pathogens. However, it may not encourage antibiotic development by small and medium-sized companies, as the funding is more likely to benefit large pharmaceutical corporations (61). It remains unclear whether this system would successfully bring such antibiotics back to market (62).

Despite these financial incentives, the rapid pace of resistance development has prompted the scientific community to explore new classes of treatments that are less susceptible to resistance.

1.10 New classes of treatment

New classes of treatments are continuously being developed to combat AMR, with the key advantage of reduced susceptibility to resistance development. One promising approach is phage therapy, which uses bacterial phages, viruses that specifically target and kill bacteria (63). These phages can be customised to attack specific bacterial strains and are often effective against MDR pathogens due to an evolutionary arms race between bacteria and phages. However, phage therapy remains largely experimental, facing challenges such as high production costs and a narrow host range, which limits their ability to target all pathogenic strains within a species (64).

Another method is the development of antivirulence drugs (AVDs), which target non-essential bacterial components to minimise selection pressure and reduce the likelihood of resistance (65). By disarming virulence factors, AVDs impair the bacteria's ability to cause disease, allowing the immune system to effectively clear the infection while mitigating the inflammatory response caused by bacterial toxins (66). Despite their potential, few AVDs have been synthesised, and production can be costly, particularly as most approved drugs are monoclonal antibody based (67).

Additionally, photodynamic therapy (PDT) employs photosensitisers (PS) and specific light wavelengths to generate reactive oxygen species (ROS) that effectively eliminate bacteria. This method, which will be the focus of this thesis, presents a promising approach to addressing AMR.

1.11 Photodynamic Therapy

Photodynamic therapy involves the use of a PS, oxygen, and visible light to generate unstable ROS (68). The PS is typically an organic molecule rich in conjugated pi bonds, allowing it to absorb light within the visible spectrum (69). After application, the PS accumulates in the target tissue with minimal toxicity. Initially, the PS exists in a singlet ground state, where it contains two electrons with opposite spins in a low-energy orbital (68).

When exposed to light of the appropriate wavelength, the PS transitions to an excited singlet state as one electron absorbs energy and moves to a higher-energy orbital. At this stage, the PS may either emit a photon or return to the ground state through internal conversion, releasing energy as light or heat, respectively (70). Additionally, the excited PS can undergo intersystem crossing, resulting in a change in the electron spin to a parallel configuration and forming a more stable triplet state. While the triplet state can potentially emit a photon through phosphorescence, this process is "forbidden" by quantum selection rules, leading to a significantly longer lifetime of microseconds for the triplet state compared to the nanosecond duration of the singlet state (71).

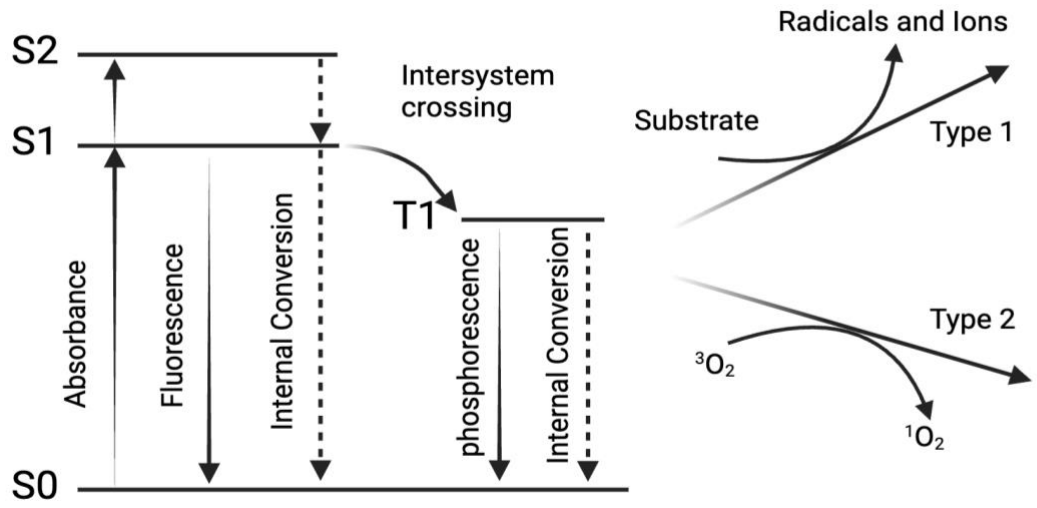

Figure 2. Jablonski diagram to indicate the absorbance of a photon by a photosensitiser and the excited state, with intersystem crossing leading to the long-lived triplet state. Transfer of electrons or protons to substrate (type 1) or energy transfer to oxygen (type 2). Created with Biorender.com

1.12 Types of Photosensitiser reaction

Photosensitisers are classified into four types (1-4) based on the chemical mechanisms that induce oxidative stress and photocytotoxicity. These types are further divided into direct and indirect PS (72).

Type 1 and Type 2 reactions are both indirect and oxygen-dependent. Type 1 photoreactions generate ROS through electron or proton transfer to molecular oxygen. This process leads to the oxidation or reduction of oxygen, producing radicals such as superoxide ($O^{2\bullet-}$), hydroxyl radicals (•OH), and hydrogen peroxide (H_2O_2) (73) . These resulting ROS can indiscriminately transfer oxygen to or extract electrons from various biomolecules, including nucleic acids, lipids, and amino acids, resulting in extensive cellular damage and cell death.

In contrast, Type 2 reactions involve the transfer of energy from the PS to change the spin of an electron in the ground state of molecular oxygen. leading to the free electron having opposite spin to an unpaired electron in the ground state, and these electrons pairing up in an unstable unparallel spin rotation, resulting in the formation of highly reactive singlet oxygen (73), which is short-lived, lasting less than 4×10^{-8} seconds, before being rapidly quenched by water (74). Despite its brief lifetime, singlet oxygen can inflict significant damage through energy transfer or chemical reactions with bioactive molecules (74). Typically, Type 1 and Type 2 reactions occur simultaneously, with the predominance of one type over the other depending on the specific properties of the PS (75).

Type 3 and Type 4 reactions are categorised as direct, oxygen-independent photosensitisation processes. Type 3 PS interact directly with biomolecules such as DNA and proteins, where the excited PS destructively combines with the biomolecule through a triplet-doublet reaction to

generate ROS (76). Type 4 PS utilise non-toxic prodrugs that undergo photoisomerisation upon irradiation, converting the PS into an active form that binds directly to the target, resulting in cytotoxicity independent of ROS generation (77).

1.13 Antimicrobial PDT

Antimicrobial photodynamic therapy (aPDT) focuses on utilising PDT to inactivate or kill bacteria that are resistant to common antibiotics. Unlike conventional antimicrobials, which target specific molecules or pathways, aPDT relies on the non-specific action of ROS generated during the photoactivation of a PS. These ROS cause oxidation and damage to various critical cellular components, particularly membranes, proteins, and DNA. Most bacteria lack sufficient antioxidant defences to withstand the overwhelming production of ROS following photoactivation (78). aPDT has demonstrated effectiveness against resistant pathogens. With 100 µM Methylene Blue (MB) reducing viable cells by more than 5log following 100mW/cm2 activation against ten of the highest-priority drug resistant pathogens following exposure identified by the World Health Organisation, including resistant strains of *A. baumannii*, *S. aureus* and *K. pneumoniae* (79). However, the indiscriminate production of reactive oxygen species during photoactivation eliminates both commensal and pathogenic bacteria, potentially disrupting the microbiome. For example, studies have shown that blue light treatment can alter the microbiome composition in mice (80).

1.14 Difficulty in development of resistance to PDT

Antimicrobial photodynamic therapy poses significant challenges for bacterial adaptation and resistance due to its rapid and non-specific action on microbial cells as, unlike with conventional antibiotics, bacteria cannot simply modify a single target to evade the action of ROS and gain resistance (81). Additionally, because the PS itself exhibits low toxicity in the absence of light, bacteria do not trigger survival responses against the PS prior to photoactivation (82). This low dark toxicity can hinder bacteria from recognising the oxidative stress as being caused by the PS, prompting them to respond through detoxification pathways or other metabolic adjustments aimed at counteracting ROS instead of a selection against the photosensitiser itself (83). Although it is possible for bacteria to develop resistance to aPDT, potentially through modifications in oxidative stress response pathways or the introduction of non-specific efflux pumps to expel the PS before activation, such adaptations prove significantly more challenging than adaptations to a conventional antibiotic (82).

1.15 Reactive oxygen species and aPDT

Central to the effectiveness of PDT is the generation of ROS upon activation of the PS by light. These highly reactive molecules induce oxidative stress in bacterial cells, causing extensive damage to essential cellular components. Among the most destructive ROS is the hydroxyl radical (•OH), which can be produced through the Fenton reaction.

This reaction occurs when H_2O_2 undergoes a redox reaction with ferrous iron (Fe^{2+}), resulting in the formation of the highly reactive •OH, which can oxidise most biological molecules at diffusion-limited rates (84). Additionally, this reaction converts Fe^{2+} to ferric iron (Fe^{3+}) (85).

The Fenton reaction can take place in bacteria when H_2O_2 accumulates in cells, where it reacts with free iron that is not bound to enzymes or iron storage proteins (84).

1.16 ROS damage to proteins

ROS can cause significant damage to bacterial proteins, primarily through the oxidation of amino acid side chains. Cysteine and methionine are particularly susceptible to this oxidation due to their sulfur-containing side chains (86). When these sulfur atoms are oxidised, they can form disulfide bonds or unstable sulfenic acid groups, disrupting the protein's structure and function (87).

Furthermore, ROS can trigger the formation of carbonylated proteins by oxidising basic amino acids such as arginine, lysine, and threonine, (88). Hydroxyl radicals can extract a hydrogen atom from these residues, leading to the formation of carbon-based radicals that subsequently react with oxygen to produce carbonyl groups (C=O) (89). In bacteria, carbonylation is an irreversible modification, with the only defence mechanism being proteolytic degradation of the carbonylated proteins via the protease pathway (90).

In addition to directly modifying amino acids, ROS can also damage iron-sulfur (Fe-S) clusters, which are common cofactors in nature. Both hydrogen peroxide and superoxide can enter the active site of the cluster containing enzyme active site and directly oxidise the clusters by removing an electron, converting them from the stable $[4Fe\text{-}4S]^{2+}$ form to the unstable $[4Fe\text{-}4S]^{3+}$ form (91). This alteration leads to the release of catalytic iron from the cluster and the formation of $[3Fe\text{-}4S]^{1+}$, rendering cluster-bound enzymes inactive. Moreover, the free iron can react with H_2O_2 to generate hydroxyl radicals via the Fenton reaction, resulting in subsequent damage (92).

The cumulative effects of these oxidative modifications can severely compromise protein stability and activity, ultimately affecting the viability and pathogenicity of the bacteria.

1.17 ROS damage to lipids

ROS can cause significant damage to bacterial cells through the radical-mediated removal of electrons from membrane lipids, leading to lipid peroxidation. However, lipid peroxidation occurs less readily in bacteria than in eukaryotes, as bacterial membranes predominantly contain poorly oxidisable saturated or monounsaturated lipids (93), while eukaryotic membranes are rich in polyunsaturated fatty acids that are more susceptible to peroxidation (93). Nevertheless, H_2O_2 can react with free iron to generate hydroxyl radicals, which can initiate lipid peroxidation. This process results in an autocatalytic radical chain reaction that degrades phospholipid acyl chains (94), decreasing membrane fluidity and compromising membrane integrity (95). Additionally, this reaction produces toxic aldehydes, which can migrate from the membrane and react with proteins and DNA, causing further cellular damage (95).

ROS can also oxidise membrane-bound proteins, altering their structure and function, and destabilising essential membrane transport proteins and enzymes (96). This impairment disrupts critical processes such as energy production and nutrient uptake (95). The combined effects of altered lipids and disrupted membrane proteins increase cellular permeability, interferes with vital functions, and can lead to the leakage of essential cellular contents. Severe oxidation of the membrane compromises its integrity and results in loss of cell viability.

1.18 ROS damage to DNA

ROS produced in bacteria can cause DNA damage through various mechanisms. While $O^{2\bullet-}$ and H_2O_2 do not directly damage DNA (97), H_2O_2 can react with unincorporated iron, some of which associates with DNA (98), via the Fenton reaction to generate •OH. •OH oxidises both the bases and the ribose moiety of nucleotides, with guanine being preferentially targeted due to its lower reducing potential, which allows electron transfer from guanine to the nearby oxidised base (99). This redirection of oxidative damage from other bases to guanine can result in the formation of 8-oxo-7,8-dihydro-2'-deoxyguanine (8-OxodG) (97). This oxidised form of guanine is difficult to replace and often leads to the misincorporation of adenine during DNA replication, resulting in point mutations if the lesion is not correctly repaired (84).

To rectify this misincorporation, the base excision repair (BER) system is activated; however, this repair process creates single-strand DNA breaks (100). Moreover, when BER is recruited to nearby damaged sites, it may lead to double-strand DNA breaks (101). These breaks disrupt the integrity of the DNA helix and can be fatal if not repaired, often by the error-prone DNA polymerase V (84), which can lead to further genomic instability. ROS mediated DNA damage is thought to be one of the most significant targets for ROS, as even a single DNA lesion can potentially be mutagenic or lethal (84).

1.19 Bacterial defence against ROS - detoxification

To mitigate the dangers posed by uncontrolled ROS, bacteria have developed systems to detoxify these harmful molecules before they can damage vital cellular components. Superoxide, for example, is detoxified by superoxide dismutase (SOD) enzymes. These metalloenzymes utilise a redox-active metal cofactor to convert two molecules of superoxide

into molecular oxygen and hydrogen peroxide (102). The presence of SODs in nearly all pathogenic bacteria underscores the significance of superoxide dismutation. Many bacteria possess multiple SODs, each with a different metal cofactor, ensuring effective detoxification even in cells with limited availability of a specific metal (103).

The hydrogen peroxide produced by SODs is further broken down into water and molecular oxygen by catalase enzymes. Catalase typically employs a two-stage mechanism for this dismutation: the first reaction uses a heme iron cofactor to reduce the first H_2O_2 to water, oxidising the iron in the process. The second reaction occurs rapidly after, with a second H_2O_2 molecule reducing the iron back to its original state, producing water and oxygen (104). Catalase enzymes are widespread to limit the H_2O_2 that can react with free iron and generate •OH that can cause severe cellular damage. To date, no protein mechanisms have been discovered that can detoxify these hydroxyl radicals (105).

In addition to these enzymatic systems, bacteria produce various small-molecule antioxidants and scavengers, such as thioredoxin, to maintain a reduced cellular environment and keep redox enzymes in their active reduced state. Thioredoxin effectively reduces thiol-disulfide bonds (106), and has been shown to directly reduce H_2O_2 (107). It also acts as a quencher for singlet oxygen and can scavenge hydroxyl radicals (108). While not essential, thioredoxin is crucial for bacterial survival and is found in most bacteria.

Overall, the ROS detoxification system is vital for regulating intracellular ROS levels; knockout studies have shown that the absence of these detoxification mechanisms significantly increases susceptibility to even low levels of ROS (96).

1.20 Bacterial defence against ROS – DNA repair

Unrepaired DNA damage from ROS poses a significant threat to bacteria, as it can lead to harmful mutations or cell death (109). To combat this, bacteria have developed robust repair mechanisms, one of which is the SOS response. This inducible system not only promotes DNA integrity but also enables the production of error-prone factors, allowing bacteria to survive and replicate despite extensive DNA damage, albeit at the cost of increased mutation rates (109).

The SOS response is activated by the accumulation of single-stranded DNA breaks, prompting RecA to bind to the single-stranded DNA and convert to its active form. This activation cleaves the SOS repressor LexA (110), leading to the expression of approximately 50 genes involved in DNA damage repair. For minor DNA damage, BER removes and replaces damaged or incorrect bases (111), while nucleotide excision repair (NER) repairs bulky DNA adducts and interstrand cross-links (112). However, in cases of severe damage where BER and NER are insufficient to restore DNA replication, a mutagenic phase called translesion DNA synthesis is initiated (110). Here, RecA activates DNA polymerase V, an error-prone polymerase that inserts nucleotides opposite DNA lesions (113), Ultimately, while this response allows bacteria to survive oxidative damage from ROS, it also significantly increases the build-up of potentially fatal mutations (114).

1.21 Photosensitisers currently used for aPDT

As more clinical attention has been paid to aPDT the repertoire of PS has been further investigated, with the effectiveness of many PS trialled for their effectiveness against a range of bacteria (table 1).

Class	Example	Excitation maximum (nm)	Bacteria inactivated	Reference
Tetra-pyrrole structures	porphyrin	447	*S. aureus* *P. aeruginosa* *E. faecalis*	(115-117)
	Phtalocyanine	670	*A. hidrophila*	(118)
Natural PSs	Curcumin	547	*S. mutans* *L. acidophilus*	(119, 120)
	Hypericin	593	*S. aureus* *E. coli*	(121, 122)
Phenothiazinium	Methylene blue	632	*S. aureus* *P. aeruginosa*	(123)
	Rose Bengal	532	*E. faecalis* *P. aeruginosa*	(124)
Nano structures	Fullerenes	532	*S. aureus* *E. coli*	(125, 126)
	Titanium Dioxide	400	*E. coli*	(127)

Table 1. The 4 most common classes of photosensitiser used for aPDT and the bacteria they have been shown to inactivate

1.21.1 Tetrapyrrole structures

Tetrapyrroles, including porphyrins and phthalocyanines, were among the first PS introduced in photodynamic therapy. These compounds are characterised by their cyclic structure, which comprises four interconnected pyrrole rings and typically contains an internal metal cofactor (128). Cationic porphyrins are particularly notable for their ability to accumulate in bacterial

cells, resulting in high yields of singlet oxygen and significant cytotoxicity when irradiated with blue light (129). For example, the cationic porphyrin 5,10,15,20-tetrakis(1-methyl-pyridino)-21H,23H-porphine, tetra-p-tosylate salt (TMP), was shown to reduce the number of viable cells within a *P. aeruginosa* biofilm by 10^4 at a concentration of 100 µM following 10 minutes of irradiation with a 400 nm mercury lamp (115).

Trimethoprim (TMP) has also demonstrated effectiveness against *S. aureus* biofilms, reducing cell survival by 70-fold compared to the untreated control when treated with 10 µM TMP and exposed to 150 J/cm² blue light (116).

Another promising tetrapyrrole-based photosensitiser is the phthalocyanine derivative $(NCH_3)_3ZnPc^{3+}$, which rapidly binds to microbial cells and effectively eliminates *S. aureus* and *E. coli* within five minutes of red-light irradiation at concentrations of 1 µM and 2.5 µM, respectively (130). Additionally, the porphyrin 5-aminolevulinic acid (5-ALA) has received FDA approval as a prodrug, which is metabolised into the active photosensitiser protoporphyrin IX. It is currently used as a photodynamic therapy (PDT) treatment for high-grade gliomas (131). Beyond oncology, 5-ALA has also been applied in the treatment of wounds and skin infections through topical administration (132).

1.21.2 Natural photosensitisers

Natural PS have been isolated from plants which were used historically to treat skin infections when combined with sunlight. Most naturally derived PS require some form of processing or encapsulation with nanoparticles to display efficient activity upon light exposure (71). However, natural PSs have been shown to effectively eliminate bacteria upon activation. One

example is the naturally derived PS, curcumin, isolated from the root of *curcuma longa*. Was shown to eliminate dental pathogens upon exposure to blue light (133).

1.21.3 Phenothiazinium dyes

Phenothiazinium dyes, such as methylene blue (MB) and Rose Bengal (RB), are dyes derived from the phenothiazine backbone, which features a three-ring system consisting of two fused benzene rings and a sulfur-containing heterocyclic ring (134). These dyes exhibit broad-spectrum photoactivity while generally maintaining low toxicity to human cells, making them effective therapeutic agents (135).

Methylene blue, in particular, has been observed to accumulate around bacterial membranes, leading to cell death when activated with 660 nm light (135). Research has demonstrated that exposure to 100 mW/cm² of light at a concentration of 100 µM MB can effectively clear ESKAPE pathogens, with no significant difference in susceptibility between antibiotic-susceptible and resistant strains (79).

Additionally, methylene blue has proven useful in clinical settings. For example, the Canadian biomedical company Ondine employs methylene blue to sterilise the anterior nares of patients prior to surgery. This approach has been shown to reduce surgical site infections caused by *S. aureus* by over 50%, with no long-term development of resistance observed (136).

Another Phenothiazinium dye, Rose bengal (RB), has been shown to eliminate clinically relevant bacteria upon activation with green light. Shrestha et. al. demonstrated the ability of 10 µM RB to reduce the viable cells of an *E. faecalis* biofilm by 3 log following 40 J/cm^2

irradiation with 540 nm light (124). Whilst also being shown to act synergistically with gentamicin, with a combination of 64 µg/ml and 40 µg/ml of RB and gentamycin, respectively, shown to completely eliminate *S. aureus* biofilms when exposed to 18 J/cm^2 green light (137).

1.21.4 Nanostructures

Nanostructures are commonly employed to enhance the delivery of PS by forming carriers that improve the solubility of the PS, ensuring effective delivery to the target site without compromising the PS's efficacy after light activation (138). Some nanoparticles can act as photosensitisers themselves, such as Fullerenes, nanostructures consisting of spherical arrangements of carbon atoms, The condensed aromatic rings present allow π conjugation and overlap of molecular orbitals, leading to excellent light absorption and high triplet state stability, allowing efficient production of singlet oxygen (126). Fullerenes have demonstrated high photostability and effective killing of *S. aureus* at 10 µM, with elimination of *E. coli* requiring a higher concentration of 100 µM (125). Moreover, chemical attachment to the structure is simple, allowing for attachment of chemical groups to improve efficiency towards specific pathogens (126).

1.22 Problems associated with conventional PS

While PDT offers significant therapeutic potential, clinically approved photosensitisers such as 5-aminolevulinic acid (5-ALA) have several limitations. One major issue is poor dosage control due to the need for metabolic conversion to the active photosensitiser, protoporphyrin IX (139). 5-ALA is also known to be quite unstable, undergoing dimerisation and subsequent oxidation at neutral and basic PH. (131) Many porphyrins exhibit high stability

towards metabolism and, hence, they exhibit a long elimination half-life, which can lead to photosensitivity lasting weeks after treatment (140). Furthermore, the large size of porphyrin structures makes it challenging for them to diffuse into target cells, often resulting in accumulation in off-target tissues. Although they are effective photosensitisers, they frequently fall short as therapeutics (140).

In contrast, phenothiazinium dyes experience fewer of these issues but still require relatively high concentrations and light intensity to achieve bacterial elimination.

Nanostructures present their own set of challenges. Their synthesis can be complex and costly, and predicting their distribution within the body is difficult, which may lead to issues with clearance and off-target accumulation (141).

Given these challenges, there is a pressing need for novel photosensitisers that can accumulate effectively in target tissues without off-target effects, while delivering a controlled dose of ROS upon activation to achieve a high bactericidal effect.

1.23 LightOx Photosensitisers

LightOx has developed a library of low molecular weight (0.4-0.6 kDa) photo-activated donor-acceptor diarylacetylenes (142). These molecules exhibit varying functionalities with a general modular structure based on a diarylacetylene core, which includes an α,β-unsaturated carboxylic acid or ester group at the acceptor end and a free amine-containing moiety at the donor end. This design makes them ideal candidates for photoactivated therapy, as their planar structures and highly conjugated structure allows for effective light absorption, and the free amine group provides a suitable site for attachment to targeting molecules.

LightOx compounds have been shown to readily penetrate mammalian cells, commonly associating with intracellular lipid droplets and organelle membranes (143). When activated by UV-A or violet light, these compounds exhibit potent cytotoxic activity, ostensibly through intracellular ROS production following light absorption, while possessing a more "drug-like" structure compared to existing photosensitisers (140). This structural advantage contributes to more favourable pharmacokinetics. The combination of low molecular weight, allowing for effective penetration of bacterial cell walls, and high phototoxicity makes LightOx compounds promising candidates for use as antimicrobial agents.

1.24 Aims of the project

In this thesis, I will screen a library of LightOx compounds using *B. subtilis* overlays to identify candidate compounds that inhibit bacterial growth upon activation with 365 nm light. From these candidates, a frontrunner will be selected based on growth inhibition assays conducted on *S. epidermidis*, *B. subtilis*, *E. coli*, and *P. fluorescens*, as well as a Propidium iodide (PI) assay in *S. epidermidis* to evaluate cytotoxic effects. The most effective compound will then be further assessed for its cytotoxic effects following activation in clinically relevant ESKAPE pathogens, with an emphasis on combating antibiotic-resistant bacteria and understanding the potential for *S. aureus* to develop tolerance after repeated sub-lethal treatments. Finally, I will investigate the mechanism of action of this compound, focusing on its localisation, the production of ROS following photoactivation, the species of ROS generated, and the cellular targets affected.

Chapter 2: Materials and methods

2.1 Compound 2 absorption and emission spectra

The structures of six diarylacetylene candidates screened for antibacterial activity are shown in Figure 4. Absorption spectra were obtained using a Perkin Elmer Cary 60 spectrometer and emission spectra using an Agilent Cary Eclipse spectrometer. For absorption spectra, 5 µM solutions of Compound **2** in $CHCl_3$ or DMSO were added to 10 mm path length quartz optical cuvettes (Hellma) and absorbances recorded at 1 nm intervals. Extinction coefficient measurements were determined in triplicate using measurements obtained from absorption readings at the respective λmax exhibited by Compound **2** in each solvent at concentrations from 5 to 30 µM. Extinction coefficient values are expressed as an average of the three independent replicates, with the standard deviation. Emission spectra were obtained at 1 nm intervals from 100 nM solutions in quartz cuvettes, as specified above, using excitation at λ = 380 nm, and normalised according to the respective maximal intensity values.

2.2 Quantum yield measurement

The quantum yield from one-photon excitation was determined using LightOx17 (quantum yield 0.67) in toluene as a standard. Compound **2** was measured at varying concentration in each of the solvents aiming for absorbances of 0.1 and below, these corresponded to concentrations in the 0.5-2 µM range. Absorbances of each compound in solution were recorded between 300 and 1000 nm and the corresponding fluorescence intensity was measured between 250 and 700 nm. Quantum yield was calculated using the relative method (144). The absorbance and fluorescence of compounds in solution were measured at multiple concentrations and compared to a reference via equation 1 (144):

$$\phi_S = \phi_R \frac{Grad_S}{Grad_R}\left(\frac{n_s}{n_R}\right)^2$$

Equation 1. Quantum yield calculation from relative absorbance and fluorescence

Where Grad is the gradient obtained by plotting the integrated fluorescence, I, against the absorbance, 1-10 A, and n is the refractive index of the solvents. The absorbance was measured at 390 nm using a Cary 60 UV-Vis, aiming for absorbances 0.1 and below. The fluorescence was measured using the same excitation wavelength (390 nm) by a Cary Eclipse Fluorescence Spectrophotometer and integrated between 400 and 700 nm. LightOx17 in toluene was used as the reference for all calculations (145). For each compound between 5 and 7 concentrations were measured with 3 repeats.

2.3 Bacterial strains used

Species	Strain	Source and genotype
Bacillus subtilis	ATCC 23857	Obtained from the American Type Culture Collection
	KS88	*trpC2 amyE*::(*spc* P*xyl*-WALP23-mcherry(B)) From Henrik Strahl, University of Newcastle
Staphylococcus epidermidis	ATCC 12228	FDA strain PCI 1200 Obtained from the American Type Culture Collection
Pseudomonas fluorescens	ATCC 13525	Obtained from the American Type Culture Collection
Enterococcus faecalis	ATCC 29212, NCTC 12697	Obtained from Public Health England
Pseudomonas aeruginosa	ATCC 25668	Schroeter, Migula; originally a clinical isolate; obtained from Public Health England
Staphylococcus aureus	FDA209P	Reference methicillin-sensitive *S. aureus* (MSSA) strain (146).

	SH1000	NCTC8325-4 derivative with repaired *rsbU* (147); from Laura Dobby, University of Newcastle
	GS3026	As SH1000, but Δ*sodA* Δ*sodM*; from Laura Dobby, University of Newcastle
	USA300	Community-associated methicillin-resistant *S. aureus* (CA-MRSA) strain JE2; from Kevin Waldron, University of Newcastle
Escherichia coli	ATCC 25922	FDA strain Seattle 1946 obtained from the American Type Culture Collection
	BW25113	*lacI*+ Δ(*araD-araB*)567, Δ*lacZ4787*(::*rrnB-3*), λ^-, *rph-1*, Δ(*rhaD-rhaB*)*568*, *hsdR514*.; wild-type strain for the Keio collection (148); all 'JW' strains below are from this collection obtained from Horizon Discovery Biosciences Limited, Cambridge
	JW3596	As BW25113, but Δ*rfaC::kan*
	JW2669	As BW25113, but Δ*recA::kan*
	JW0097	As BW25113, but Δ*mutT::kan*
	JW3879	As BW25113, but Δ*sodA::kan*
	JW1648	As BW25113, but Δ*sodB::kan*
	JW1638	As BW25113, but Δ*sodC::kan*
	JW0598	As BW25113, but Δ*ahpC::kan*
	JW3914	As BW25113, but Δ*katG::kan*
	JW2663	As BW25113, but Δ*gshA::kan*
	JW3024	As BW25113, but Δ*rfaE::kan*
	JW3606	As BW25113, but Δ*rfaG::kan*
	JW3607	As BW25113, but Δ*rfaQ::kan*
	JW2203	As BW25113, but Δ*ompC::kan*
	JW5580	As BW25113, but Δ*tatB::kan*
	JW5646	As BW25113, but Δ*envC::kan*
	JW5503	As BW25113, but Δ*tolC::kan*
	JW0452	As BW25113, but Δ*acrA::kan*
	JW0212	As BW25113, but Δ*lpcA::kan*
	JW3933	As BW25113, but Δ*oxyR::kan*
	JW3610	As BW25113, but Δ*mutM::kan*
	JW0018	As BW25113, but Δ*nhaA::kan*
	JW5276	As BW25113, but Δ*ydiQ::kan*
	JW1176	As BW25113, but Δ*fadR::kan*
	JW2277	As BW25113, but Δ*nuoH::kan*
	HS564	F^+ Sm^R *fabA*(Ts) *fabF* Crc- *atpB*-mNeonGreen; from Henrik Strahl, University of Newcastle

Table 2. Bacterial strains used in this thesis.

2.4 Photoactivated bacterial growth inhibition

Bacteria were cultivated in LB (Miller) broth in an orbital shaker (VWR) at 150 revolutions per minute (RPM) at a temperature of either 30 or 37°C, depending on the bacteria cultured. Overnight cultures were prepared by inoculating a single, isolated colony into 10 mL of LB broth followed by incubation with shaking for 16-20 h. Bacteria exposed to photoactivatable compound were placed in a LightOx PhotoReact 365 Lightbox (Merck) and exposed to light at a wavelength of 365 nm for 5 min, with an energy intensity of 13 mW/cm^2 (total energy delivered: 3.9 J/cm^2). For assays requiring half of a 96-well or agar plate to be irradiated, a section of black card was used to mask the relevant samples.

For bacterial overlays, 50 mL of 1.5% LB agar was poured into a 100 × 100 × 20 mm square petri dish (Sarstedt) and once solidified, 15 mL of 0.75% LB soft agar inoculated with 200 µL of bacteria from an overnight culture was poured onto the surface. Serially diluted concentrations of compound were applied to the overlay in 6 µL volumes. Plates to be photoactivated were then exposed to light at 365 nm and incubated at 30°C for 24 h before imaging in a Bio-Rad Gel Doc XR+ System.

For growth curves, 5 mL of LB broth in a 15 mL Falcon tube (Sarstedt) was inoculated with 50 µL of bacteria from an overnight culture. Compound **2** was added to give a final concentration of 2 µM and incubated in the dark with 150 RPM shaking at 30°C for 30 min. Samples (100 µL) were pipetted into the wells of a 96-well plate, with 8 technical repeats per sample. Half of the plate was covered, and the rest irradiated at 365 nm. Growth was monitored at $OD_{600n\ m}$ every 5 min for 24 h in a plate reader (Biotek Synergy HT) and data normalised against the negative control containing media alone.

2.5 Bacterial growth inhibition assay

All bacteria were grown in Muller-Hinton broth (Merck) in an orbital shaker at 30-37˚C; 25 µL of an overnight culture was added to 2 mL of Muller-Hinton broth in a sterile semi-micro cuvette (Sarstedt) and incubated at 30 or 37˚C with shaking until an $OD_{600\ nm}$ of 0.07, equivalent to a 0.5 MacFarland standard (240 µM $BaCl_2$ in 0.18 M H_2SO_4 aq). Appropriate concentrations of compound **2** (2-fold dilutions) were mixed with 50 µL Muller-Hinton broth in a 96-well plate with relevant controls. The culture was diluted 10-fold by adding 1 mL of the culture to 9 mL fresh Mueller-Hinton broth in a 15 mL sterile Falcon tube and inverted to mix before 50 µL of the diluted culture was pipetted into the sample wells of a 96 well plate already containing 50 µL of diluted compound. Plates were the irradiated in a PhotoReact 365 Lightbox, with settings as detailed above, and then incubated for 16 h with 120-130 rpm agitation. Readings at $OD_{600\ nm}$ were taken in a plate reader to quantify amounts of growth. Values were normalised against a negative control containing media only and relative growth determined as a percentage of growth of a positive control without compound treatment. The minimum inhibitory concentration (MIC) was determined as the lowest concentration that prevented >90% growth.

2.6 Minimum Bactericidal Concentration

A 15 mL Falcon tube with 6 mL of LB broth inoculated with 50 µL of bacteria from an overnight culture was incubated with shaking at 30-37°C until early log phase, $OD_{600\ nm}$ 0.2. Samples (1 mL) were transferred to a 24-well plate and incubated with Compound **2** at concentrations of

0. 0.1, 0.25, 0.5 and 1 µM for Gram-positive bacteria and 0, 2, 4, 8 and 16 µM for Gram-negative species for 30 min at 30°C. Serial dilutions (10-fold) were performed, 20 µL sample in 180 µL LB, in a 96-well plate. Samples in the 24-well plate were irradiated, incubated for 15 min at room temperature and 30 µL samples removed and serial 10-fold dilutions made as before. Samples (10 µL) were applied to an LB agar plate in triplicate and incubated for 16-20 h. Colonies at appropriate dilutions were enumerated and viability determined in CFU per ml. Minimum Bactericidal Concentration was detrmined as the lowest concentration which yielded a CFU/mL of $<10^3$ relative to the untreated control.

2.7 Bacterial viability assay

A semi-micro cuvette (Sarstedt) containing 2 mL of LB broth was inoculated with 50 µL of bacteria from an overnight culture and incubated with shaking at 30-37°C until early log phase, $OD_{600\ nm}$ 0.2. Samples of 1 mL were transferred to a 24-well plate and incubated with Compound **2** at 2 µM for 30 min at 30°C. Serial dilutions (10-fold) were performed, 30 µL sample in 270 µL LB, in a 96-well plate. Samples in the 24-well plate were irradiated in the PhotoReact 365 lightbox, incubated for 15 min at room temperature, 30 µL removed and serial 10-fold dilutions performed as before. Samples (10 µL) were applied to an LB agar plate in triplicate and incubated for 16–20 h. Colonies at appropriate dilutions were enumerated and viability determined in colony forming units (CFU) per mL.

2.8 Propidium iodide assay for loss of membrane integrity

Bacteria were cultivated as in viability assays ($OD_{600\ nm}$ 0.2) and 500 µL of the culture transferred to a 1.5 mL microcentrifuge tube containing Compound **2** to give a final concentration of 2 µM. Controls containing 500 µL of the culture and 0.2% DMSO were set up in parallel. Samples were incubated at 30°C for 30 min and cells pelleted by centrifugation at 17,000 g for 4 min. Cell pellets were resuspended in 200 µL 1× PBS containing 7.5 µM propidium iodide (PI; ThermoFisher). Samples (3 × 50 µL) were applied to a 96-well plate, transferred to a Biotek Synergy HT and fluorescence measurements made every 2 min for 20 min with excitation at 485 nm and emission at 645 nm. PBS (50 µL) was then added to sample wells and 50 µL 100% ethanol added to additional samples as a positive control for loss of membrane integrity and cell killing. The plate was placed in the PhotoReact 365 lightbox, irradiated for 5 min, returned immediately to the plate reader and fluorescence monitored every 2 min for 1 h.

2.9 Confocal microscopy

For confocal microscopy, cell pellets were prepared as in the propidium iodide assays with 500 µL of the culture transferred to a 1.5 mL microcentrifuge tube containing Compound **2** to give a final concentration of 2 µM unless specified otherwise. Samples were incubated at 30°C for 30 min and cells pelleted by centrifugation at 17,000 *g* for 4 min, then resuspended in 200 µL of Baclight solution containing 10 µM SYTO9 and 60 µM PI. A 10 µL sample was applied to a 1 cm x 1 cm 1% agarose (Bioline) pad on a microscope slide with a cover slip placed on top. The slide was imaged using a 63× lens on a confocal microscope (Zeiss 800 Airyscan) with Compound **2** being imaged with the Airyscan function using a 405 nm laser and an emission filter of 450-550 nm, SYTO 9 using a 488 nm laser and 550-580 nm filter, PI using a 488 nm

laser and an emission filter of 600-650 nm, Nile Red using a 488 nm laser and an emission filter of 550-620 nm and mCherry using a 560 nm laser and an emission of 600-650 nm. Samples were irradiated using the 405 nm laser at 30% power for 1 min (total energy: 90 mJ/cm^2) on the microscope.

2.10 Confocal microscopy in a low less stress environment

A 50 mL Falcon containing 5 ml LB broth inoculated with 50 µL *B. subtilis* (ATCC 23857 or KS88) was grown to mid-log phase ($OD_{600\,nm}$ 0.4). A culture sample (100 µl) was transferred to a 1.5 ml microcentrifuge tube and Nile Red added to a final concentration of 3.3 µM if required. Cells were then incubated for 20 min before Compound **2** was added and cells incubated again under the same conditions for 20 min. A 10 µL sample was applied to a 1 cm x 1 cm 1% agarose (Bioline) pad on a microscope slide with a cover slip placed on top immediately before imaging using the confocal microscopy settings described above.

2.11 Scanning Electron Microscopy

Bacteria were cultured as in viability assays, transferred to microcentrifuge tubes containing compound **2** to give a final concentration of 1 µM and incubated at 37˚C for 30 min with agitation. Samples were transferred to 12-well plates, irradiated and returned to 37˚C with agitation before transfer to a fresh microcentrifuge tube at 20, 40 and 60 min timepoints after irradiation. Controls were set up in parallel contained 1 µM compound **2** incubated for 60 min in the absence of irradiation and 0.1% DMSO irradiated and incubated for 60 min. Cells were pelleted by centrifugation at 13,000 *g* for 5 min, washed with 1x PBS and resuspended in 50

µl 2% glutaraldehyde followed by incubation at room temperature for 1 h. Cells were once again pelleted by centrifugation, resuspended in 30 µL sterile milliQ (MQ) water, with 1 µL spotted onto a silicon chip submerged in sterile water. Each chip was submerged in 1% osmium tetroxide (Sigma) for 10 min prior to ethanol treatment, with each chip submerged for 2 min as specified:

Step 1, Sterile MQ water

Step 2, Sterile MQ water

Step 3, 50% ethanol

Step 4, 95% ethanol

Step 5, 100% ethanol

Once submerged in 100% ethanol each chip was critical point dried (Bal-Tec CPD 030), coated in chromium (Cressington coater series 328) before imaging on a Hitachi S-500 Scanning Electron Microscope, with images taken at magnifications of 60,000x and 200,000x imaging was carried out by Dr Chieko Itakura, Electron Microscopy facility, Durham University.

2.12 Experimental evolution approach

Five groups were selected for treatment with sublethal concentrations of compound **2** and appropriate controls (Table 3) and each group was repeated in triplicate to give 15 samples. A single colony of *S. aureus* was used to inoculate 5 mL of LB in a 15mL Falcon tube and incubated for 16 h at 37˚C with 150 RPM shaking. The $OD_{600\,nm}$ was measured and each sample diluted to an $OD_{600\,nm}$ of 0.5 in a microcentrifuge tube, with appropriate treatment added to give a final volume of 1 mL and incubated with agitation. Appropriate samples were irradiated

for 5 min at 13 mW/cm^2 using a PhotoReact 365 Lightbox. Serial (10-fold) dilutions using 10 µL of culture were performed and 10 µL volumes applied to an LB agar plate and incubated at 37˚C for 16 h and CFU/ml determined. A 50 µL sample from each culture was used to inoculate 5 mL of fresh LB to create the next overnight culture and the cycle was repeated 15 times. On days 3, 6, 9, 12 and 15 all samples were treated with 2 µM Compound **2** and exposed to light with CFU/ml determined as described. On these days, MICs for ampicillin and H_2O_2 treatment groups (3 and 4) were also determined. A single, isolated colony from each sample was taken from the daily treatment plate on days 3, 6, 9, 12 and 15 and added to a 1.5 mL microcentrifuge tube containing 500 µL LB broth and 500 µL 80% glycerol (Fisher) for longer-term storage at -80˚C.

Group	Daily treatment
1	0.1 µM activated Compound **2**
2	365 nm light only
3	0.25 µg/ml Ampicillin
4	0.01% H_2O_2
5	no treatment

Table 3. Sub lethal daily treatment groups used to assess the evolution of tolerance and resistance over 15 treatment cycles

2.13 Whole Genome sequencing

Whole genome sequencing was performed by GenomicsNG following standard commercial protocols and an Illumina HiSeq platform with 60x coverage. Bioinformatic analysis was carried out by Dr Wenbin Wei, Bioinformatics facility, Durham University. *S. aureus* genome sequences (chromosome AP014942.1 and plasmid AP014943.1) and annotation were downloaded from GenBank. Read quality was analysed using fastqc

(https://www.bioinformatics.babraham.ac.uk/projects/fastqc/) and multiqc (https://multiqc.info/). Adaptors and low-quality sequences were trimmed using fastp (https://academic.oup.com/bioinformatics/article/34/17/i884/5093234). Reads were aligned to the genome sequence using bwa-mem2 (https://github.com/bwa-mem2/bwa-mem2). Alignment statistics were generated using samtools (http://www.htslib.org/doc/samtools.html) and combined using multiqc. Duplicated reads were removed using sambamba (https://academic.oup.com/bioinformatics/article/31/12/2032/214758). The resulting bam files and metrics files were analysed using samtools and multiqc to collect read statistics. Coverage statistics were generated using mosdepth (https://github.com/brentp/mosdepth). Variants (SNPs, indels, structural variants) that exist in a sample of interest but not in the wild type control were identified using strelka2 (https://github.com/Illumina/strelka) and manta (https://pubmed.ncbi.nlm.nih.gov/26647377/). Variants that passed filters were selected using GATK tool SelectVariants. Impact and effect of variants were predicted using software snpEff (http://pcingola.github.io/SnpEff/). Variant information in the vcf files were extracted using software SnpSift (http://pcingola.github.io/SnpEff/ss_introduction/). Variants with allele frequency <0.2 were removed. Variants were visually checked using Integrative Genomics Viewer (IGV, https://software.broadinstitute.org/software/igv/).

2.14 Proteomics

LB broth (48 mL) was added to 250 mL conical flasks, sealed with a foam bung and foil top and sterilised by autoclaving at 121°C for 15 min. 2 mL of a *S. aureus* (FDA209P) overnight culture was added to each flask and incubated at 37°C with shaking at 150 rpm until cells reached mid-log phase ($A_{600\ nm}$ of 0.4). Compound **2** was added to give a final concentration of 1 μM, a concentration that reduces cell viability by 10^3 following photoactivation. Each sample was incubated for a further 15 min before transfer to a square petri dish (Sarstedt) then irradiated at 13 mW/cm^2 for 5 min in the PhotoReact 365 lightbox. Samples were transferred to 50 mL Falcon tubes and incubated at 37˚C with 150 rpm shaking for 30 min. Cells were pelleted by centrifugation at 2,000 g for 15 min. The supernatant was discarded, and cell pellets were centrifuged at 2,000 g for a further 7 min. Cell pellets from quadruplicate biological analyses were analysed by Dr Adrian Brown at the Proteomics Facility, Durham University, including further processing and addition of isobaric tags for relative and absolute quantitation (iTRAQ) analysis.

Cell pellets were suspended in 20 μL 20% SDS and frozen at -20°C for 10 min. Samples were thawed at room temperature before vigourous vortexing and return to -20°C. This process was repeated for three freeze-thaw cycles. Urea (180 μL of 8M) was added and samples sonicated for 5 min in a water bath sonicator (Sigma-Aldrich). Following further vigorous vortexing for 30 sec, samples were sonicated for a further 5 min and then pelleted by centrifugation at 18,000 x *g* for 10 min. The supernatant was transferred to a fresh tube and total soluble protein content determined by the Pierce BCA assay.

Aliquots of 30 μg protein from each sample were precipitated and processed for labelling using an iTRAQ Reagent-Multiplex Buffer Kit (Sigma-Aldrich, 4352135) following the manufacturer's instructions, and 50% of each sample was loaded on a protein gel to check equivalence of precipitation and resuspension. Protein samples were digested with trypsin

overnight at 37°C and subsequently labelled using an 8-plex iTRAQ reagent kit, according to the manufacturer's instructions. The 4-replicate untreated control samples were labelled with iTRAQ tags 113, 114, 115 and 116, while Compound **2**-treated samples were labelled with tags 117, 118, 119 and 121. After labelling, all samples were pooled and subsequently cleaned-up using hydrophobic interaction chromatography (HILIC) solid phase extraction (SPE) to remove unincorporated label and buffer salts. The HILIC eluate was freeze-dried and re-suspended in 0.1% formic acid for liquid chromatography-mass spectrometry (LC-MS). LC-MS/MS and mass spectrometric analyses were conducted on peptides originating from 5 µg of sample. LC-MS/MS was conducted using a Triple TOF 6600 Q-TOF mass spectrometer (AB Sciex) linked to an Eksigent 425 LC system via a Sciex Duospray source (AB Sciex). The acquisition of mass spectrometer data was carried out using the AB Sciex Analyst TF 1.8.1 instrument control and data processing software.

Protein identification and relative quantification was conducted by processing raw .wiff data files against the UniProt protein sequences of the specific bacterial proteome of interest and known proteomic experiment contaminants (keratins, trypsin etc.) using the AB Sciex ProteinPilot 5.02 software. Raw protein identification data were exported from ProteinPilot to Microsoft® Excel for manual data-handling and filtering. All duplicate proteins were manually removed from the dataset and for each iTRAQ experiment, the relative quantification of the CHA-responsive proteins was generated as a ratio of each protein relative to the 113-tagged DMSO control sample. An average ratio of each protein was calculated across all four biological replicate samples, and a Student's t-test at $p \leq 0.05$ was used to compute the statistical significance in the ratios.

Proteins with fold changes >1.20 or <0.83 and with $p \leq 0.05$ were classified as differentially expressed proteins (DEPs). These proteins were mapped to gene ontology (GO) terms using

the GO Consortium (https://geneontology.org) powered by PANTHER (Ashburner et al., 2000; Thomas et al., 2022; Aleksander et al., 2023). DEPs were compared to a reference list of the relevant organism's entire genome and a Fisher's Exact test used to determine which GO terms were significantly enriched ($p < 0.05$) in each of the three GO components: Biological Process, Cellular Component and Molecular Function.

Chapter 3. Determining efficacy of LightOx compounds in representative Gram-positive and Gram-negative organisms

3.1 Aims

Antimicrobial photodynamic therapy uses a PS as a bactericidal agent to reduce infections. This approach using methylene blue was shown to eliminate resistant bacterial infections colonising wound surfaces (149). LightOx has developed a range of potent PS designed to eradicate dysplastic oral mucosal cells. Early work has shown some of these compounds were also able to enter the bacteria *S. epidermidis* and *B. subtilis* and plate reader growth assays appeared to show growth arrest upon light activation (150). Therefore, it was hypothesised that LightOx compounds could prove to be a potent antimicrobial agent against a range of species, including clinically relevant bacteria.

In this chapter, I screened a library of LightOx compounds for their bacteriostatic effect upon photoactivation in *B. subtilis*. 26 compounds were tested and the six compounds most effective at inhibiting growth of *B. subtilis* when exposed to 365nm light were further assessed for their bacteriostatic and bactericidal effects. From this initial selection, compounds were screened subsequently for those with light-specific cytotoxicity at concentrations < 8μM and showed minimal impacts without light-irradiation.

Once the 26 compounds had been narrowed down to 6 candidates, candidates were tested further for bacteriostatic and bactericidal effects in four representative species, the Gram–positive bacteria *S. epidermidis* and *B. subtilis*, and the Gram–negative bacteria *P. fluorescens* and *E. coli*. Some candidates were further tested for efficacy against the clinically relevant ESKAPE pathogen group, *E. faecalis*, *P. aeruginosa* and *S. aureus*.

Finally, I tested if *S. aureus* was able to develop tolerance to the most promising LightOx compound through repeated cycles sub-lethal drug exposure. The workflow for this chapter is shown below:

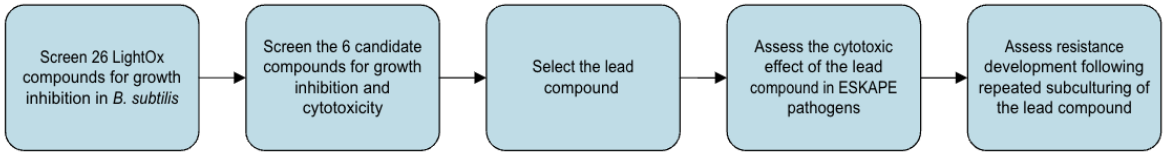

3.2 Results

3.2.1 Initial screening of the LightOx compound catalogue and determination of the six candidate compounds

I screened 26 LightOx compounds, each consisting of a diarylacetylene core backbone with different functional groups attached to the acceptor or donor ends , for their ability to inhibit growth of B*. subtilis* following activation with 365nm light using soft agar overlays. *B. subtilis* was chosen as it is a safe, easily cultivatable organism used as a model organism for decades. As well as having established gene knockouts for future work (151). This rapid screening method was employed to screen compounds in this Gram–positive bacteria as, in general, Gram–positive bacteria are more susceptible to antibiotics and thus more likely to allow for penetration of novel compounds, Susceptibility of bacteria to light-activated compounds was determined by examination of growth suppression as detected by the presence of dark circles on the agar assays (figure 3).

Dilutions of each compound were prepared at concentrations ranging from 1 µM to 5 µM in DMSO, based on previous mammalian cell-based assays indicating that LightOx compounds

elicited a cytotoxic effect in human cells in this range (140). Compounds were applied to the surface of a soft agar overlay inoculated with *B. subtilis* and activated by exposure to light at 365 nm, followed by incubation for 24h. The volumes of agar and inoculation volume were kept consistent to ensure uniform cell density across overlays. The overlays were imaged using a Gel-doc and compound mediated zones of inhibition identified. The six compounds that showed the most significant inhibition of growth were selected for further testing. This number was chosen because six is the maximum amount that can be spotted on a square plate without the risk of mixing.

Of the twenty six compounds screened, six candidate compounds, 1,3,5,6,11 and 17 were identified that showed the most growth inhibition in *B. subtilis* at 5 µM upon activation (figure 3) The properties and chemical structures of the 6 candidate compounds are shown in figure 4.

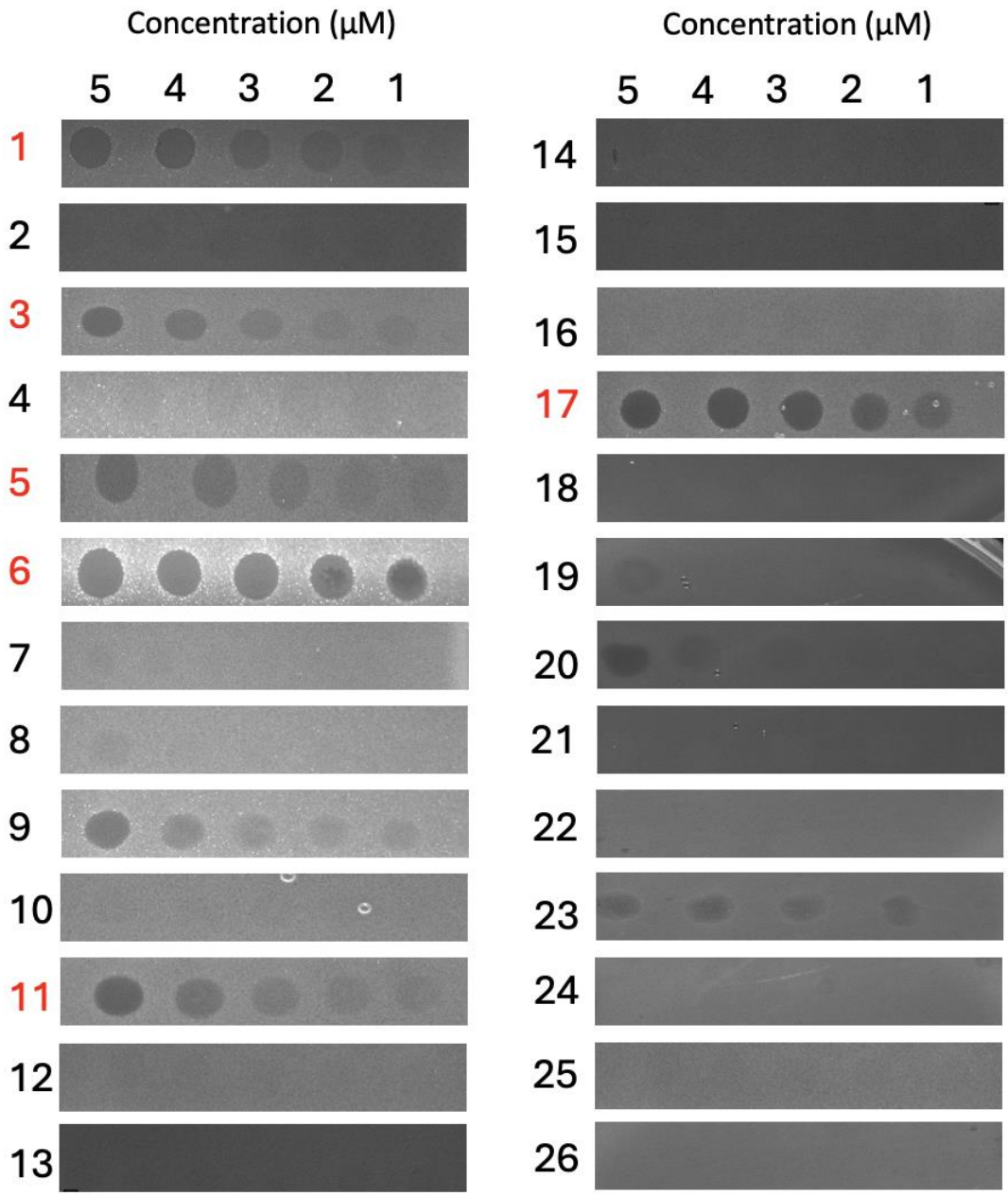

Figure 3. Initial screening of the 26 LightOx compounds. Compound concentrations of 1 µM to 5 µM were applied in 6 µl volumes to the surface of a soft agar overlay inoculated with *B. subtilis*, and exposed to 365 nm light for 5 min. The LB agar plates were incubated for 24 hours at 37°C prior to imaging. The six compounds taken forward as the candidates are highlighted in red

A

Compound	MW (g/mol)	Peak Excitation (nm)	Peak Emission (nm)	LogP
1	388.51	362	477	5.26
2	394.53	380	530	5.31
3	334.42	368	530	3.95
4	729.69	368	530	9.11
5	383.49	378	531	6.04
6	397.52	393	526	6.69

B

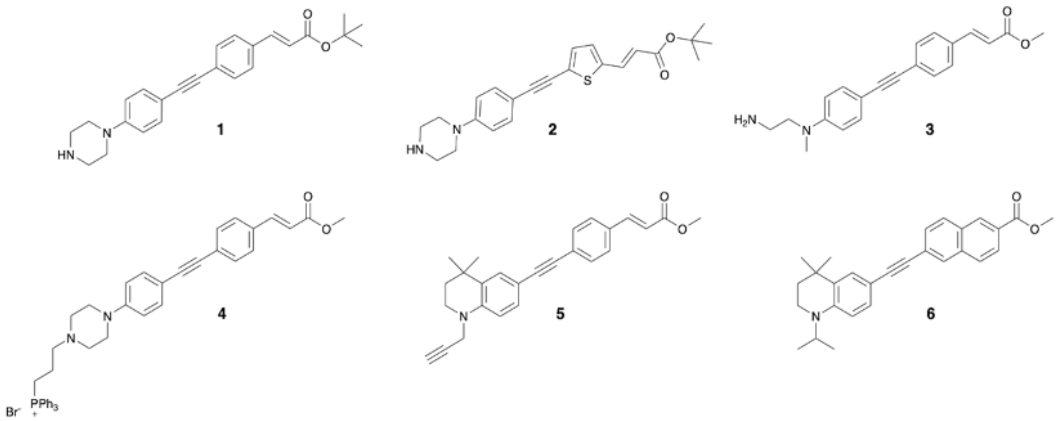

Figure 4. (**A)** Molecular weight, peak excitation/emission wavelength in toluene and calculated hydrophobicity of the candidate LightOx photosensitising compounds. (**B)** structure of the six candidate LightOx compounds.

The concentration range of each candidate compound was reduced to a range of 0.01 µM to 1 µM to evaluate growth inhibition across four representative species, two Gram-positive (*B. subtilis and S. epidermidis*) and two Gram-negative (*E. coli* and *P. fluorescens*). Non-irradiated and DMSO-only controls were conducted in parallel (figure 6) and none of the tested compounds affected the growth of any of the four bacterial species under these conditions.

S. epidermidis and *P. fluorescens* were selected because they are safe and easy to culture in a hazard group 1 lab, where the work was conducted. They also serve as proxies for the more pathogenic species, *S. aureus* and *P. aeruginosa*, respectively. Activation of the six-candidate compound resulted in distinct zones of growth inhibition, particularly in the Gram-positive bacteria *B. subtilis* and *S. epidermidis* at a concentration of 1 µM (Figure 5). Compound **2** exhibited the highest efficacy, demonstrating growth inhibition at 0.1 µM in *B. subtilis* and *S. epidermidis* (figure 5). In contrast, the Gram-negative species *E. coli* and *P. fluorescens* showed less growth inhibition, with only Compound **2** demonstrating any effect (Figure 5). The size of each zone of inhibition remained consistent across the compounds, suggesting the compound itself does not diffuse across the soft agar and bacterial growth is only inhibited at the spot location (figure 5).

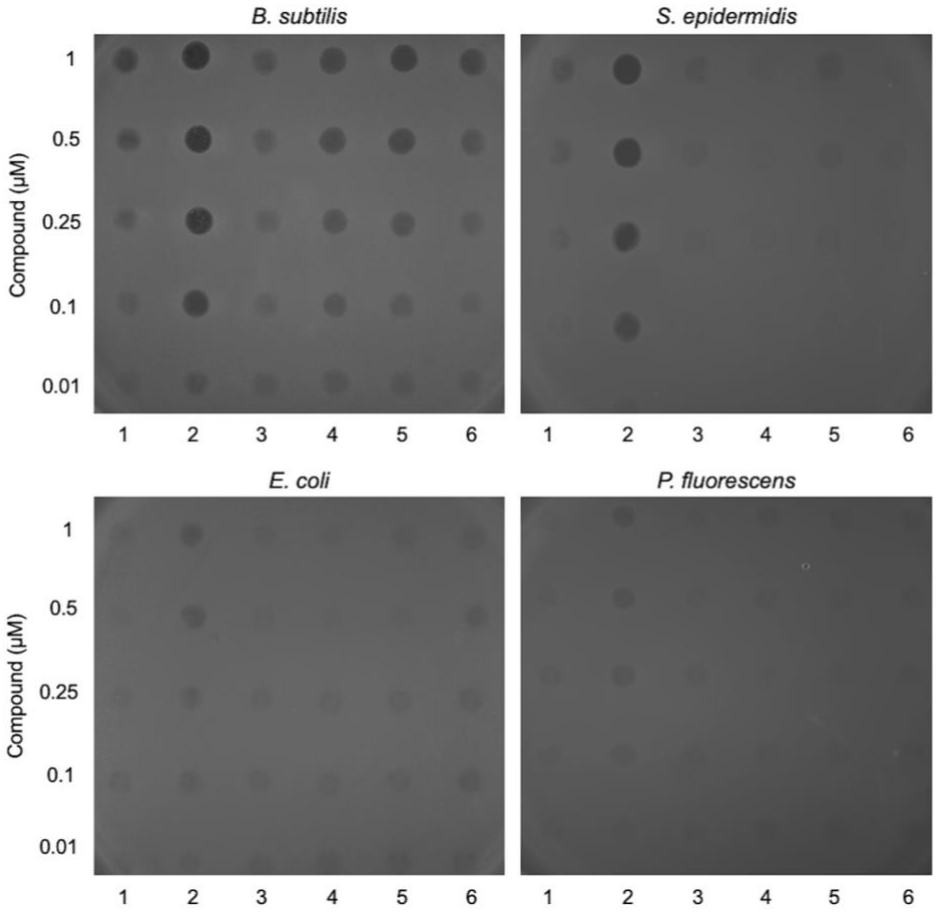

Figure 5. Screening lead compounds for antibacterial activity against Gram-positive and Gram-negative bacteria. Dilutions of six lead compounds (labelled 1-6) were applied in 6 µl volumes to the surface of a soft agar overlay inoculated with *B. subtilis*, *S. epidermidis*, *E. coli* or *P. fluorescens*. The agar plates were exposed to 365 nm light for 5 minutes and then incubated for 24 hours prior to imaging. Controls without light activation or with application of DMSO are shown in Figure 6.

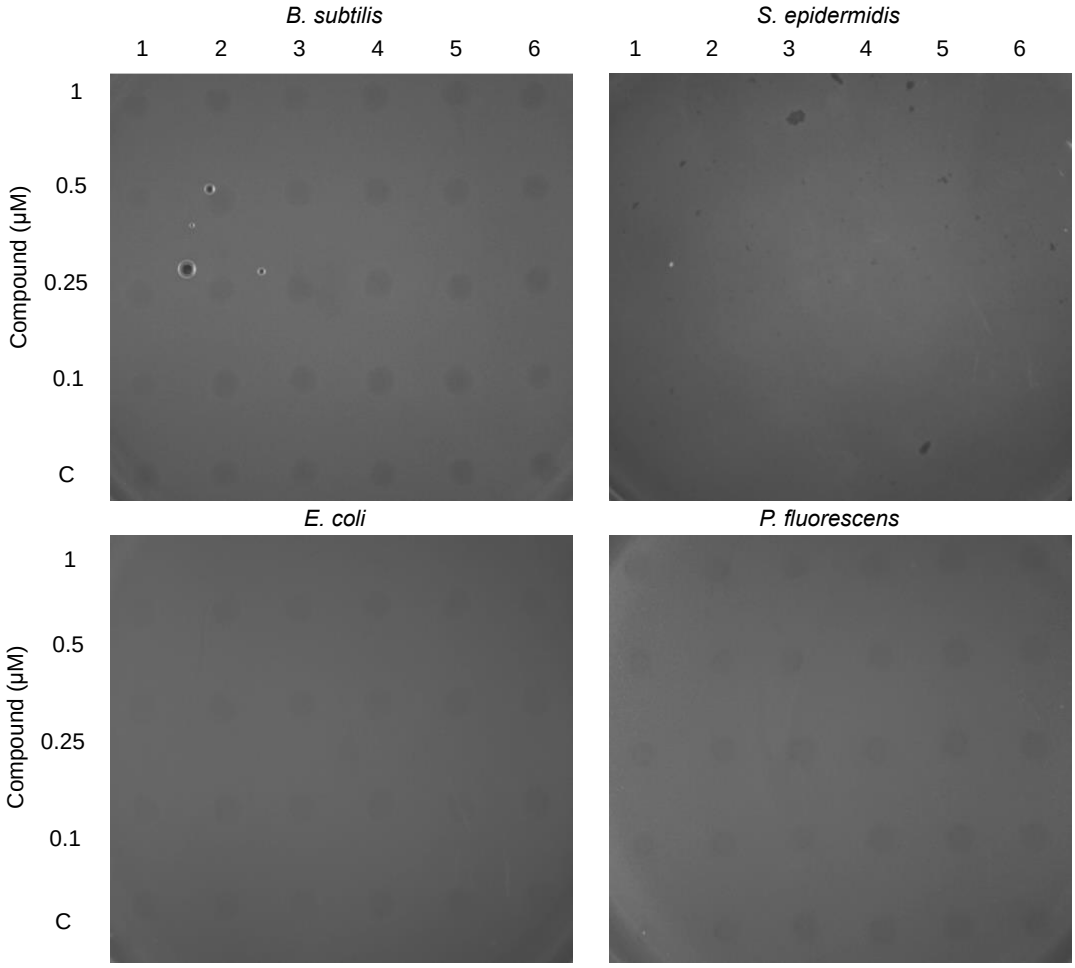

Figure 6. Controls for screening candidate compounds for antibacterial activity against Gram-positive and Gram-negative bacteria. Two-fold dilutions of six candidate compounds were applied in 6 µL volumes to the surface of a soft agar overlay inoculated with *B. subtilis, S. epidermidis, E. coli or P. fluorescence*. With a control of 0.1% DMSO spotted onto the bottom row. The LB agar plates were incubated for 24 hours at 37˚C prior to imaging. Minimal zones of inhibition were seen relative to the irradiated plates

3.2.2 Growth comparisons of the six candidate compounds in *S. epidermidis* liquid cultures

To investigate the effect of photoactivation on the candidate compounds in liquid culture, a growth curve was conducted using Luria-Bertani (LB) broth. The growth of *S. epidermidis* was monitored in response to treatment with 2 µM Compound, in line with exploratory experiments conducted by Candace Adams, which indicated that this concentration inhibits growth of this bacterium. *S. epidermidis* was incubated with compound for 30 min in LB broth then transferred to a 96 well plate, with half of the plate irradiated and the other half covered with black card to block the light. Optical density measurements were then taken over a 24-hour period in samples irradiated with 365 nm light and unirradiated controls (figure 5A).

In the absence of irradiation, Compounds **3** and **5** exhibited growth rates similar to the DMSO control for the first 5 hours before showing reduced growth rates (figure 7A). Compounds **1**,**2**,**4** and **6** experienced a longer lag phase before logarithmic growth resumed after 6 to 8 hours (figure 7A). Compound **2** demonstrated the most significant growth inhibition under these conditions (figure 7A,D).

Upon photoactivation, Compound **5** mirrored the growth rate of the DMSO control, indicating that 365 nm light activation of this compound had no effect on growth rate at this concentration (figure 7B). Compound **3** displayed a 4-hour lag before aligning its growth rate with the control (figure 7B). Compounds **4** and **6** exhibited a lag period of 10 and 14 hours respectively, before starting logarithmic growth (figure 5B). When activated at 2 µM, Compounds **1** and **2** inhibited growth for 20 hours. *S. epidermidis* treated with Compound **1** resumed growth after this period (figure 7B,C), in contrast Compound **2** completely arrested

growth for up to 24 hours following photoactivation (figure 7B,C). These results were consistent with the overlay assays, confirming that Compound **2** was the most effective at inhibiting growth in *S. epidermidis*, both upon photoactivation and in the absence of light.

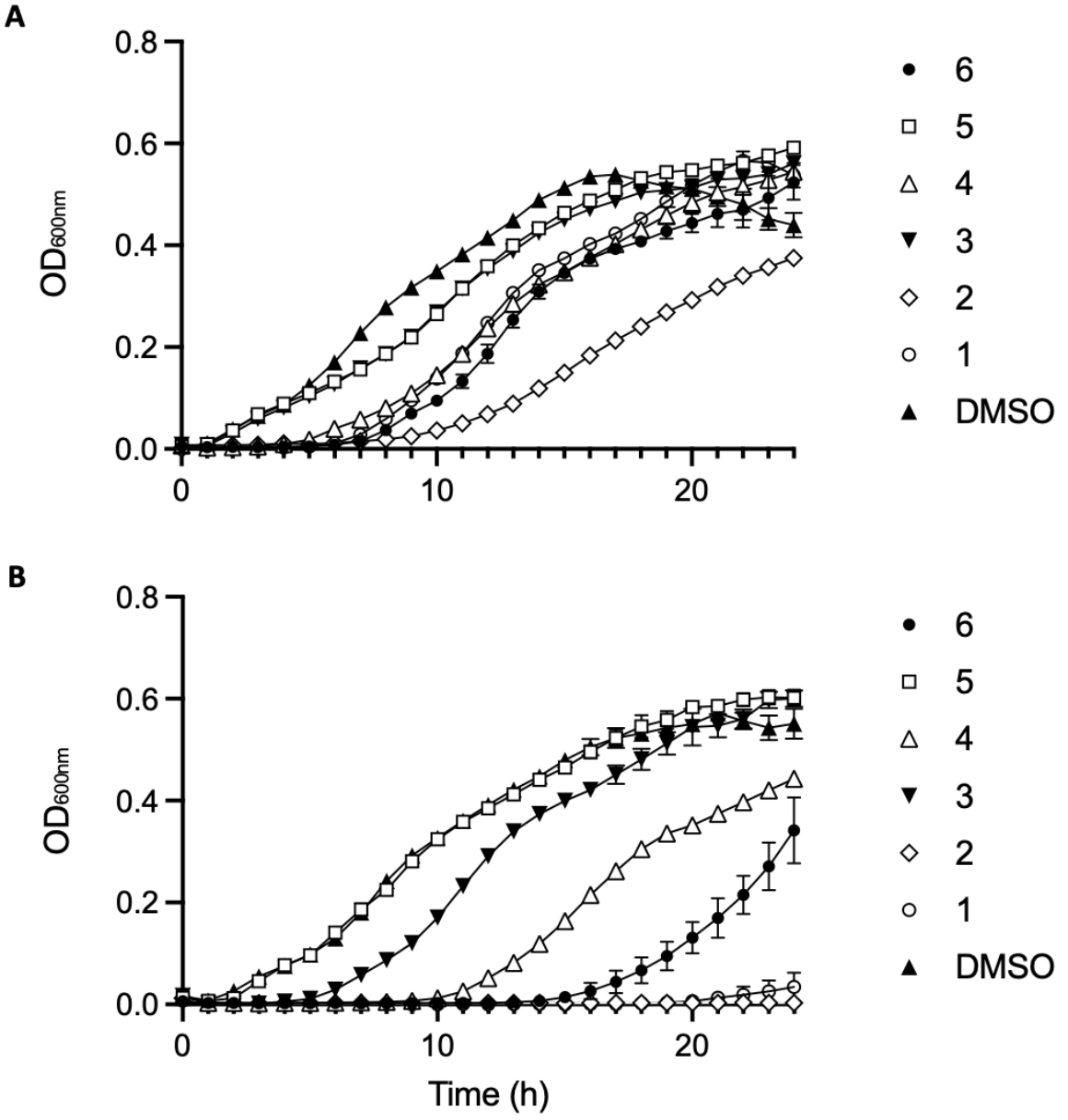
A
0.8
0.6
0.4
0.2
0.0
OD600nm
0
10
20
6
5
4
3
2
1
DMSO
B
0.8
0.6
0.4
0.2
0.0
OD600nm
0
10
20
Time (h)
6
5
4
3
2
1
DMSO

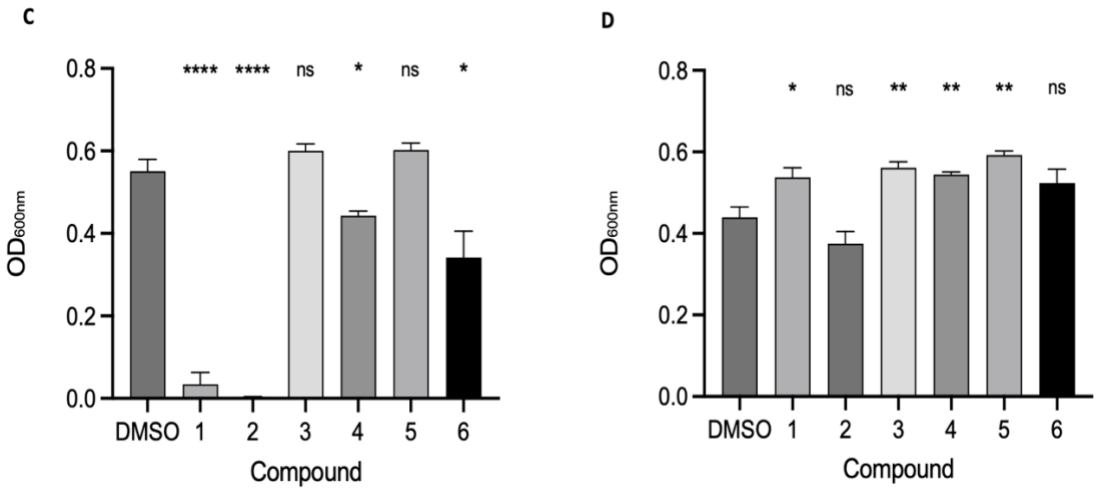
C
0.8
0.6
0.4
0.2
0.0
OD600nm
**** **** ns * ns *
DMSO 1 2 3 4 5 6
Compound
D
0.8
0.6
0.4
0.2
0.0
OD600nm
* ns ** ** ** ns
DMSO 1 2 3 4 5 6
Compound

Figure 7. Effect of the six candidate compounds on bacterial growth in liquid culture. The six candidate compounds were added to *S. epidermidis* in LB broth in a 96 well plate to give a final concentration of 2 µM and cultivated in LB broth at 37 °C in 96-well plates in a plate reader with intermittent shaking. Growth was monitored at OD_{600nm} in samples without light treatment (**A**) and samples exposed to light at 365 nm for 5 minutes (**B**). OD600nm values were plotted after 24 hours and unpaired t tests perfomed to determine significance of each compound compared to the DMSO control in samples with Light treatment (**C**) and without light treatment (**D**).

3.2.3 Effect of the candidate compounds on *S. epidermidis* membrane integrity

I used a propidium iodide (PI) assay to assess membrane integrity in cells exposed to the candidate Compounds. PI is a membrane-impermeable dye that fluoresces only in the presence of chromosomal DNA when it penetrates the cell envelope and thus serves as a reporter for severe membrane damage and, with some caveats, of cell death (152). This assay allows for a rapid assessment of compound effects on cell viability in both the absence and presence of irradiation. *S. epidermidis* was incubated in the presence of 2 µM of each candidate compound and then exposed to 365 nm light after 20 min. PI fluorescence was monitored throughout the experiment from 0 to 80 min (figure 8).

Cells treated with Compound **1** displayed the highest level of PI fluorescence before photoactivation, suggesting dark toxicity in this compound at this concentration. This was in

contrast with the growth assays where Compound **2** displayed the most growth inhibition in the absence of light (figure 7A,D) Following activation, a modest increase in PI fluorescence was observed, indicating a bactericidal effect at 2 μM (figure 8).

A significant increase in PI fluorescence was observed following activation of Compound **2**, consistent with a rapid loss of membrane integrity and therefore cell viability. This suggests that Compound **2** exerts a potent bactericidal effect following activation. The other 4 compounds (**3**,**4**,**5** and **6**) showed a small increase in fluorescence after activation, which then dropped back down, with the exception of compound 5 this was significant relative to the DMSO control, indicating some cell death following activation of compounds **3**,**4** and **6**

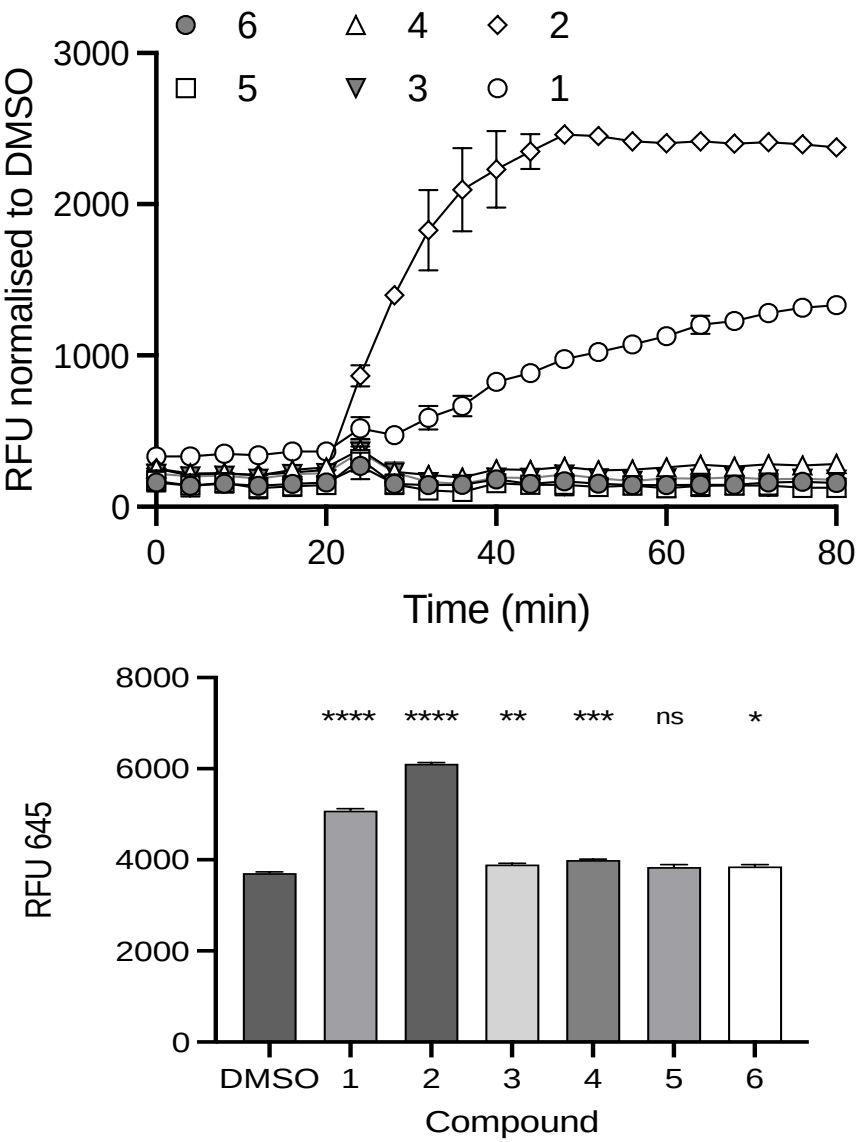

Figure 8. Cytotoxic effect of the 6 lead compounds. Bacteria were grown to mid-log phase in the presence of 2 µM compound. (**A**) The relative fluorescence units (RFU x 10^3) at an emission of 645 nm were normalised against controls containing appropriate control concentrations of DMSO. All samples were exposed to light at 365 nm after 20 min and incubation continued for another 60 minutes.(**B)** RFU 645 of all samples after 80 min, with significance displayed from an unpaired t – test of each sample compared to the DMSO control.

3.2.4 Structure and photophysical properties of the lead compound, Compound 2

Compound **2** was identified as the most effective candidate, exhibiting the highest bacteriostatic and bactericidal effects upon activation with 365 nm light (Figures 7 and 8). While growth reduction was observed in the absence of light (Figure 7A), Compound **2** exhibited lower PI fluorescence, suggesting a bactericidal effect, than Compound **1**. In contrast Compound **1**, which showed the second-highest bactericidal effect following photoactivation, exhibited a higher PI fluorescence prior to photoactivation. (figure 8) Consequently, Compound **2** was selected for further assessment.

Compound **2** exhibits similar solvatochromatic absorption (figure 9B) and emission (figure 9C) behaviour in toluene, chloroform and ethanol as other donor-acceptor structures (140, 142) In nonpolar solvents, high intensity, shorter wavelength fluorescence emission (toluene, λmax = 491 nm, Φ = 0.8 and chloroform λmax = 531 nm, Φ = 0.50) was observed, while much weaker emission with a significant bathochromic shift in the considerably more polar solvent, DMSO (λmax = 588 nm, Φ = 0.001) was shown, presumably due to aggregation and self-quenching effects.

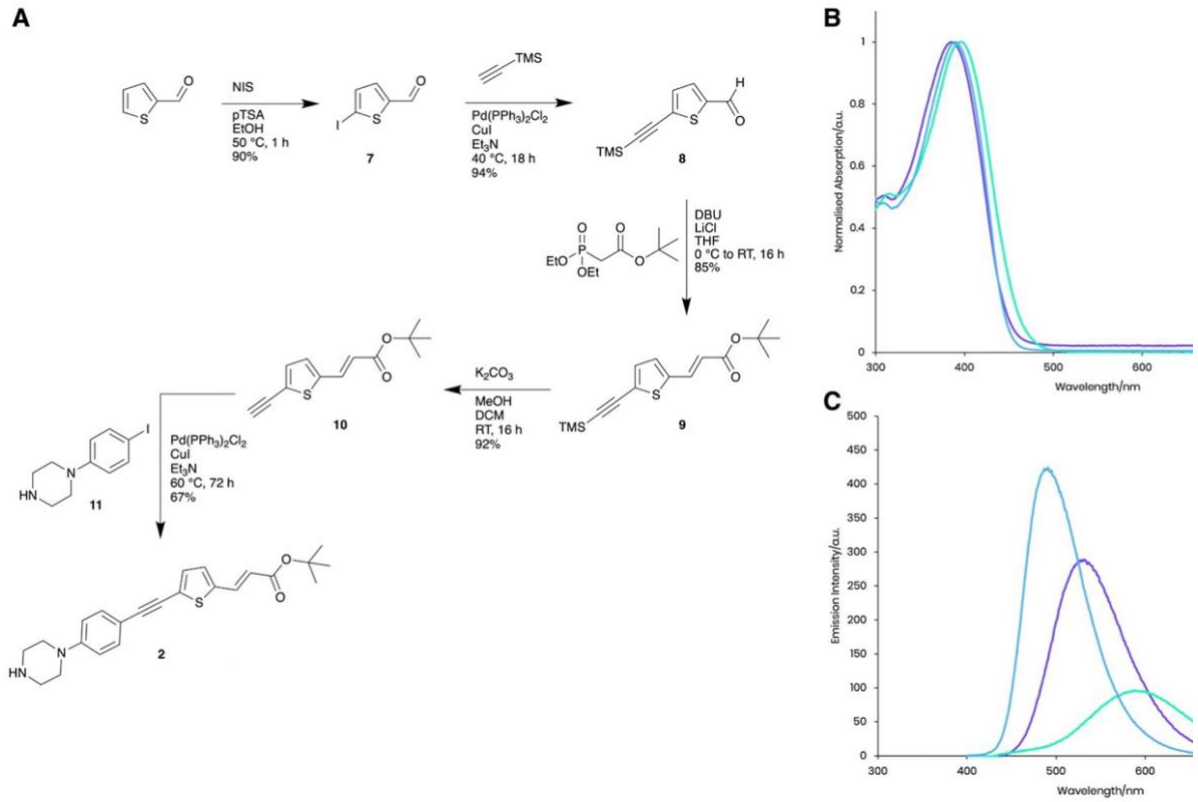

Figure 9. Photophysical properties of Compound **2**. **(A)** Synthesis and structure of Compound **2**. **(B)** Normalised absorption spectra of Compound **2** in chloroform (blue), DMSO (purple) and toluene (green). **(C)** Emission spectra of Compound **2** in chloroform (blue), DMSO (purple) and toluene (green) with excitation at the respective absorption peak maxima. (72)

3.2.5 Effect of Compound 2 on bacterial growth

Compound **2** was next examined for its ability to inhibit the growth of *E. coli*, *B. subtilis*, and *S. epidermidis* in liquid cultures. Unfortunately, *P. fluorescens*, as an obligate aerobe, was unable to grow under these conditions, potentially due to a combination of the low oxygen environment of the 96 well plate and the intermittent shaking in the plate reader. Bacterial growth in response to treatment with 2 µM Compound **2** was followed by optical density measurements over a 24-h period with half of the samples irradiated with 365nm light at the outset alongside unirradiated controls (Figure 10).

2 µM was selected as the concentration due to the difference in susceptibility displayed in liquid cultures and on agar, with bacterial lawns being shown to be more susceptible than the corresponding species in a liquid growth assay. Therefore, 2µM was selected as this was the lowest concentration of Compound **2** that would completely inhibit the growth of *S. epidermidis* in LB broth following photoactivation (Figure 10).

E. coli exposed to the light-activated Compound **2** experienced a substantial (10 h) lag in growth relative to an unirradiated control, although there was a resumption in growth beyond this time point (Figure 10A). Unirradiated *E. coli* grown in the presence of the compound did show a modest delay in growth but quickly recovered thereafter (Figure 10A). The two Gram-positive species, *B. subtilis* and *S. epidermidis,* showed much greater susceptibility to Compound **2** exposure (Figures 10B, C). In light-exposed samples, growth ceased immediately and did not resume over the 24-h monitoring period. Growth inhibition was also evident in unirradiated cultures exposed to Compound **2** and indicates some, albeit reduced, toxicity in the absence of light activation in these species at this treatment concentration. No

differences in growth were detected with appropriate vehicle in the presence or absence of light, demonstrating that the compound is solely responsible for bacterial growth inhibition in these species.

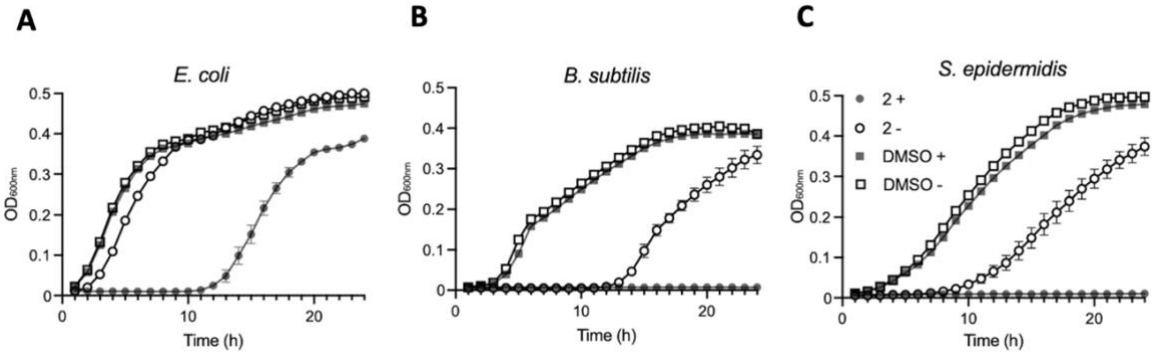

Figure 10. Effect of Compound **2** on bacterial growth. *E. coli*, *B. subtilis* and *S. epidermidis* were cultivated in LB broth at 37 °C in 96-well plates in a plate reader with continuous shaking. Growth was monitored at OD_{600nm} in samples exposed to light at 365 nm for 5 minutes (filled symbols) or without light treatment (open symbols). Samples contained 2 µM Compound **2** or 0.2% DMSO indicated by circles or squares, respectively.

3.2.6 Effect of Compound 2 on viability

The growth curves performed above showed complete growth inhibition for 24 hours in *B. subtilis* and *S. epidermidis* following photoactivation of Compound **2**, with a 12-hour lag period observed in E. coli. A PI assay was performed in four representative species (*E. coli*, *P. fluorescens*, *S. epidermidis* and *B. subtilis*) above to probe whether activation of Compound **2** leads to significant membrane damage and loss of viability in these species. The four species were grown to early log phase (OD_{600nm} 0.2) then incubated with Compound **2** at a treatment concentration of 2 µM, then centrifuged, resuspended in PI solution and exposed to 365 nm light after 20 minutes. PI fluorescence was monitored throughout the experiment from 0 to 80 minutes.

S. epidermidis and *B. subtilis* displayed an increased PI fluorescence relative to the DMSO control in the 20 minutes prior to irradiation. indicating a slight loss of membrane integrity, the fluorescence of *B. subtilis* gradually increases even without irradiation suggesting dark toxicity in this species at 2 µM. A significant increase in PI fluorescence was evident with both Gram-positive species following photoactivation (figure 11A).

E. coli and *P. fluorescens* treated with the 2 µM Compound **2** showed only a minor increase in PI fluorescence following photoactivation. Ethanol controls conducted in parallel confirmed that significant membrane damage in Gram-negative bacteria leads to PI uptake, as evidenced by a rapid increase in fluorescence (figure 11B). This indicates Compound **2** does not compromise the viability of *E. coli* and *P. fluorescens*.

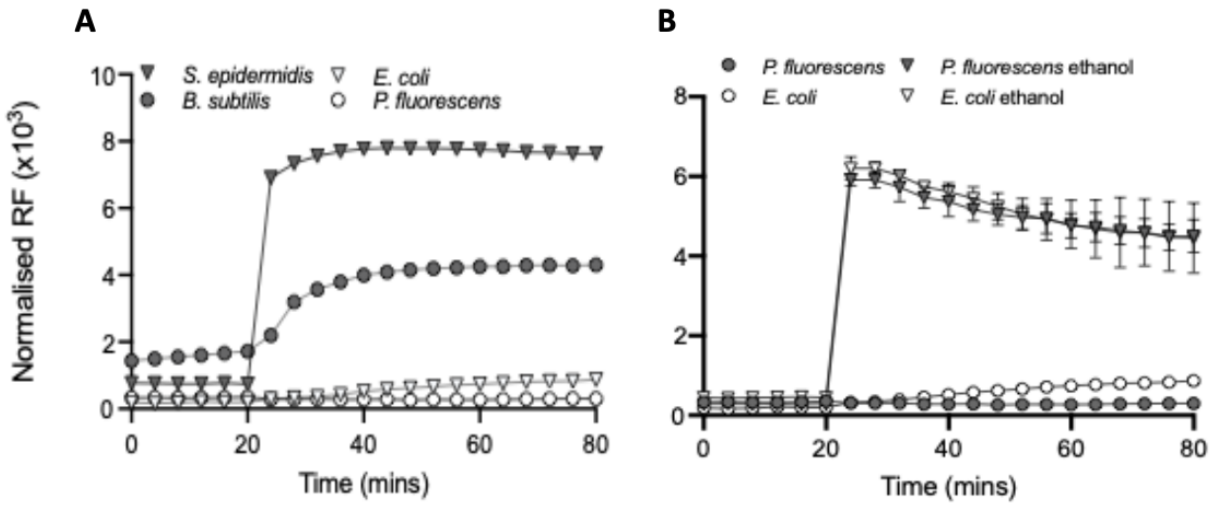

Figure 11. Effect of compound **2** on bacterial membrane integrity. Bacteria were grown to mid-log phase in the presence or absence of 2 µM compound **2** as described in the Material and Methods. (A) The relative fluorescence units (RFU x 10^3) at an emission of 645 nm were normalised against controls containing appropriate control concentrations of DMSO. samples were exposed to light at 365 nm after 20 min and incubation continued for another 60 minutes. (B) Positive controls for membrane damage and subsequent entry of PI conducted in parallel for *E. coli* and *P. fluorescens* using 50% ethanol.

The PI assays performed above offered a fast way to determine severe membrane damage in bacteria which can be used as a proxy for cell viability. However, there are problems with using PI as a direct measurement of cell viability, as severe membrane damage is not always indicative of cell death (152). Therefore, a colony forming unit (CFU) assay was performed to confirm the bactericidal properties of Compound **2** at 2 μM. The four representative bacterial species were grown to early-log phase prior to addition of 2 μM Compound **2** and exposure to 365 nm light. Controls without irradiation and equivalent concentrations of DMSO were conducted in parallel (figure 12). Serial ten-fold dilutions of the bacteria were applied to the surface of agar plates and CFU/ml calculated.

No reduction in viability of any of the bacterial species was observed in the controls, with or without light, or samples incubated with Compound **2** but without irradiation (figure 12). Similar results were obtained with the two Gram-negative species, *E. coli* and *P. fluorescens*, consistent with a tolerance towards the light-activated effect of the compound (figure 12). *S. epidermidis* and *B. subtilis*, in contrast, showed a dramatic reduction in viability after light exposure, with both displaying a 6-log reduction in survival following photoactivation compared to the non-irradiated controls (12).

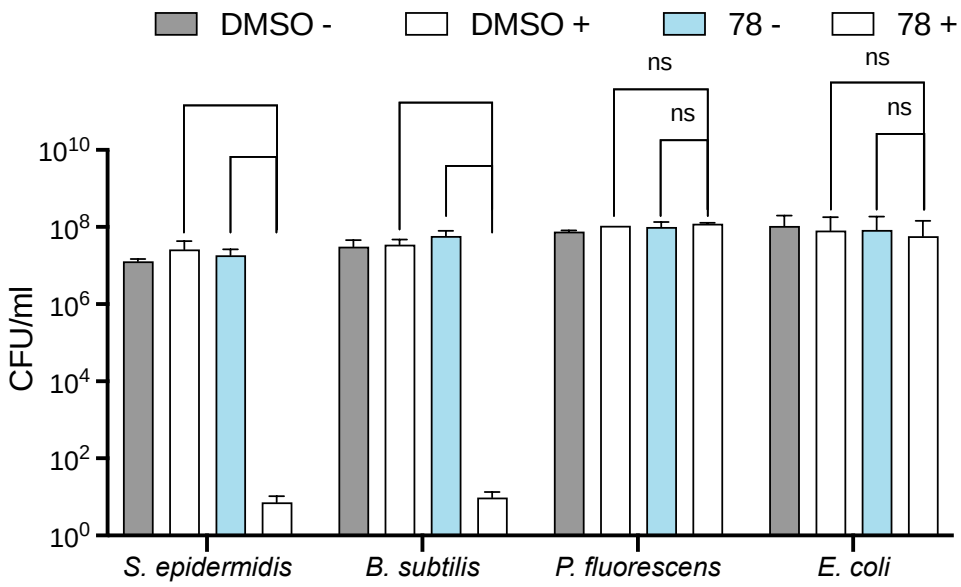

Figure 12. Effect of Compound **2** on bacterial viability. Bacteria at mid-log phase of growth (30µL) were transferred to a clear 24-well plate were mixed with 270µL LB broth. Serial (10-fold) dilutions were performed and 10µL of each dilution was applied to the surface of an LB agar plate in the presence of 2 µM Compound **2** or 0.2% DMSO. The 24 well plate was then activated by irradiation at 365 nm, and samples diluted and spotted again. Both irradiated and non-irradiated plates were incubated for 24h before enumeration of colonies to determine CFU/ml. Data are the mean and standard error of three independent experiments with an unpaired t-test to determine significance.

3.2.7 Effect of Compound 2 on growth inhibition at a range of concentrations

To determine the range of concentrations at which growth inhibition can be observed a Minimum Inhibitory Concentration (MIC) assay was performed. MIC assays are used to determine the effect of compounds on growth at a range of concentrations to calculate the minimum concentration in which growth is completely inhibited, defined as growth less than 10% of the untreated control. Bacterial cultures were grown in Muller Hinton (MH) broth to early log phase (OD_{600nm} 0.07) and added to microtitre plates containing serial dilutions (2-fold) of Compound **2**. Then incubated for 24 hours, with the OD_{600nm} plotted as a percentage of the untreated control.

S. epidermidis and *B. subtilis* showed complete growth inhibition at 8 µM (Figure 13A), a much higher concentration than the 2 µM required in previous liquid growth assays (figure 10A, B). This difference may be due to variations in media, or that The MIC plates were incubated in a constantly shaking environment, whereas the plate reader only shakes every 5 minutes. This difference in conditions means that bacteria in the MIC assay experienced a more favourable growth environment, potentially allowing them to recover more effectively following activation. In contrast, *P. fluorescens* and *E. coli* exhibited over 10% growth at 8 µM, indicating an MIC greater than the highest concentration tested (Figure 11A).

The relative growth of *S. epidermidis* with activated Compound **2** differed significantly 8 hours and 24 hours post-activation (figure 13B). Suggesting an initial cytotoxic effect following

photoactivation of compound in Gram–positive bacteria, with surviving cells able to resume logarithmic growth and repopulate the culture (figure 13B).

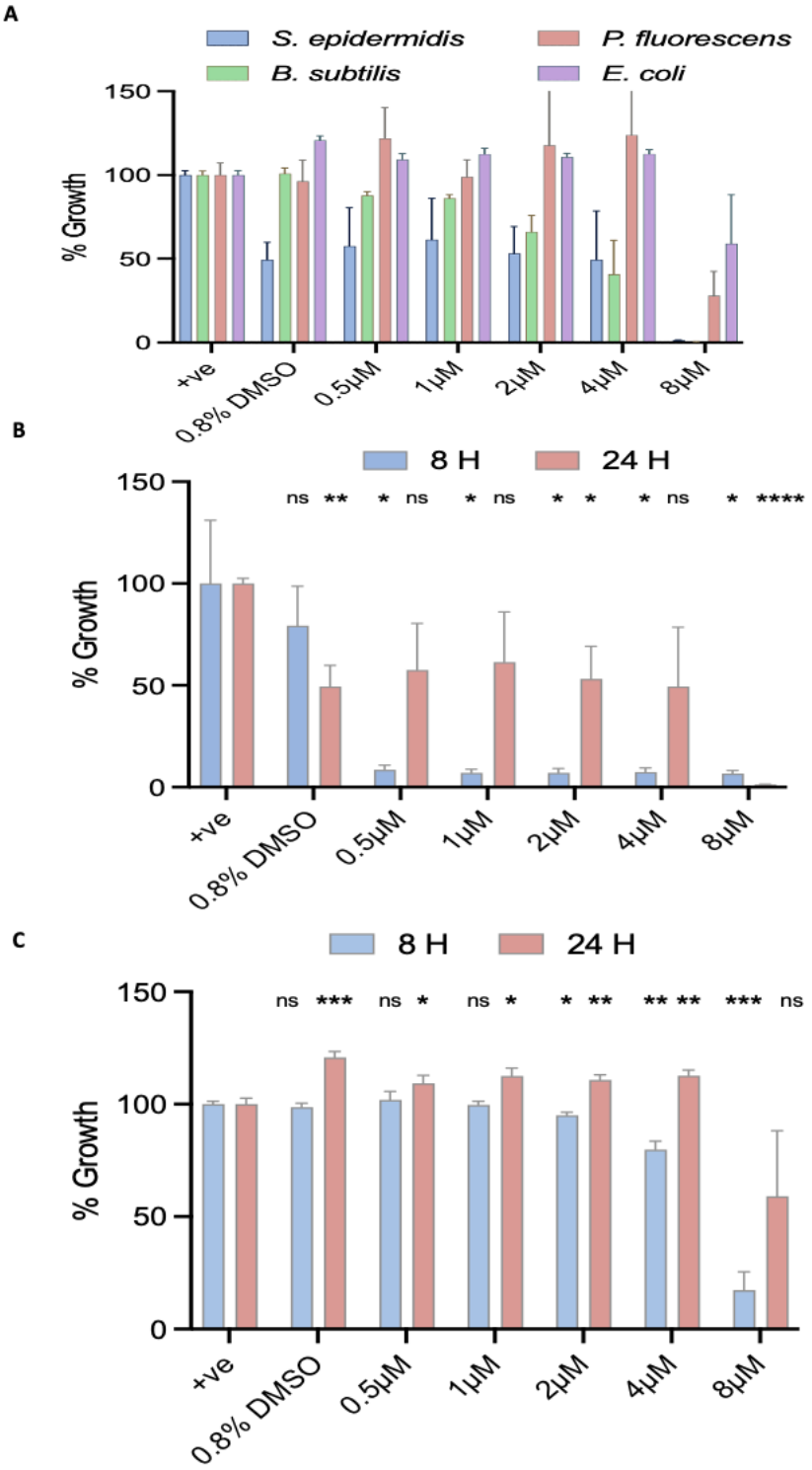

Figure 13. Effect of Compound **2** on bacterial growth at a range of concentrations. Bacteria were grown to an OD_{600nm} of 0.07 and then added to a 96 well plate with serial dilutions of Compound **2** as described in the Material and Methods. The plates were grown with constant agitation before the OD_{600nm} was read using a plate reader and normalised as a percentage to the positive control of bacteria only. Each bar shows the mean and standard error of 3 repeats. (**A**) Normalised growth in 4 representative species following incubation with Compound **2** at a range of concentrations 24 hours following photoactivation. (**B**) *S. epidermis* OD_{600nm} measured 8 and 24 hours following light exposure, displaying the difference in relative growth at these time points with unpaired t-tests comparing the growth of each concentration at each time point relative to the positive control at the same point. (**C**) *E. coli* OD_{600nm} measured 8 and 24 hours following light exposure, displaying the difference in relative growth at these time points with unpaired t-tests comparing the growth of each concentration at each time point relative to the positive control at the same point.

3.2.8 Effect of Compound 2 on bacterial viability at a range of concentrations

To evaluate the effect of Compound **2** on cell viability across various concentrations, a minimum bactericidal concentration (MBC) assay was performed. The MBC is a CFU experiment that determines the lowest concentration at which a compound reduces viable cells by more than 10^3 relative to the DMSO control, indicating elimination of 99.9% of cells. The four representative species were prepared as described above and incubated with different concentrations of Compound **2**, along with untreated and solvent-only controls.

Both *S. epidermidis* and *B. subtilis* showed a 10^3 reduction in viable cells at 0.25 µM (figure 14), indicating the potent bactericidal effect of photoactivated Compound **2** in Gram–positive species. *S. epidermidis* was particularly susceptible, with fewer than 10 cells recovered following activation at 1 µM (figure 14). In contrast, the MBC values for *E. coli* and *P. fluorescens* were considerably higher, exceeding 16 µM (Figure 14). Due to solubility issues Compound **2** starts to precipitate in DMSO at concentrations higher than this, therefore it was not possible to test at a higher concentration. This provides further evidence that Gram - negative bacteria effectively tolerate much higher concentrations of Compound **2** than Gram – positive bacteria.

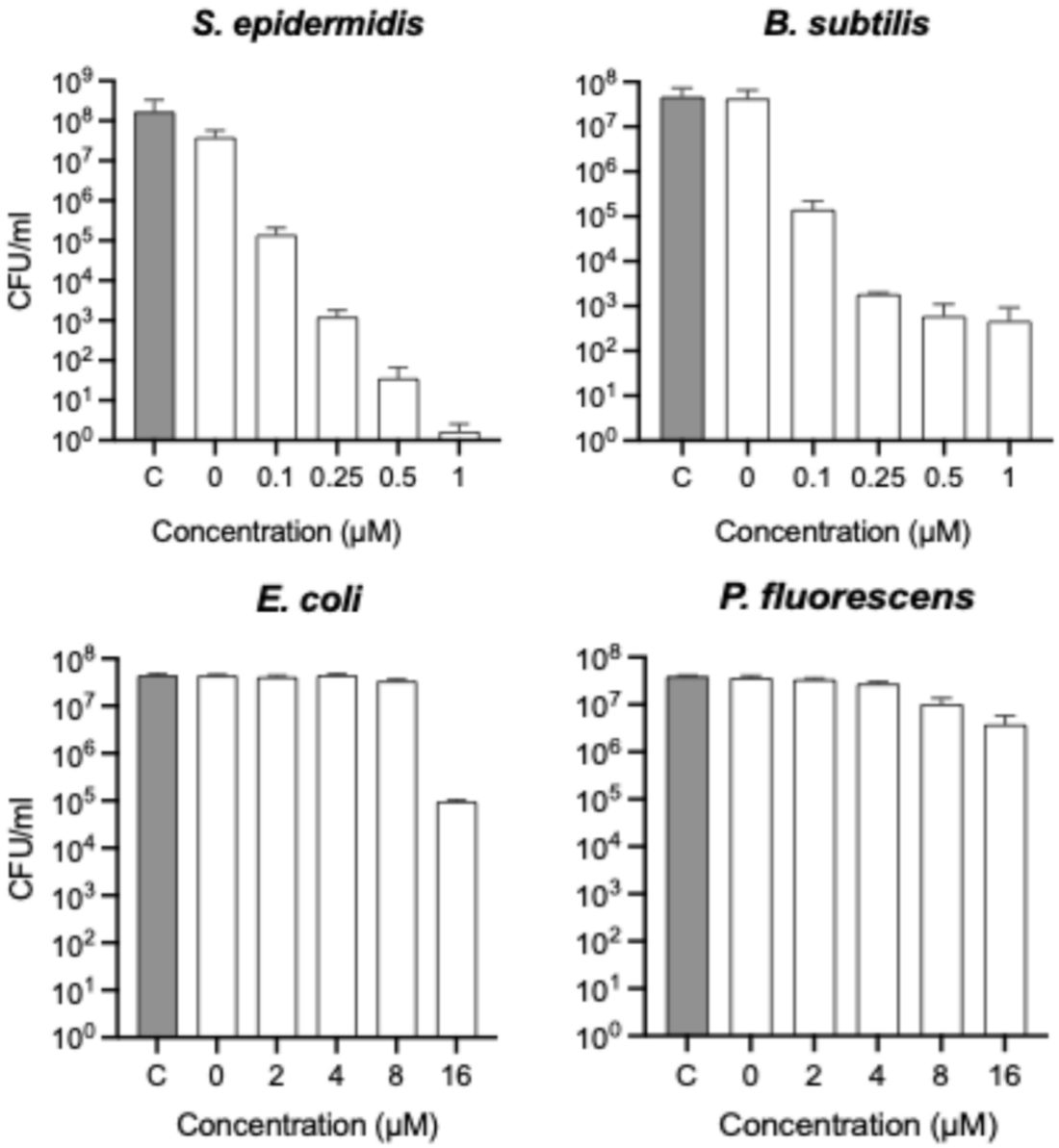

Figure 14. Minimum bactericidal concentration of the 4 representative species following treatment with Compound **2**. Samples were grown to mid log phase and then incubated with a series of concentrations of Compound **2** in a 24 well plate, The plate was then activated by irradiation at 365 nm and serial (10-fold) dilutions were performed with 10 µl of each dilution applied to the surface of an LB agar plate. Plates were incubated for 24 hours before enumeration of colonies to determine CFU/ml.

3.2.9 Real-time monitoring of bacterial membrane integrity

To provide further evidence that membrane disruption by Compound **2** is dependent on photoactivation, a real time BacLight assay was employed. The assay utilises SYTO 9, a membrane permeable dye that fluoresces when bound to chromosomal DNA, while PI, as mentioned above, only enters cells when membrane integrity is severely compromised and displaces SYTO 9 due to its higher affinity for DNA (153). Bacteria were grown to early-log phase, treated with 2 µM Compound **2** in the presence of the two dyes and visualised by microscopy. Compound **2** was activated by light at 405 nm and images were captured over 10 min to monitor changes in fluorescence. The fluorescence of SYTO 9 was adjusted from green to yellow and the fluorescence of PI was adjusted from red to magenta to allow visualisation by people with red-green colour blindness.

Most of the *B. subtilis* and *S. epidermidis* bacteria were stained with SYTO 9 prior to light activation (Figures 15A,B; SYTO 9 coloured yellow) indicating these cells possessed intact cell envelopes and were alive. Photoactivation resulted in a rapid fluorescence change, with all cells stained with PI after 10 min (Figures 15A,B; PI coloured magenta). These changes indicate significant membrane damage, and likely cell death, due to the activated Compound **2**, allowing the influx and subsequent fluorescence from PI. In contrast, *E. coli* and *P. fluorescens* with cells exposed to Compound **2** retained the SYTO 9 dye after light activation with no indication of membrane disruption (Figures 15C,D).

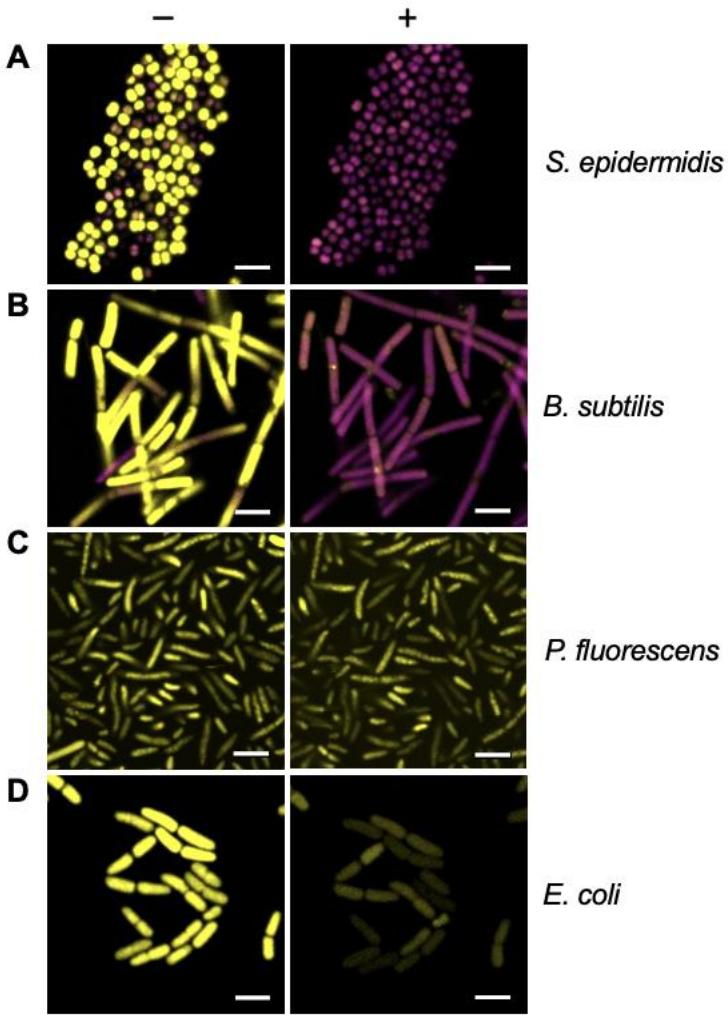

Figure 15. Real-time monitoring of bacterial membrane integrity. The BacLight assay of membrane integrity following photoactivation of compound **2**. *S. epidermidis* (A), *B. subtilis* (B), *P. fluorescens* and *E. coli* (D) in mid-log phase of growth were stained with PI (adjusted to magenta) and SYTO 9 (adjusted to yellow) and imaged by confocal microscopy without light activation (–) or 10 minutes after photoactivation with the 405 nm laser (+). The laser was applied at 30% power for 1 minute. The bar represents 3 µm.

3.2.10 Effect of Compound 2 on the viability of clinically relevant bacteria

Compound **2** proved effective at eliminating the Gram-positive organisms *S. epidermidis* and *B. subtilis* upon photoactivation. However, *B. subtilis* is widely considered to be non-pathogenic in humans (154) and *S. epidermidis* has been shown to be less virulent than the more concerning bacteria of the same genus *S. aureus* (155).

The MBC assay was conducted as previously described to assess the bactericidal effects of Compound **2** against three clinically relevant ESKAPE bacteria: *S. aureus*, *E. faecalis*, and *P. aeruginosa*, commonly associated with nosocomial infections (156). This included two strains of *S. aureus*: the methicillin-susceptible SH1000 strain and the MRSA strain USA300.

Both strains of *S. aureus* and *E. faecalis* demonstrated high susceptibility to Compound **2**, with MBC values of 1 µM and 0.25 µM, respectively (Table 4), indicating that Compound **2** could serve as a potent treatment for clinically relevant infections. Notably, the MSSA and MRSA strains exhibited nearly identical susceptibility to photoactivated Compound **2** (Figure 16A), suggesting that modifications to PBPs do not affect susceptibility, making Compound **2** a viable option for treating drug-resistant bacteria.

In contrast, *P. aeruginosa* showed no decrease in growth relative to the control, even at 8 µM of Compound **2** (Figure 16B). Overall, these results highlight the potential of Compound **2** to effectively target clinically relevant Gram-positive infections.

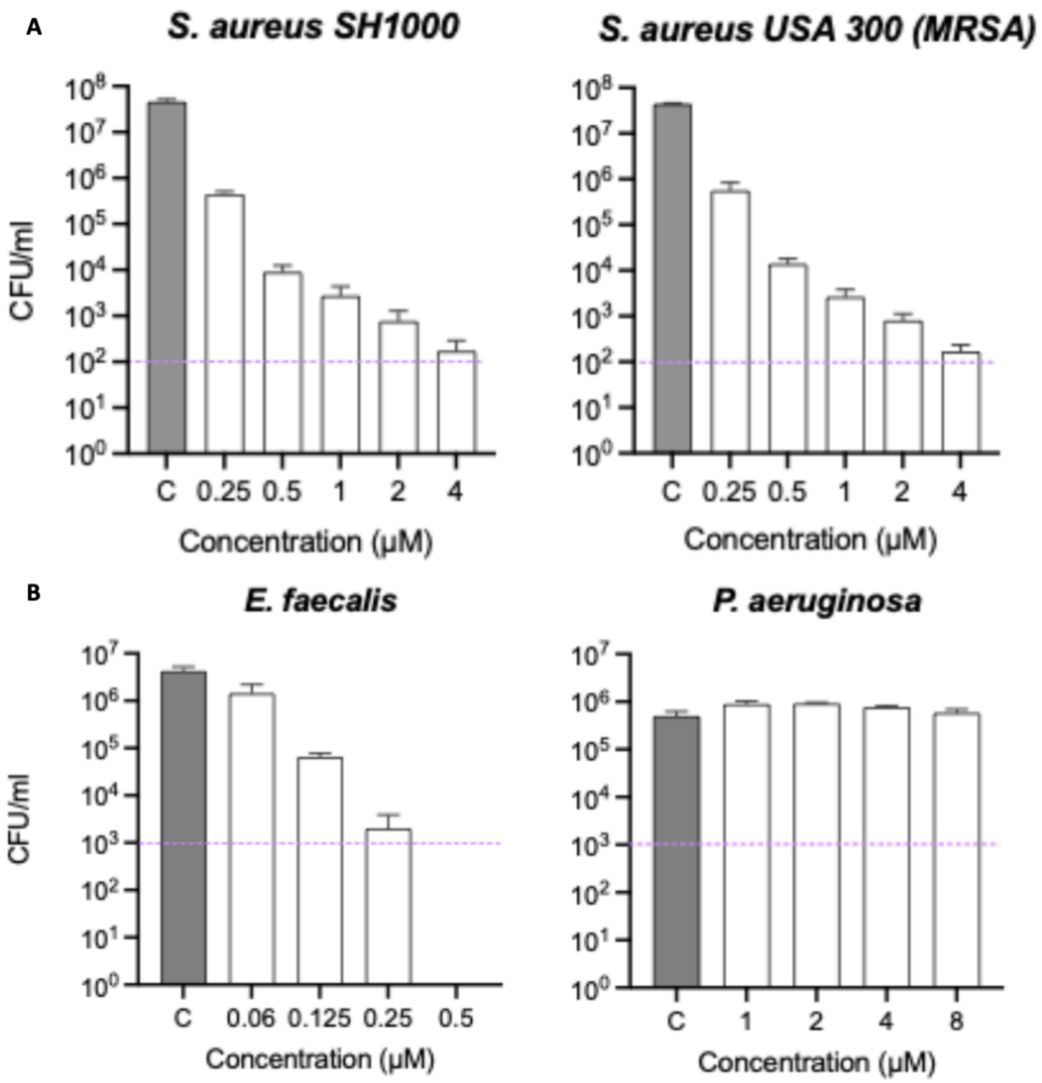

Figure 16. Effect of Compound **2** on the ESKAPE Pathogens *S. aureus*, *E. faecalis* and *P. aeruginosa*. Bacteria at mid-log phase of growth (20µL) were transferred to a clear 96-well plate were mixed with 180µL LB broth. Serial (10-fold) dilutions were performed and 10µL of each dilution was applied to the surface of an LB agar plate in the presence of Compound **2** or a DMSO control. (**A**) Minimal Bactericidal concentration of a Methicillin susceptible lab strain of the ESAKPE pathogen *S. aureus* (SH1000) and a methicillin resistant strain (USA300). (**B)** Minimum bactericidal concentration of the ESKAPE pathogens *E. faecalis* and *P. aeruginosa*. Purple lines represent the detection limit.

Bacteria	MBC (µM)
S. epidermidis	0.25
B. subtilis	0.25
E. faecalis	0.25
S. aureus	1
P. aeruginosa	>8
P. fluorescens	>16
E. coli	>16

Table 4. Minimum bactericidal concentrations of all species assayed when incubated with Compound **2** and exposed to 365nm light for 5 minutes.

3.2.11 Development of tolerance following sub-lethal treatment of Compound 2

I next determined whether repeated exposure to sub-lethal concentrations of Compound **2** would lead to the emergence of a mutant with reduced susceptibility to treatment at 2 µM Compound **2**, a lethal concentration that previously reduced viability by 10^4-fold in *S. aureus* (figure 16A). *S. aureus* cultures were treated with 0.1 µM activated Compound **2,** a concentration selected to elicit an approximate 10-fold reduction in viability based on 0.25 µM leading to a 100-fold reduction in viability, alongside appropriate controls (table 3) and assessed for viability by plating serial dilutions onto agar plates to calculate CFU/ml, as described previously. Each treated culture was then used to subculture the next treatment cycle. This was repeated for 15 cycles. By directly transferring the treated culture to fresh media, rather than using a single surviving colony for subculturing, a higher degree of genetic diversity was transferred from one cycle to the next, thereby increasing the likelihood of developing a tolerant mutant (157).

After 15 cycles of repeated subculturing, no tolerance of statistical significance was observed in any of the 5 groups after treatment with 2 µM Compound **2** (figure 17A) MBC assays conducted on day 1 for the wild type and on Group 1 after 15 cycles indicated that while there was an increase in viable cells at lower concentrations, it was not statistically significant (Figure 17B). Fewer viable cells were recovered after treatment with 2 µM, but this difference was also not significant (figure 17B), MIC assays for group 4 showed no development of resistance to H_2O_2 at higher concentrations (figure 17C), at day 9, some growth was observed at 0.0075% and 0. 015% H_2O_2, with growth also noted at 0.0075% on day 12. However, this was not observed on day 15 and suggests this reading may have been erroneous. Taken together, this suggests that tolerance to activated Compound **2** and H_2O_2 did not develop in *S. aureus* following 15 cycles of subculturing with sub-lethal doses.

In contrast, treatment with ampicillin showed growth at higher concentrations after 9 days of exposure to 0.25 µg/ml. By day 15, growth was observed at 128 µg/ml, approximately 500 times the sub-lethal dose (Figure 17D), indicating that resistance to ampicillin developed due to selection pressure from sub-lethal treatment.

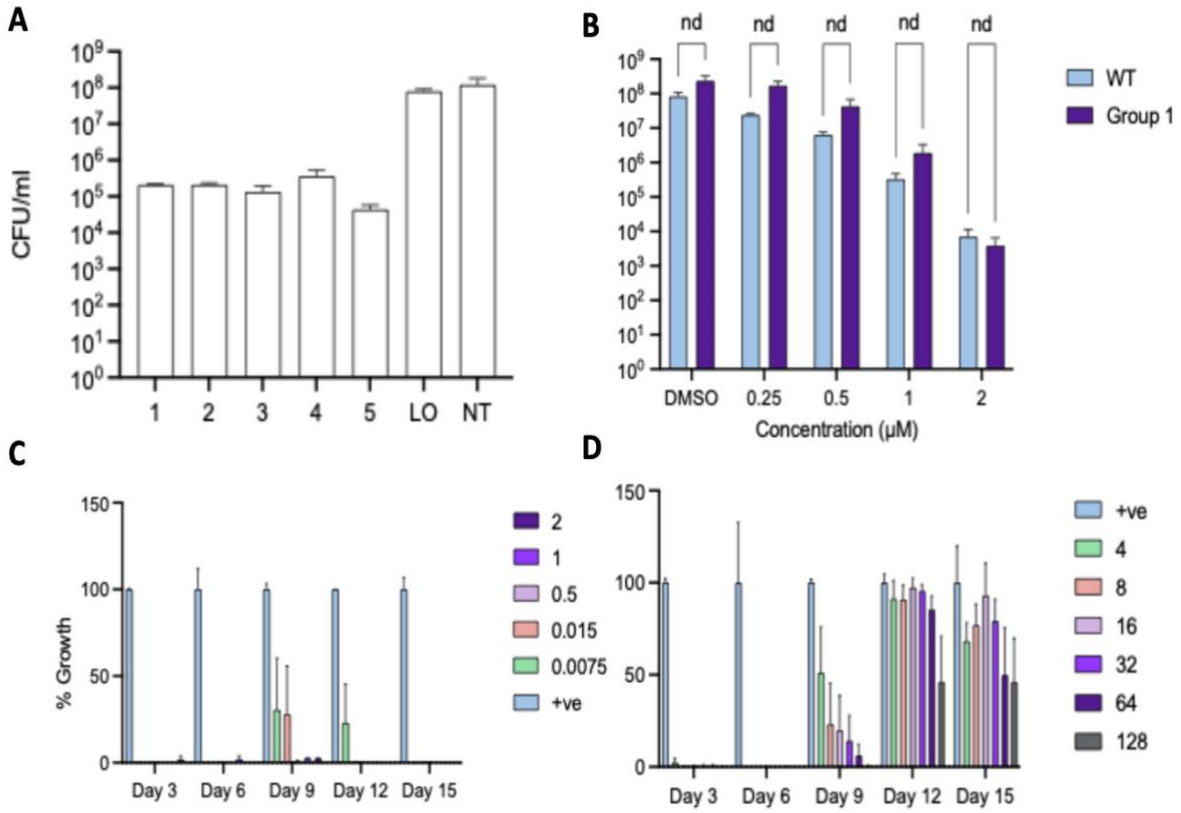

Figure 17. Resistance assay probing the development of resistance in *S. aureus* following repeated subtreatments. Bacteria were treated with sub lethal doses of Compound **2** and other controls then used to re seed the next cycle of growth, with lethal treatments performed every 3 cycles. A: CFU/ml experiment with all 5 groups treated with 2 μM Compound **2** after 15 cycles of subculturing of the respective groups. Light only treatment and no treatment control were performed in parallel. B: MBC assay of the Wild type *S. aureus* compared to group 1 after 15 cycles showing no significant difference in susceptibility at a range of concentrations. C: MIC assay of group 4 showing no development of resistance to Hydrogen peroxide after repeated cycles of subculturing with a sub lethal treatment. D: MIC assay of group 3 showing the development of resistance to ampicillin after repeated cycles of subculturing with a sub lethal treatment.

The three strains treated for 15 cycles with 0.1 µM light-activated Compound **2** (Group 1) were sent for whole genome sequencing (WGS), and their sequences were aligned to and then compared to a reference strain from the untreated Group 5 to determine if there were any single nucleotide polymorphisms (SNPs) or structural variants. Of the three strains sequenced, only one (Group 1 strain 2) exhibited SNPs or structural variants relative to the untreated strain. The observed SNPs are detailed in Table 5.

Fumarate hydratase (FumC), which catalyses the interconversion of fumarate and L-malate in the TCA cycle (158), and NhaC, a Na^+/H^+ antiporter that contributes to osmotolerance and halotolerance in alkaline environments (159), were both identified. However, neither protein has an obvious role in a tolerance response to activated Compound **2**.

Additionally, Group 1 strain 2 had a 4 kb deletion. The presence of multiple repeat proteins, likely contributing to the deletion, suggests that these mutations occurred due to repetitive DNA sequences. Most of the deleted proteins belonged to the TIGR01741 family, which has unknown functions. Overall, none of these mutations provided clear insights into potential mechanisms of resistance or tolerance to photoactivated Compound **2**.

Genome position	Gene	Base change	Amino acid change
305719	TIGR01741 family protein	T - A	Met - Lys
305725	TIGR01741 family protein	A - G	Lys - Arg
1897058	fumC	C - A	Val - Leu
2328148	nhaC	A - T	Upstream variant

Table 5. Details of the genes affected and base/amino acid changes of group 1 strain 2 *S. aureus* following 15 cycles of treatment with 0.1 µM Compound **2** exposed to light. Changes were mapped to the genome of the untreated culture group 5 strain 1.

3.3 Discussion

LightOx compounds were screened to identify those most effective in arresting growth and eliminating four representative species. Compound **2** demonstrated the highest toxicity across all species when exposed to 365 nm light. While growth inhibition was observed, minimal cytotoxicity occurred in *S. epidermidis* at 2 µM in the absence of light. Consequently, Compound **2** was selected as the frontrunner for further testing.

Compound **2** exhibited strong bactericidal properties against Gram-positive bacterial species upon photoactivation, while Gram-negative bacteria displayed significantly greater tolerance to the compound. The rapid influx of propidium iodide (PI) confirmed the photoactivatable nature of Compound **2**. Within 10 minutes of activation, PI fluorescence was markedly higher than in untreated controls, indicating a swift cytotoxic effect upon photoactivation (Figure 15A, B). ROS are highly reactive and quickly lead to cytotoxic effects (96). Thus, the rapid influx of PI and subsequent cell death can likely be attributed to the overwhelming surge of ROS generated following absorption of 365 nm light. This mechanism could explain the observed differences between MIC and MBC values in the tested bacteria. Since ROS are inherently short-lived (160), their cytotoxic effects occur rapidly after photoactivation. Growth inhibition may simply reflect a reduced number of

viable cells, some of which were initially damaged by the oxidative burst. These cells could later recover and re-seed the population once sufficiently repaired.

This also provides an alternative explanation for the zones of inhibition observed in soft agar assays (Figure 5). Rather than representing areas where the compound inhibited growth, these zones may instead indicate regions where activated compound killed the bacteria. This would also explain the uniformity of the inhibition zones, as compound which diffused after the initial activation would not be subsequently activated, preventing further spread of the zone (figure 5) If the plates were incubated for a longer period, colonies might eventually appear within the zones, as surviving cells could recover and repopulate the area.

The ability of Compound **2** to eliminate clinically relevant Gram-positive bacteria, including *S. aureus* (both standard and MRSA strains) and *E. faecalis*, is promising. Importantly, after 15 cycles of subculturing at a sub-lethal concentration, no development of resistance was observed. This aligns with existing literature indicating that resistance to PDT does not readily develop (161) (162). However, resistance to H_2O_2 did not develop as expected, despite literature suggesting that it should. Painter et al. demonstrated that exposure to 0.1 mM (0.0034%) H_2O_2 led to phenotypic changes and the formation of small colonies with increased resistance to 1 mM (0.034%) H_2O_2 (163). Additionally, Rapacka-Zdonczyk et. al. demonstrated that sub-lethal PDI treatments led to a measurable increase in resistance to H_2O_2 (157), something that was not tested during this assay. Given this discrepancy, the experiment could be repeated with more robust controls, using a higher sub-lethal concentration of Compound **2** and H_2O_2 over additional cycles, while measuring H_2O_2 MICs in all samples. The failure to observe H_2O_2 resistance raises concerns about the experiment's ability to generate mutants with enhanced oxidative stress resistance.

The excellent activity of Compound **2** may be due to two unique structural characteristics. First, the basic phenylpiperazine moiety of the donor region will likely be protonated under the bacterial culture conditions. This would aid localisation to the net negatively charged membrane structures (164) of most bacteria and, thus, potentially aid internalisation. Second, the thiophene moiety of the acceptor region may aid the generation of suitably reactive excited states during photoactivation by promoting intersystem crossing (165) and thus potentially increase/modulate the elicitation of ROS generation.

Taken together, this chapter underscores the potential of Compound **2** as a valuable candidate for light-based antimicrobial treatments targeting clinically relevant Gram-positive infections, thus contributing to the reduction of AMR.

Chapter 4: Gram – positive bacteria are eliminated via a type 1 ROS based mechanism requiring compound accumulation on the membrane and cell cytosol

4.1 Aims

In the previous chapter, screening LightOx compounds identified Compound **2** as the most effective agent able to eliminate clinically relevant Gram-positive bacteria upon activation with 365 nm light. It maintained high efficacy against MRSA and did not promote tolerance after repeated sub-lethal treatments. However, the mechanism by which Compound **2** induces cytotoxicity remained unclear.

Photosensitisers typically generate ROS upon activation through either a type 1 or type 2 mechanism (73), with the ROS rapidly reacting with nearby molecules. Thus, the localisation of Compound **2** is crucial in determining its cellular targets. At physiological pH, Compound **2** is hydrophobic (LogD of 3.1 at pH7), suggesting it could have a strong affinity for the hydrophobic phospholipids and glycolipids that predominantly make up Gram-positive membranes (166). In contrast, the Gram-negative outer membrane may repel the compound due to the charged groups on lipopolysaccharides (LPS), which create a hydrophilic environment (167). This difference may account for the varying susceptibility of these bacterial types, as Compound **2** might struggle to penetrate the Gram-negative envelope. As

a result, the ROS produced upon photoactivation may interact with outer membrane components rather than targeting vulnerable intracellular components.

In this chapter, I assessed the bacterial response to oxidative damage using *S. aureus* strains lacking superoxide dismutase activity. I also employed proteomic analysis, scanning electron microscopy (SEM), and the oxidative stress detector CellRox to investigate ROS-mediated damage. Additionally, I utilised the fluorescent properties of Compound **2** in confocal microscopy to examine its localisation in the Gram-positive species *B. subtilis* and *S. epidermidis*, as well as the Gram-negative species *E. coli* and *P. fluorescens*. These methods provide insights into the mechanism of cytotoxicity of photoactivated Compound **2** in Gram-positive bacteria.

4.2 Results

4.2.1 Effect of superoxide dismutase knockouts on susceptibility to Compound 2

To test if the the generation of $O^{2\bullet-}$ upon Compound **2** photoactivation occurs in *S. aureus* and leads to cellular phenotypes, a double knockout strain Δ*sodAM* was used as this had been previously provided from the Strahl lab at Newcastle University . SodA (Mn) and SodM (Mn/Fe) are the two superoxide dismutases currently identified in *S. aureus* (168). The double knockout exhibits no superoxide dismutase activity, resulting in increased sensitivity to $O^{2\bullet-}$ mediated damage (169).

S. aureus Δ*sodAM* and wild-type strains were grown to mid-log phase, diluted to an OD_{600nm} of 0.2 to account for the reduced growth rate of the double knockout, then incubated with

Compound **2** at concentrations ranging from 0.25 µM to 4 µM, a range in which *S. aureus* has shown drug susceptibility (Figure 14). CFU/ml were calculated before and after irradiation. No loss of viability was detected at any concentration of Compound **2** without irradiation (Figure 18A). In contrast, the knockout strains lacking superoxide dismutase activity had an increase in susceptibility compared to the wild-type, with a 100-fold decrease in cell viability at concentrations of 0.5 µM to 4 µM (Figure 18B). Notably, no cells were recovered at 4 µM in *S. aureus* Δ*sodAM* following light exposure (Figure 18B). The increased susceptibility of the double SOD knockout to Compound **2** implies that the expected $O^{2\bullet-}$ production following photoactivation is likely exerting damaging effects on bacterial survival (Figure 18B).

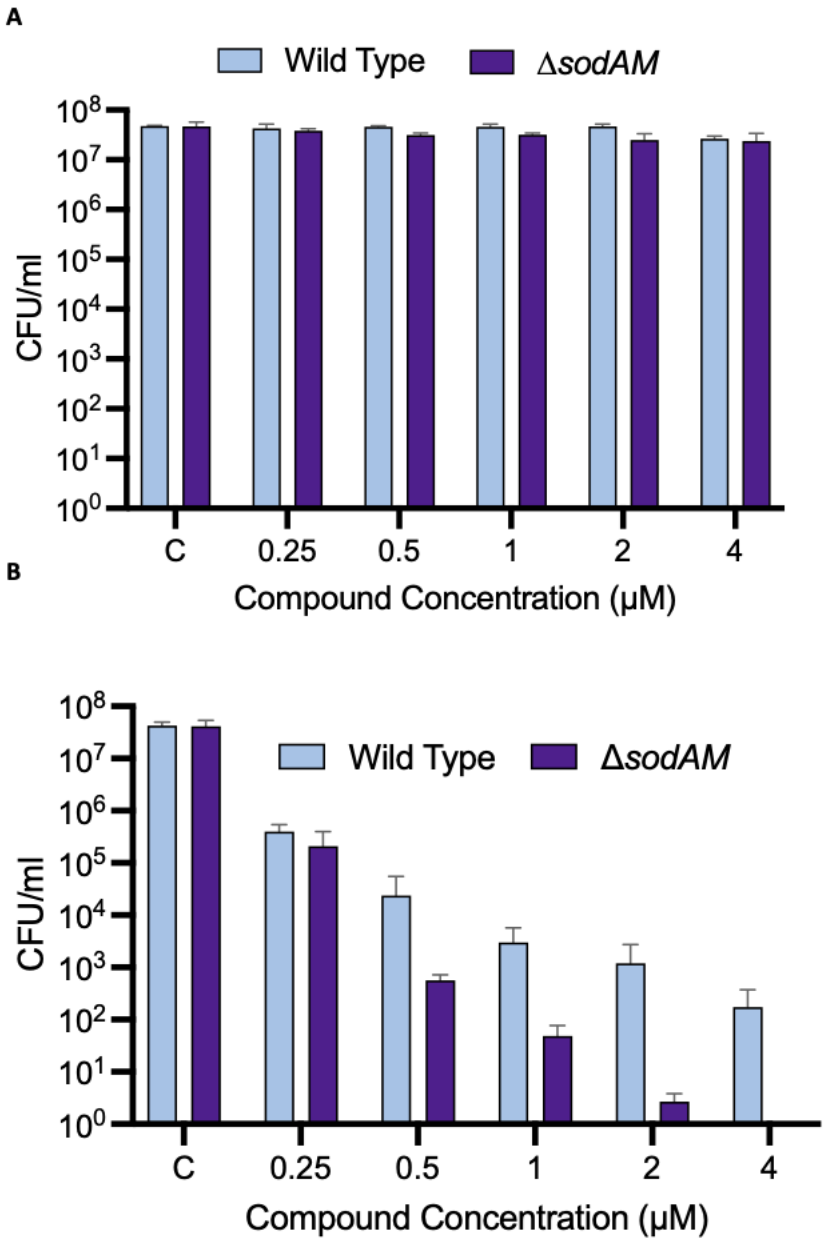

Figure 18. Susceptibility of a *S. aureus* strain deficient in superoxide dismutase activity. The viability of bacteria exposed to a range of concentrations of Compound **2** and a control of 0.4% DMSO before (**A**) and after (**B**) photoactivation shown. Serial dilutions of bacteria were applied to LB agar plates and colonies counted to determine CFU/mL. The CFU/mL represents the mean and standard error of three independent experiments.

4.2.2 Detection of Intracellular oxidative following Compound 2 photoactivation

To confirm that photoactivation of Compound **2** causes an increase in detectable reactive oxygen species, the fluorescent**,** oxidative stress responsive dye CellRox was used. CellRox is a membrane-permeable dye that localises in the cell cytosol, in its reduced state the dye will not fluoresce, but once oxidised will become fluorescent. Indicating the presence of oxidative stress molecules (170).

B. subtilis and *E. coli* were grown to mid log phase, incubated with Compound **2** and CellRox, and then exposed to 365nm light after 20 minutes. CellRox fluorescence was monitored on microscope from 0 to 80 min (Figure 19A). CellRox fluorescence was also imaged in fixed samples of *B. subtilis* and *E. coli*, following 365 nm activation of 2 µM and 8 µM Compound **2** respectively.

Both the Gram–positive *B. subtilis* and Gram–negative *E. coli* displayed a slight concentration-dependent increase in CellRox fluorescence during the 20 minutes prior to photoactivation, suggesting mild increase in oxidative stress was occurring and this could be due to exposure to Compound **2** alone in the absence of light (figure 19A). After photoactivation, a significant increase in detectable fluorescence was observed in both species at 2 µM (figure 19A). With a more modest but still statistically significant increase in fluorescence seen at 1 µM, approximately 0.33x that observed at 2µM (figure 19A), indicating oxidative stress following activation likely due to ROS production.

Imaging of fixed samples of *B. subtilis* showed no statistically significant increase in corrected total cell fluorescence (CTCF), the fluorescence of 3 technical repeats with

background fluorescence subtracted, after the photoactivation of 2 µM Compound **2,** relative to irradiated DMSO control. Due to high variance in fluorescence intensity between images (Figure 19B). It was noted however, *B. subtilis* cells appeared larger when irradiated in the presence of Compound **2** than with DMSO, indicating Compound **2** activaition, potentially indicating damage to the cell wall and subsequent swelling (171). Similarly, a significant increase in CTCF was not detected in *E. coli* at 8 µM compared to the control (Figure 19C). The lack of significant fluorescence increase may be due to the fixation of the cells altering the microenvironment within the cell, leading to increased variance in fluorescence. Overall, these results may indicate that intracellular oxidative stress occurred in both species following photoactivation of Compound **2**.

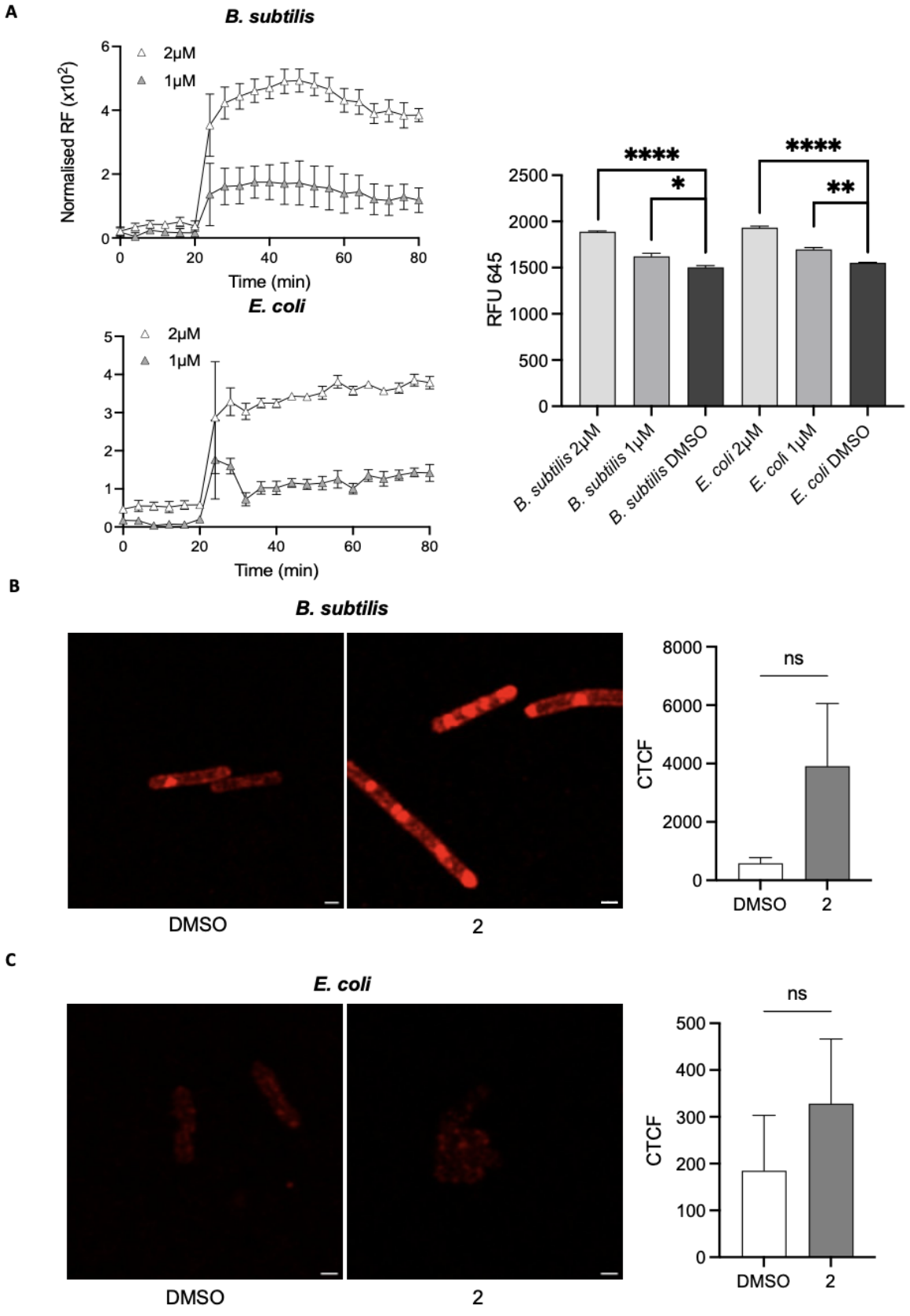
A
B. subtilis
2μM
1μM
Normalised RF (x10²)
Time (min)
E. coli
2μM
1μM
Time (min)
****
*
****
**
RFU 645
B. subtilis 2μM
B. subtilis 1μM
B. subtilis DMSO
E. coli 2μM
E. coli 1μM
E. coli DMSO
B
B. subtilis
DMSO
2
ns
CTCF
DMSO
2
C
E. coli
DMSO
2
ns
CTCF
DMSO
2

Figure 19. Effect of Compound **2** on intracellular oxidative stress. Bacteria were grown to mid-log phase in the presence or absence of Compound **2** as described in the Material and Methods. **A.** The relative fluorescence units (RFU × 10^2) at 645 nm were measured every 4 mins and normalised against controls containing appropriate control concentrations of DMSO. With Unpaired t-tests of the fluorescence after 80 min to determine significance of each sample relative to the irradiated DMSO control. **B.** Confocal microscopy of 4% paraformaldehyde fixed *B. subtilis* with 0.2% DMSO and 2 µM Compound **2** exposed to 365 nm light with fluorescence quantification normalised for the field of view. The scale bar represents 1 µm. **C.** Confocal microscopy of 4% paraformaldehyde fixed *E. coli* with 0.8% DMSO and 8 µM Compound **2** exposed to 365 nm light with fluorescence quantification normalised for the field of view. The scale bar represents 1 µm.

4.2.3 Visualisation of Compound 2 in bacterial cells

Compound **2** is inherently fluorescent in the visible detection range when excited by 365-405 nm of light and I used confocal microscopy to determine compound localisation in the four bacterial species under investigation. In all species, compound was detected on the cell surface and in both Gram-positive species evaluated, fluorescence was detected in discrete, foci. The shape and location of these foci suggested possible labelling of aggregates at the surface or accumulation within the cytosol (Figure 20A,B). Compound **2** localisation at the poles of *B. subtilis* cells was particularly noticeable (Figure 20A) between cells undergoing division. These bright foci were absent in the two Gram-negative species examined and Compound **2** detected solely at the cell surface (Figure 20C,D).

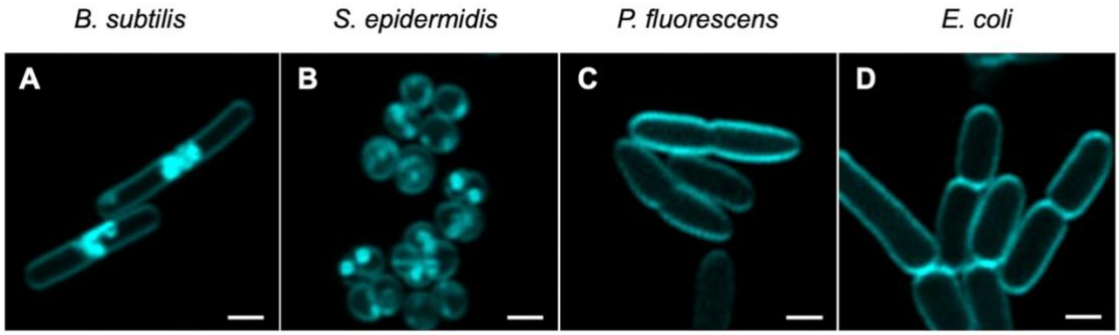

Figure 20. Location of Compound **2** fluorescence in bacterial cells. Mid-log phase bacteria were incubated with 2 µM of Compound **2** for 30 min before centrifugation and resuspension in 1x PBS. Resuspended cells were applied to a 1% agarose pad and imaged using confocal microscopy with cyan false colour imaging of the compound using a 405 nm laser with detection at 450–550 nm using the Airyscan function. The bar represents 1 µm.

4.2.4 Effect of Compound 2 on bacterial membranes

Bright membrane fluorescence was observed in all species investigated suggesting the majority of Compound **2** localises to the cell wall and/or membrane. Other anti-bacterial photosensitisers, such as methylene blue, work through ROS-mediated destruction of cell walls and membranes. Therefore, I used Scanning Electron Microscopy (SEM) to examine the effect of Compound **2** activation on cell surface integrity in *S. epidermidis.* Cells were grown to mid-log phase and treated with 1 µM Compound **2**, a concentration shown to be highly bactericidal following photoactivation (figure 16) then fixed before and at several timepoints following light exposure (20, 40, 60 min) and imaged using SEM. Control samples included irradiated DMSO and 1 µM Compound **2** without light exposure to evaluate the impact of the compound in the absence of light and the effects of light exposure alone on the membrane.

Irradiated DMSO control (figure 21) and Compound **2** treated cells without irradiation (figure 21) showed no obvious surface changes to membrane morphology, with cells displaying a uniform spherical shape (figure 21). Upon light-activation, Compound **2** treated cells became distorted, with patches of bumpiness and wrinkling evident on the cell surface accompanying a loss of regular morphological structure (figure 21). This was most likely a consequence of membrane aggregation and loss of cell turgor, likely resulting from direct membrane damage or lysis following cell death (figure 21). This effect did appear to be lessened after 40 minutes however, indicating a non – uniform effect across cells and timepoints Taken together, these data suggest potential membrane damage occurs following photoactivation of Compound **2**.

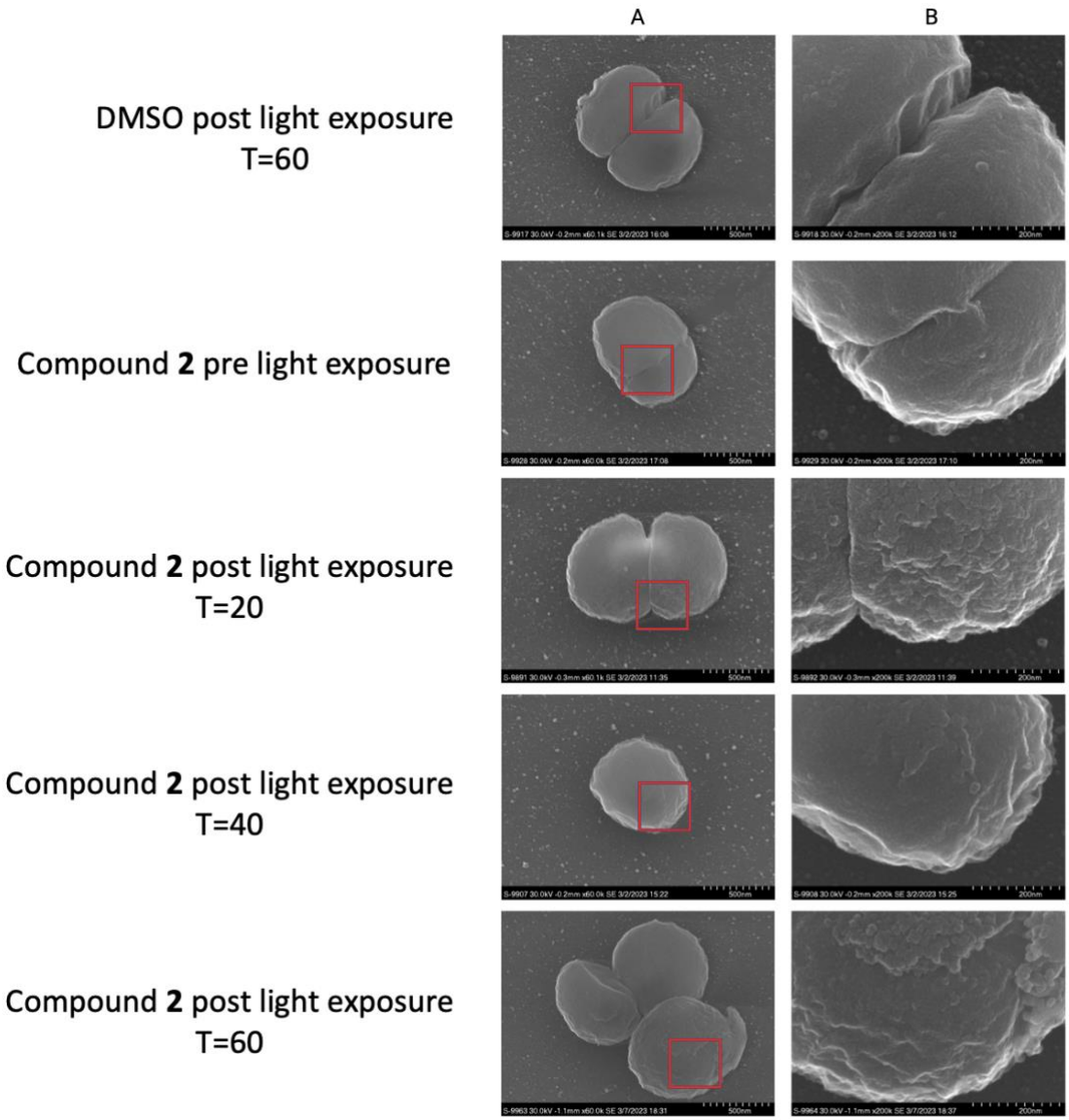

Figure 21. SEM of *S. epidermidis* with 1 µM Compound **2** and 0.1% DMSO. *S. epidermidis* was grown to mid log phase and incubated with Compound **2** before been exposed to 365 nm light for 5 min, then fixed using glutaraldehyde and paraformaldehyde at the timepoints above as described in the materials and methods. Images of cells were taken before irradiation of Compound **2** and at 20, 40 and 60 mins after irradiation, with the DMSO control imaged 60 min after exposure to light, using SEM with two fields of view, 60,000x magnification (**A**) and 200,000x magnification (**B**). The red square represents the magnified area of **B**. The figure

includes one representative image from each treatment group, of which 5 images were taken per group.

4.2.5 Effect of Compound 2 on protein expression

I next investigated the biochemical and protein responses following Compound activation in *S. aureus*. As above, cells were grown to mid log phase and treated with 1 µM Compound **2** and then light irradiated for 5 mins. 1 µM was chosen as this concentration was shown to induce a significant bactericidal effect yet some viable cells remained allowing changes in protein expression to be measured in these cells (figure 16). One-hour post-irradiation, protein was extracted and iTRAQ proteomics were performed to quantify the expression changes of the 362 proteins recovered compared to the untreated control.

Among the 362 proteins identified (Figure 22), 99 showed significant up-regulation (greater than 1.2-fold increase). The molecular functions of up-regulated proteins were evaluated using Gene Ontology (GO) (figure 22). Notably, 41 of the up-regulated proteins were ribosomal subunit proteins, suggesting a stress response that enhances translation. Additionally, six proteins were identified with roles in oxidative stress response and DNA repair. Relative fold changes and GO molecular functions are detailed in Table 6, however it was interesting that both DNA gyrase subunits A and B were upregulated by 1.6-fold.

DNA gyrases cause negative supercoils into DNA and plays critical roles in replication and DNA repair (172), with increased production typically detected following DNA damage (173). Additionally, four proteins involved in ROS detoxification were also upregulated: Catalase (2.71), which works in conjunction with superoxide dismutases (SODs) to eliminate H_2O_2

generated by these enzymes (97); Alkyl hydroperoxide subunits C (1.5) and F (1.9), which form a complex to detoxify H_2O_2 and organic hydroperoxides (174); and thioredoxin reductase (1.56) protects cells from oxidative stress by maintaining thioredoxin in its reduced state (175). Thioredoxins are essential for oxidative stress detoxification, facilitating the reduction of H_2O_2 and scavenging hydroxyl radicals (169).

Despite previous evidence showing increased susceptibility of the *ΔsodAM* mutant, neither SodA nor SodM were isolated. This is most likely due to the low number of proteins successfully quantified after treatment with Compound (figure 22). Taken Together, these results support my hypothesis that intracellular H_2O_2 production and DNA damage occur in *S. aureus* following the activation of Compound **2**.

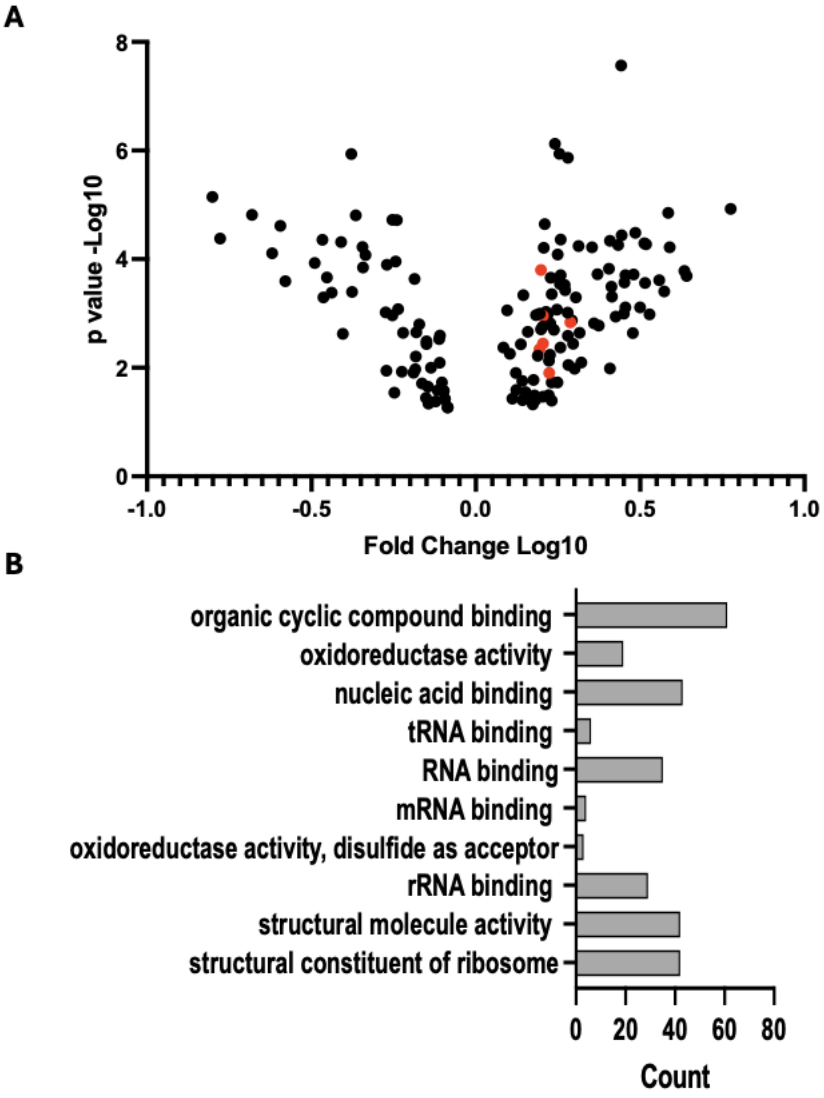
A
8
6
4
2
0
p value -Log10
-1.0
-0.5
0.0
0.5
1.0
Fold Change Log10
B
organic cyclic compound binding
oxidoreductase activity
nucleic acid binding
tRNA binding
RNA binding
mRNA binding
oxidoreductase activity, disulfide as acceptor
rRNA binding
structural molecule activity
structural constituent of ribosome
0
20
40
60
80
Count

Figure 22. Volcano Plot of significantly upregulated and down-regulated proteins following treatment with 1 μM Compound **2** and 5 mins of 365 nm light activation. The relative quantification of each protein was generated as a ratio of the DMSO control sample. An average ratio of each protein was calculated across all four biological replicate samples, and a Student's t-test at $p \leq 0.05$ was used to compute the statistical significance in the ratios. (**A**)Relative fold change was calculated with significant up-regulation (>1.2) and down-regulation (<0.83) converted to Log10 and plotted against the -Log10 of the P value. Red dots represent the proteins of interest described in table 6. (**B**) GO molecular function of the 99 upregulated proteins of *S. aureus* following ITRAQ proteomics.

Protein name	Log 10 Fold change	-Log 10 P Value	GO Molecular function
DNA gyrase subunit A	0.20	2.95	Nucleic Acid Binding
DNA gyrase subunit B	0.20	2.44	Nucleic Acid Binding
Alkyl hydroperoxide reductase C	0.20	3.80	Oxidoreductase
Alkyl hydroperoxide reductase F	0.29	2.83	Oxidoreductase
Thioredoxin reductase	0.19	2.34	Oxidoreductase
Catalase	0.43	4.26	Oxidoreductase

Table 6. Selected proteins up-regulated following activation of Compound **2**. Molecular function categorised using the GO Consortium (https://geneontology.org)

4.2.6 Compound 2 localisation to membranes and lipid droplets in Gram–positive bacteria

As described in section 4.2.3. bright foci of Compound **2** fluorescence were detected in *B. subtilis.* Compound **2** is solvatochromatic (72) and fluoresces brighter in lipid-rich environments and to better characterise labelled foci, I carried out co-staining with another fluorescent lipid stain, Nile red. Nile red displays strong fluorescence only in hydrophobic environments and is used to image membranes and intracellular lipid droplets (176).

B. subtilis was grown to mid log phase before Nile red and 2 µM Compound **2** were added and visualised using confocal microscopy (figure 23). Clusters of Nile Red fluorescence mirrored the bright fluorescent foci seen in Compound **2** stained cells with clustering primarily at cell poles (figure 23). The high Pearson Co-localisation Coefficient (PCC) value (0.904) confirmed the strong co-localisation of Compound **2** and Nile Red to neutral lipids in *B. subtilis* as predicted due to the lipophilic nature of Compound **2**.

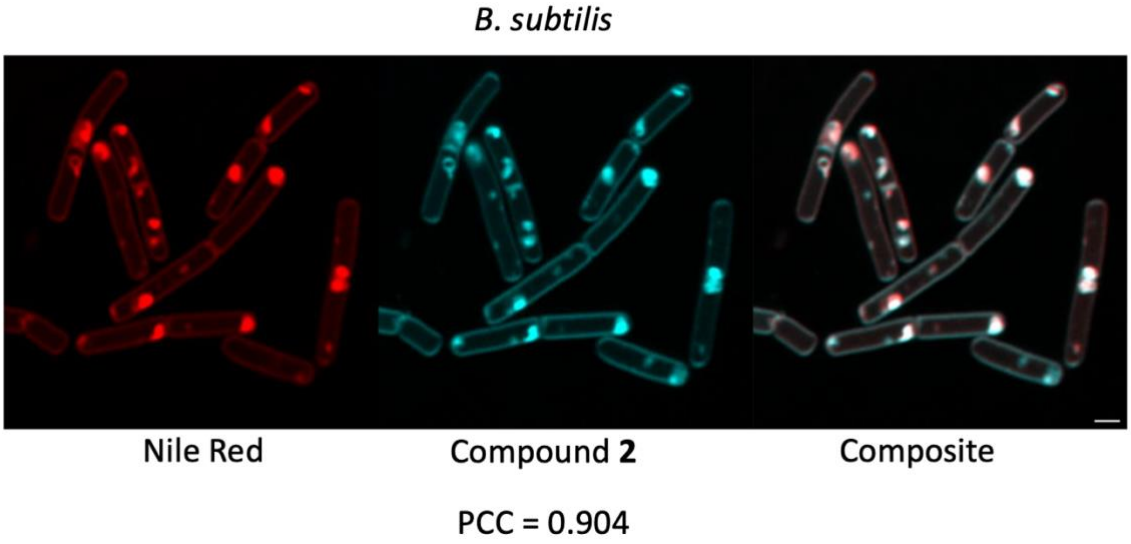

Figure 23. Colocalisation of Compound **2** and the neutral lipid dye Nile Red in *B. subtilis*. Bacteria were incubated with 2 µM of Compound **2** and 3.3 µM Nile Red for 30 min before centrifugation and resuspension in 1x PBS. Resuspended cells were applied to a 1% agarose pad and imaged immediately using confocal microscopy using the filters described in the materials and methods before the Pearson Colocalisation Coefficient was calculated. The bar represents 1 µm.

4.2.7 Lipid droplet formation following stress in *B. subtilis*

When bacteria experience stress from factors such as nutrient starvation, lack of oxygen or exposure to antimicrobial compounds, lipid droplets can form due to membrane damage and subsequent depolarisation, with irregular membrane domains accumulating in the cell cytoplasm (177). *B. subtilis* is particularly prone to developing these irregular membrane domains under stressful conditions (178).

I hypothesised that culturing and imaging conditions could induce *B. subtilis* stress response and affected the localisation of Compound **2** and Nile Red. Therefore, experiments were repeated using modified protocols to minimise the cell stress; cells were incubated in LB instead of PBS following dye addition to ensure sufficient nutrient availability and wash steps after the addition of Compound **2** were omitted, as centrifuging is known to induce stress in bacteria (179). Cells were immediately imaged after the addition of 2 µM Compound **2** for no more than 20 minutes to avoid oxygen deprivation caused by the low oxygen environment under a cover slip.

Under these conditions *B. subtilis* showed minimal signs of lipid internalisation, with only membrane fluorescence detected under low stress conditions (figure 24, T=0). This supported my hypothesis that intracellular lipid droplets seen previously were evidence of a stress response from nutrient starvation, lack of oxygen or from the dark toxicity of Compound **2**. After repeated imaging, fluorescence from both Nile Red and Compound **2** was noted building from the poles (figure 24, T= 2), indicating cell sensitisation due to the activation of Compound **2** upon exposure to the 405 nm laser. After 5 minutes small fluorescent structures emerged from the cell cell septum, potentially indicating compound targeting of proteins involved in septation. (figure 24, T=5) and by 10 minutes, lipid droplets were clearly visible (figure 24, t=10). Microscopy conditions including a combination of oxygen deprivation and cell sensitisation from repeated, on-microscope activation of Compound **2** likely triggered the stress response and subsequent formation of irregular membrane domains (Figure 24, T=20) in these cells.

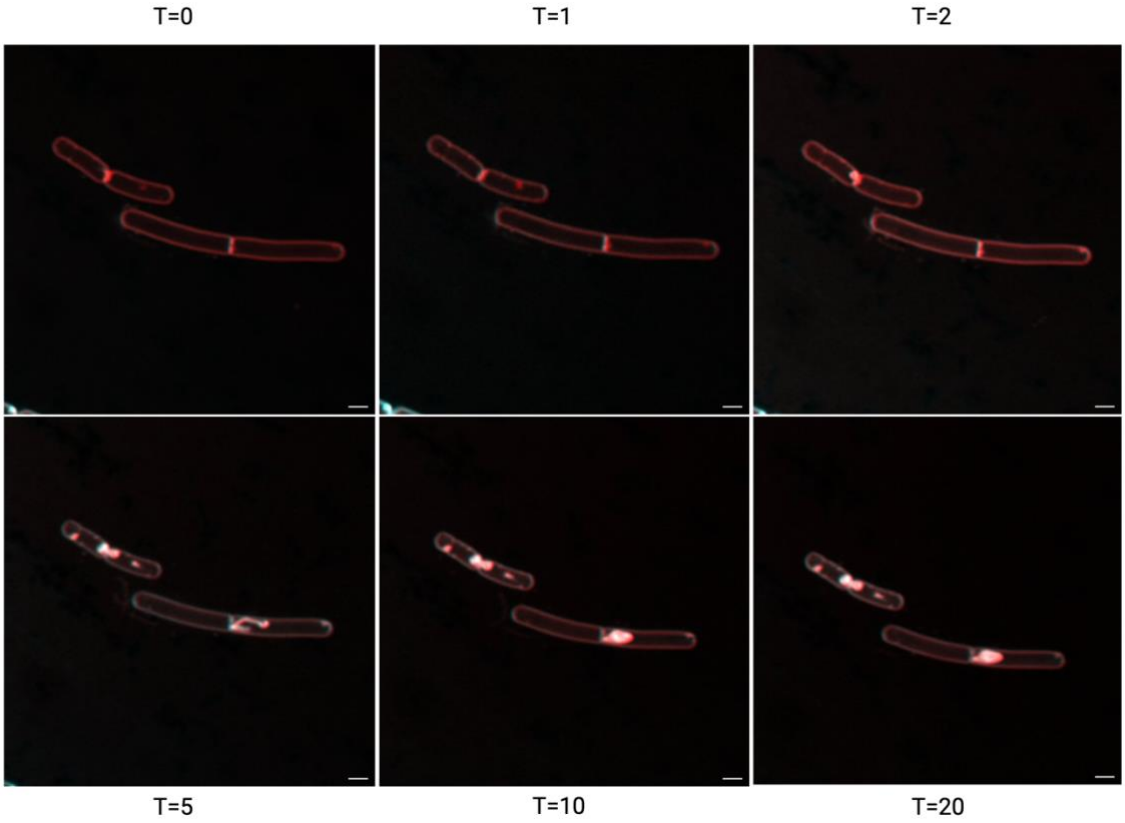

Figure 24. Visualisation of Compound **2** and Nile Red in *B. subtilis* grown in a low stress environment. Mid-log phase bacteria were incubated with 3.3 µM Nile Red for 30 min in 100 µL LB broth within a 1.5 mL microcentrifuge tube. Compound **2** was added and spotted onto a 1% agarose pad and imaged using confocal microscopy. Images were taken every minute to visualise membrane internalisation. The bar represents 1 µm.

4.2.8 Effect of Compound 2 on irregular membrane domain formation

It is possible that exposure to Compound **2** and/or Nile Red could be the trigger of stress-mediated lipid internalisation in *B. subtilis*. Therefore, I repeated the previous experiments using an Mcherry WALP23 fusion tagged strain of *B. subtilis*, designated KS88, to label lipids. WALP23 is an α-helical protein that is fully integrated into the bacterial membrane (180), allowing the Mcherry-tagged WALP23 to be used to investigate whether the internalised lipid droplets originate from the membrane.

Under the low-stress conditions previously described, WALP23 did not form membrane droplets in the absence of Compound **2** or DMSO vehicle controls (Figure 25A). This indicates that incubating *B. subtilis* in LB broth with sufficient oxygen and without wash steps does not induce stress-related irregular membrane domain formation. When *B. subtilis* was incubated with DMSO, small clusters appeared on the membrane, accompanied by some internalisation (Figure 25B), suggesting that DMSO induced a minor stress response and irregular membrane domain formation in these cells.

In contrast, Compound **2** exposure resulted in significant irregular membrane domain formation, distributed throughout the cell. The high PCC of 0.86 of Mcherry and compound **2** fluorescence suggests that internal domains derived from the membrane are formed. What is not clear is how these occur. One possibility is that membrane depolarisation is caused by the innate non-light activated toxicity of Compound **2** at 2 µM, which pulls compound-bound membrane into the cytoplasm (Figure 25C).

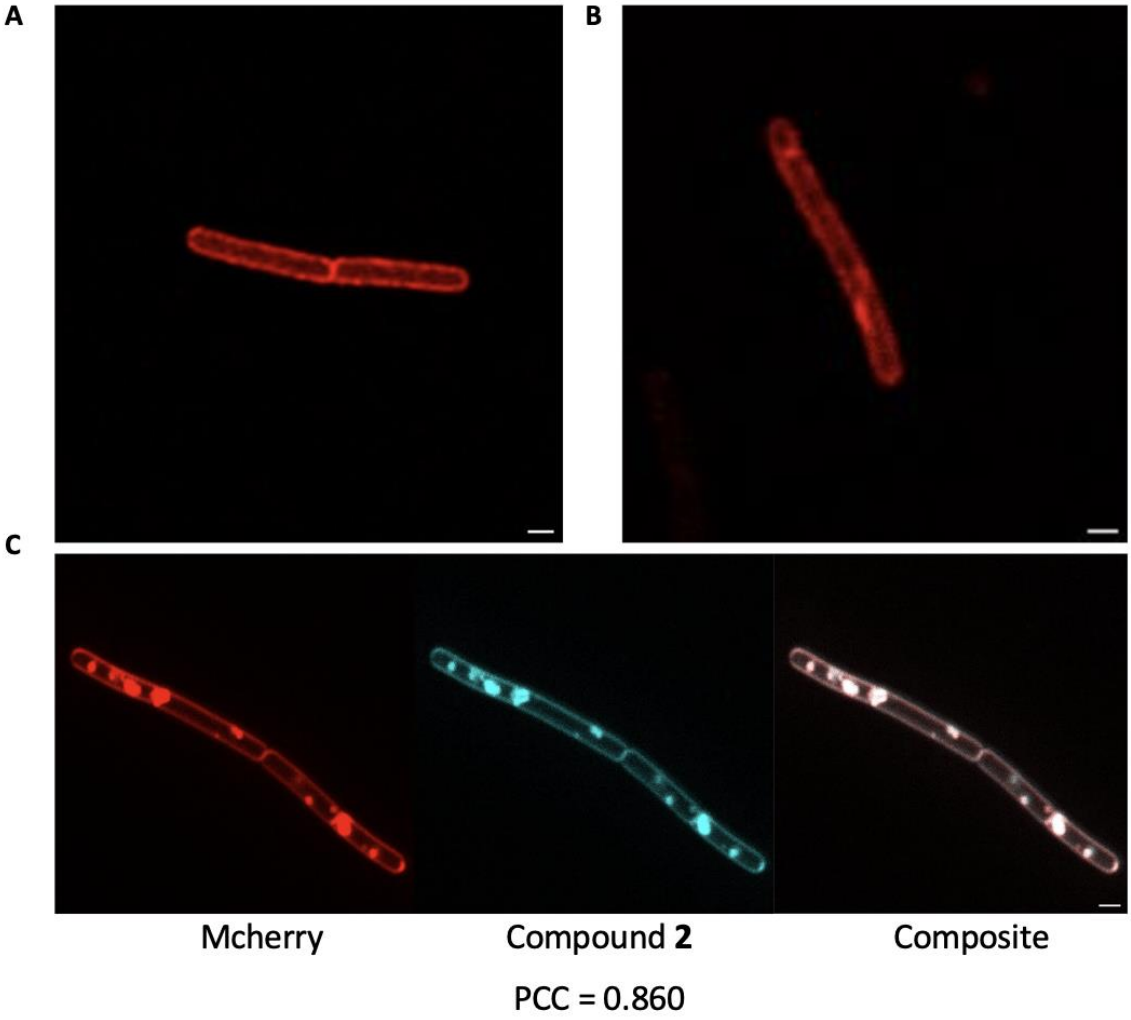

Figure 25. Airyscan of *B. subtilis KS88 Walp23::Mcherry*. Cells were incubated in LB broth until mid log phase before treatment was added and incubated for 20 minutes in a microcentrifuge tubes A. Visualisation of the KS88 after incubation in a microcentrifuge tube for 20 min B. *KS88* incubated with 0.2% DMSO showing minor membrane internalisation. C. *KS88* incubated with 2 µM Compound **2** showing significant membrane internalisation and high colocalisation of Mcherry fluorescence with Compound **2** in intracellular structures.. Scale bars represent 1 µm.

4.3 Discussion

Compound **2** acts as a highly potent photosensitiser upon activation, ostensibly due to a significant surge of ROS generated when exposed to 365 nm light, strains of *S. aureus* lacking superoxide dismutase activity proved hypersensitive to Compound **2** upon photoactivation. photoactivation. $O^{2\bullet-}$ is produced following electron transfer to oxygen via a type 1 or type 3 photodynamic pathway (77). And so, the increased susceptibility of the Δ*sodAM* mutant implies Compound **2** generates $O^{2\bullet-}$ via one of, or both, of these pathways following light activation.

In support of this hypothesis, proteomic analysis revealed a significant upregulation of proteins involved in the detoxification of H_2O_2, which arises either directly from hydrogen transfer to molecular oxygen (77) or from the dismutation of $O_2^{\bullet-}$ (97). This production of radicals supports the involvement of a type 1 or type 3 photodynamic mechanism for Compound **2**. However, it is important to acknowledge the limitations of this proteomics analysis, as only 342 proteins were successfully quantified. The cells were pelleted one hour after Compound 2 was photoactivated. Given that *S. aureus* has a typical generation time of 20 minutes in rich media (181), up to three generations may have replicated within that period, likely reverting to their original proteome expression by the time the cells were harvested and frozen.

Additionally, eliminating 99.9% of the cells may have been excessive. A lower concentration that resulted in a tenfold reduction in cell numbers could have allowed for the recovery of

more cells while still inducing detectable changes in proteome expression. This approach would have likely improved protein quantification and provided deeper insights into the *S. aureus* protein response.

Fluorescence microscopy confirmed strong membrane localisation of Compound **2** in all species assayed. Notably, the Gram-positive species exhibited internalisation of Compound **2**. Identified as aggregates of compound and lipid from the Nile red assays (figure 23). When grown in a low-stress environment, it was determined that Compound **2** induces stress on the cell, potentially causing membrane depolarisation and subsequent internalisation into the cytoplasm (figure 24). However, due to the solvatochromatic properties of Compound **2**, fluorescence is primarily observed in lipid-rich environments. Therefore, it is possible that the compound permeates the Gram-positive envelope but exhibits low fluorescence in the cytoplasm, only becoming visible when localised to lipid droplets formed after membrane depolarisation. Raman imaging, a non-fluorescent technique that uses the inelastic scattering of photos from molecular bond vibrations to generate images (182), could help determine whether Compound **2** is present in the cytoplasm or localised solely to the membrane. However, it is important to note that performing Raman imaging in bacteria is challenging (183).

Following activation, an increase in intracellular oxidative stress was observed in *B. subtilis* (figure 19). The upregulation of cytoplasmic ROS detoxification enzymes and DNA repair mechanisms indicates intracellular ROS production and oxidative stress (table 6). Scanning SEM images also suggested that membrane damage occurs post-activation (figure 21), aligning with my hypothesis that Compound **2** hits multiple cellular targets via a non-specific mechanism.

In summary, the results suggest a potential mechanism where Compound **2** readily binds to the membrane, induces membrane depolarisation, and is internalised. Upon photoactivation, Compound **2** generates ROS via a type 1 and/or a type 3 photodynamic mechanism, leading to extensive damage to both the membrane and intracellular components, ultimately resulting in loss of cell viability.

Chapter 5: *E. coli* compound 2 resistance mechanisms

5.1 Aims

The Gram-negative species *E. coli* and *P. fluorescens* showed minimal susceptibility to photoactivated Compound **2**, even at a concentration of 16 µM (table 4). Gram-negative bacteria are known for their greater tolerance of many antibiotics relative to Gram-positive species, a feature highlighted in the World Health Organisation's critical priority list, which comprises solely of Gram-negative pathogens (184). In most cases drug resistance can be attributed to the impermeability of their lipopolysaccharide(LPS)-rich outer membrane (OM) to hydrophobic molecules (185). Given that Compound **2** is hydrophobic at physiological pH (LogD of 3.1 at pH 7), the limited antibacterial efficacy against Gram-negatives fits with its inability to permeate the LPS barrier. Nonetheless, transport of hydrophobic molecules across the OM is vital for bacterial survival (186). To facilitate this, Gram-negative bacteria possess OM channel-forming proteins that allow passive diffusion of compounds that cannot penetrate LPS (187). However, it remains unclear whether Compound **2** is completely unable to enter Gram-negative cells, or if it can enter through OM channels, resulting in low levels of internalisation.

E. coli has been extensively investigated as a model organism and investigations have benefitted from the creation of the Keio collection, a library of 2 independent deletion-insertion mutants for 3985 non-essential genes (148). This was created by replacing a open reading frame coding region with a kanamycin cassette, which, upon excision of the resistance

cassette, leads to inactivation of the gene (148). *E. coli* was chosen as the organism for this chapter instead of a pathogenic knockout library such as *A. baumanni* because it could be used in the hazard group 1 laboratory where the work was conducted, in addition this collection was readily available.

In this chapter, 20 single-gene knockouts were selected based on their involvement in LPS synthesis, efflux and passive transport, ROS detoxification, and DNA damage repair. The susceptibility of these knockout strains to photoactivated compound **2**, confirmed the role of *E. coli* LPS in tolerance to this compound whilst also highlighting the importance of compound expulsion, and the bacterial response to ROS generated upon exposure to light.

5.2 Results

5.2.1 Differences in susceptibility of *E. coli* strains

The experiments performed in Chapter 3 utilised *E. coli* strain ATCC 25922, a clinical isolate obtained from Public Health England. In contrast, the Keio library used for mutant screening is derived from the *E. coli* K12 laboratory strain BW25113. The susceptibility of these two strains to compound **2** was therefore compared. Each strain was grown to mid-log phase and exposed to a range of concentrations of Compound **2**. Following irradiation, samples were spotted onto agar plates and incubated for 16 h and viability determined in CFU/mL. No loss of viability was apparent with both strains at concentrations up to 8 µM (Figure 26). However, at 16 µM, a drop in cell viability was observed in both strains, with the K12 strain showing a ten-fold decrease in viability relative to the clinical strain at 16 µM (Figure 26). This difference in susceptibility can be attributed to the 'smooth' phenotype of the clinical *E. coli* strain which possesses a typical arrangement of O-antigens decorating the lipid A core (188). In contrast,

the K12 laboratory strain of *E. coli* lacks these O-antigen polysaccharides, rendering it slightly more permeable to hydrophobic compounds (189).

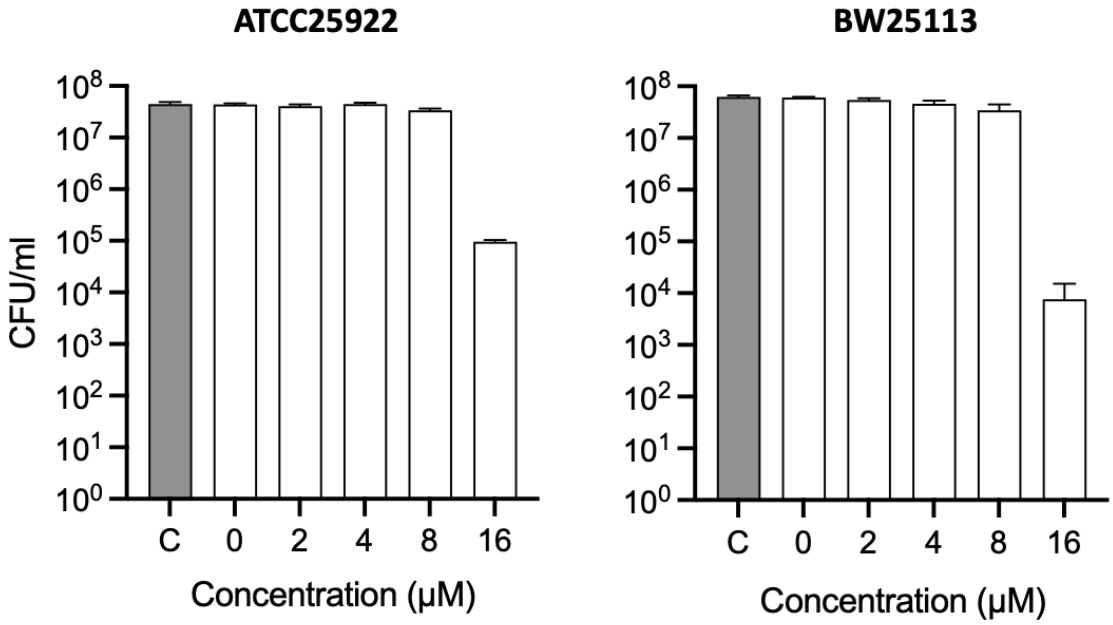

Figure 26. Susceptibility of the clinical isolate (ATCC25922) and the laboratory strain (BW25113) of *E. coli* following light activation of a range of concentrations of Compound **2** and 1.6% DMSO as a control (C). Serial (10-fold) dilutions of bacteria were applied to LB agar plates and colonies enumerated to determine CFU/mL. Values represents the mean and standard error of three independent experiments.

5.2.2 Efficacy of compound 2 against *E. coli* mutants with defects in LPS biosynthesis

The experiments performed so far suggested that the tolerance of compound **2** by *E. coli* and *P. fluorescens* is due to the presence of an impermeable outer membrane and that entry to the cytosol is a requirement for toxicity. To explore this further, I examined the susceptibility of *E. coli* strains with varying LPS compositions. Five knockout strains were analysed to determine the effects of LPS component removal on tolerance (Figure 27).

rfaG (*waaG*) encodes a glucosyltransferase responsible for adding the first glucose molecule, the initial residue of the LPS outer core, to the heptose II residue in the LPS chain (190). The knockout causes an 80% reduction in inner core heptose phosphorylation (191) (Figure 27A,B). *rfaQ* (*waaQ*), encodes a heptosyltransferase, catalysing the addition of a third heptose to the second heptose residue of the inner core. Its absence produces a truncated inner core consisting of two heptose residues and the loss of heptose phosphorylation (192) (Figure 27C).

The final three mutants, *rfaE* (*waaE*), *lpcA* (*gmhA*), and *rfaC* (*waaC*), result in the loss of inner core heptoses (figure 27D). LpcA and RfaE facilitate the production of the ADP-D-glycero-D-manno-heptose 1-phosphate precursor (193, 194), while RfaC catalyses addition of the first heptose residue to the 3-deoxy-α-D-manno-octulosonic acid (KDO) residue (195). Collectively, these three mutants result in a severely truncated LPS inner core and substantially increased permeability to hydrophobic molecules (figure 27D).

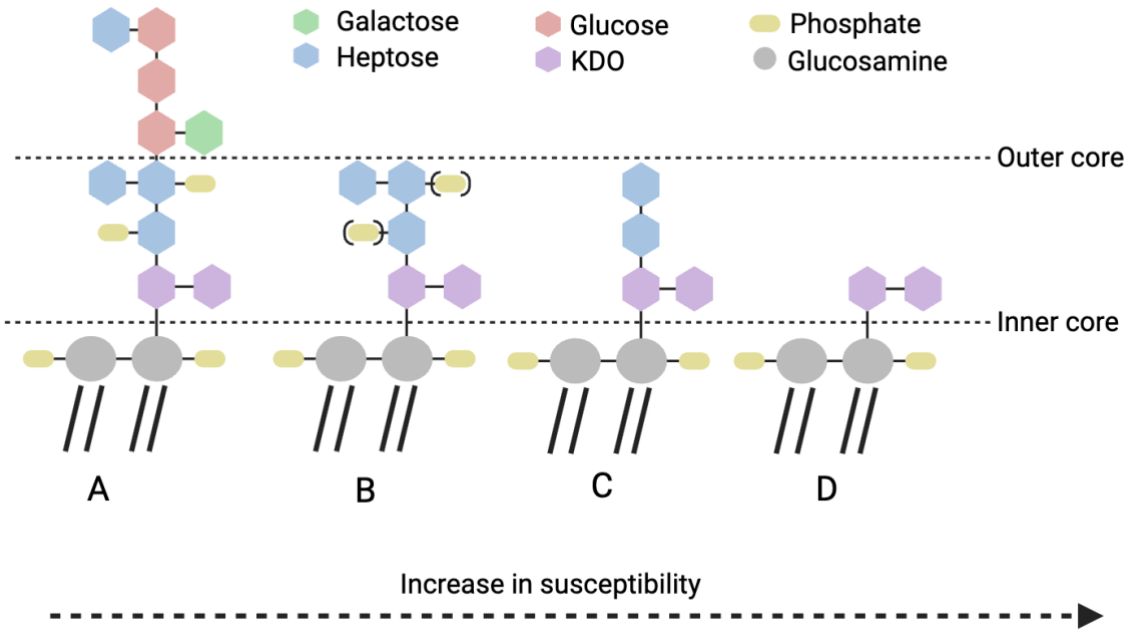

Figure 27. Diagram representing the LPS structure bound to Lipid A in *E. coli* and increasingly truncated LPS arising from different mutants involved in outer membrane biogenesis. (**A**) Wild type *E. coli* with the full LPS structure. (**B**) Mutation of *rfaG* eliminates glucose from the LPS outer core, leading to a truncated outer core and an 80% reduction in phosphorylated heptose, shown in parenthesis. (**C**) Deletion of *rfaQ* prevents heptose III addition to heptose II and loss of phosphorylation of the inner core heptose. (**D**) In *rfaE*, *lpcA*, and *rfaC* mutants, heptose I in the inner core KDO is absent, leading to a significantly truncated LPS inner core and a hyper-permeable phenotype. Created with Biorender.com

The five mutants were examined, alongside the WT, for any increased susceptibility to Compound **2** (Figure 28). To account for differences in growth rates between the strains, each sample was diluted in fresh LB to an OD_{600nm} of 0.2 immediately before the addition of compound. Increased sensitivity was evident in all the mutants, correlating with the loss of sugar residues in the LPS structure and corresponding increases in outer membrane permeability (Figure 28). When photoactivated at 8 μM, exposure to Compound **2** resulted in a 10-fold decrease in cell viability in the Δ*rfaG* knockout, suggesting that losing the outer core of LPS confers a relatively mild increase in compound penetration (Figure 28A). The Δ*rfaQ* knockout, which led to the complete removal of phosphate groups and the third heptose of the inner core, showed a more substantial decrease in viability, with a 10^4-fold reduction in CFU/mL following treatment activated Compound **2** (Figure 28A). This indicates that the inner core heptose fulfils an important role in denying entry to hydrophobic compounds. The final three mutants, Δ*rfaE*, Δ*rfaC*, and Δ*lpcA*, proved even more susceptible, to compound **2**, with Δ*rfaC* and Δ*rfaE* falling below the 100 viable cell detection limit (figure 28A). The results demonstrate that the antibacterial efficacy of Compound **2** is improved by easier access through the cell envelope, consistent with an inner membrane or cytosolic mode of action.

The BacLight assay was employed to visualise any real-time change in membrane integrity caused by Compound **2** in individual *E. coli* WT and an Δ*rfaC* mutant cells. A small number of the *E. coli* WT cells showed an increase in PI fluorescence in response to light activation of the compound (figure 28B). In contrast, all of the Δ*rfaC* cells stained with PI (figure 28B) following photoactivation of Compound **2**, indicative of rapid loss of membrane integrity and cell death. Additionally, the *ΔrfaC* cells were noticeably larger both before and after compound activation. This increase in size may be attributed to stress induced by the dark toxicity of

Compound **2** or could be a result of the deep rough phenotype, which is characterised by the loss of outer core LPS (190). Collectively, these results demonstrate that mutations that result in a decrease in outer membrane permeability significantly enhance the antibacterial activity of Compound **2**, and therefore it is the outer membrane that is likely protective against Compound **2** toxicity in all Gram-negative bacteria assayed in Chapter 3 (Table 4).

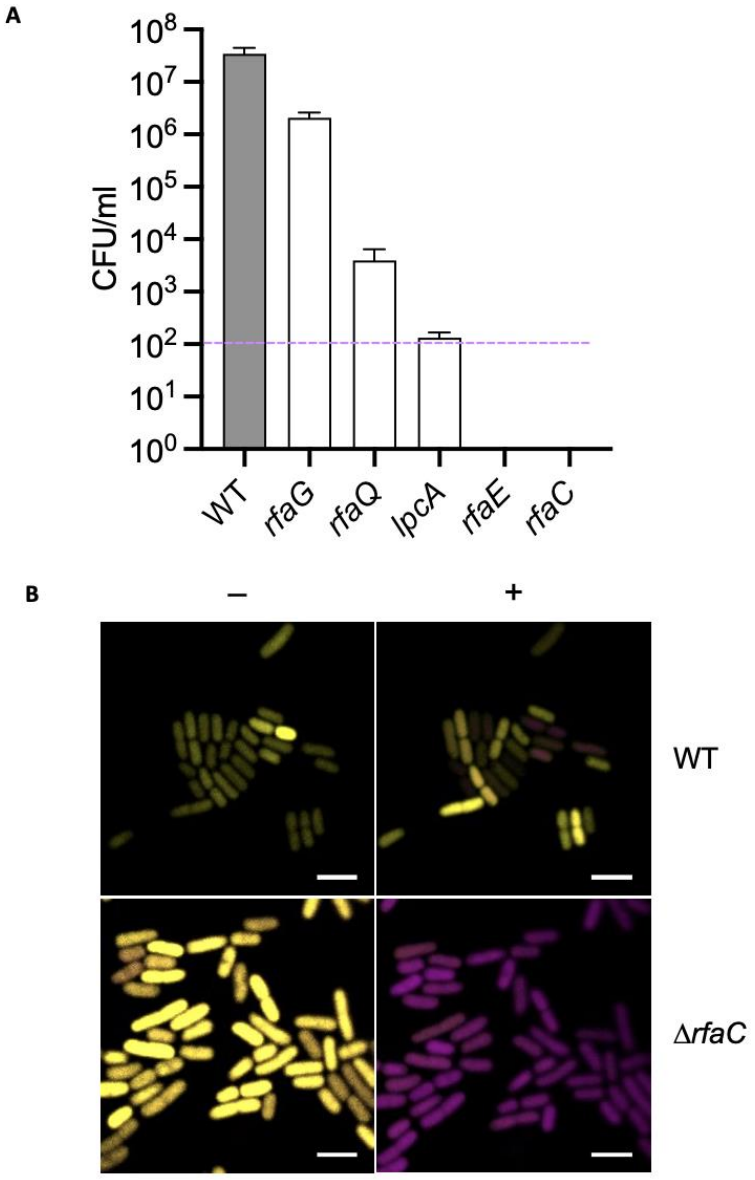

Figure 28. Susceptibility of *E. coli* strains with deficiencies in LPS biosynthesis. (**A**) Viability of bacteria exposed to Compound **2** (8 µM) activated by 365 nm light. Serial dilutions of bacteria were spotted onto LB agar plates, incubated at 37°C for 16 h and colonies counted to determine CFU/mL. Values represent the mean and standard error of three independent experiments. Purple line represents the 100 cell detection limit (**B**) Baclight assay showing the displacement of SYTO9 (yellow) and uptake of PI (magenta) before (–) and 10 min after (+) activation of Compound **2** (2 µM) in WT and Δ*rfaC* strains. The scale bar represents 3 µm.

5.2.3 Effect of Compound 2 on *E. coli* mutants with defects in efflux and passive transport

In addition to the limited permeability of the Gram-negative outer membrane, many Gram-negative bacteria possess complex efflux pumps that effectively expel toxic hydrophobic compounds from the cytoplasm (196). To determine the role of active and passive removal of Compound **2** from the cell, five *E. coli* mutants, Δ*tolC*, Δ*nhaA*, Δ*ompC*, Δ*acrA* and Δ*tatB*, lacking efflux components or transport systems were assessed.

TolC functions as the outer membrane component of the AcrAB-TolC pump, facilitating removal of hydrophobic compounds from the periplasm to the extracellular environment (197). The Δ*tolC* mutant exhibited the least susceptibility among the tested mutants, although it still showed a 10-fold decrease in viability when exposed to photoactivated Compound **2** (Figure 29). This suggests that the presence of Compound **2** in the periplasmic space is moderately toxic. Strains lacking the OmpC outer membrane porin and the NhaA Na^+/H^+ antiporter both displayed an approximately 100-fold increase in susceptibility when treated with light-activated Compound **2** (Figure 29). OmpC forms a passive diffusion channel in the outer membrane for small molecules (198) and the increased susceptibility indicates a role for passive removal of compound from the periplasmic space. NhaA regulates intracellular pH by importing H^+ (199) and may suggest an increase in Compound **2** effectiveness in an alkaline environment, potentially due to increased compound hydrophobicity at a higher pH.

Strains lacking AcrA, the key component of the AcrAB-TolC efflux pump, and TatB, an essential part of the Twin-Arginine-Translocation (TAT) pathway responsible for transport of pre-folded proteins across the cytoplasmic membrane (200), both showed a 10^5-fold decrease in viable

cells when exposed to activated Compound **2** (figure 29). The tripartite AcrAB-TolC efflux pump is responsible for the non-specific efflux of a variety of hydrophobic dyes, detergents and antibiotics from the cytoplasm to the extracellular milieu (201). The inability to fully assemble this pump compromises the cell's capacity to expel antimicrobial compounds from the cytoplasm and consistent with toxicity associated with Compound **2** entry into the cytoplasm. The susceptibility of the Δ*tatB* knockout implies Compound **2** damages proteins which are subsequently exported by this pump when available, its involvement in exporting folded proteins needed for compound tolerance. Taken together, the results suggest that Compound **2** can be internalised even in strains with fully intact outer membranes, and hint at an important role for compound export from the cytosol for *E. coli* tolerance.

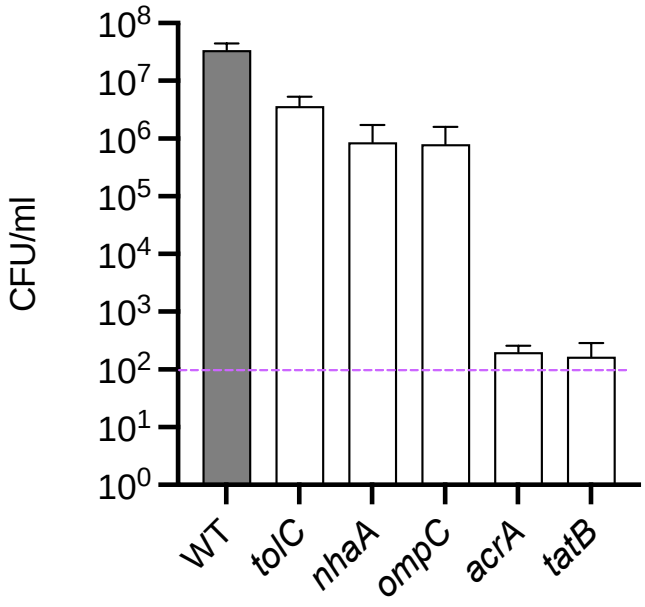

Figure 29. Susceptibility of *E. coli* strains deficient in efflux and passive transport pathways. *E. coli* WT and mutants were exposed to Compound **2** (8 µM) and exposed to 365 nm light. Serial (10-fold) dilutions of bacteria were applied to the surface of LB agar plates, incubated at 37°C for 16 h and colonies counted to determine CFU/ml. Values represent the mean and standard error of three independent experiments.

5.2.4 Effect of Compound 2 on *S. aureus* and *E. coli* mutants with defects in oxygen radical detoxification

The proposed mode of action of the photoactivatable Compound **2** is via the production of toxic ROS (140). *S. aureus* strains lacking $O^{2\bullet-}$ detoxifying enzyme superoxide dismutases SodA and SodM were found to be more susceptible to the effects of activated Compound **2** (figure 18). To further investigate the role of oxygen radicals in Compound **2** toxicity, a series of *E. coli* mutants defective in various ROS detoxifying pathways were tested.

The mutants Δ*ahpC* and Δ*oxyR* showed no greater susceptibility to activated Compound **2** than the WT strain (figure 30). AhpC, in conjunction with AhpF (174), detoxifies hydrogen peroxide and organic hydroperoxides. The absence of increased susceptibility in the Δ*ahpC* strain suggests that peroxides are not a significant product of Compound **2** activation. OxyR regulates, via a conformational change induced following oxidation by H_2O_2, the expression of a number of antioxidant genes, including the catalase *katG* and *ahpC* (202). The lack of increased susceptibility in the Δ*oxyR* mutant suggests that the expression of genes activated by OxyR are not essential for tolerance or that toxicity rapidly overwhelms the cell meaning that elevated levels are insufficient for recovery (figure 30).

The Δ*gshA* knockout experienced a 100-fold decrease in viability following compound activation (figure 30). GshA is required for the biosynthesis of the antioxidant glutathione and the knockout strain is known to be more sensitive to a range of oxygen radicals (203). The genes *sodA* [Mn], *sodB* [Fe], and *sodC* [Zn-Cu] encode metalloenzymes that detoxify superoxide by converting it into the less toxic H_2O_2 and O_2. Each enzyme is distinguished by

its metal cofactor and the latter differs in its cellular location. SodC is located in the periplasm (204), and the lack of susceptibility of the knockout suggests that the majority of ROS damage from Compound **2** photoactivation is confined to the cytosol (figure 30). The two cytosolic SODs, SodA and SodB, showed significant reductions in cell viability, 10^3 and 10^2-fold, respectively (figure 30), indicating that superoxide production in the cytosol is a key feature of compound activation, with *E. coli* SOD activities being critical for tolerance. This reinforces the previous data in chapter 4 showing increased susceptibility of the *S. aureus ΔsodAM* mutant (figure 18).

Finally, the Δ*katG* mutant exhibited a dramatic increase in susceptibility, with a 10^5-fold decrease in viable cells in response to light-activation of Compound **2** (Figure 30). KatG is a catalase that detoxifies cytosolic H_2O_2 by catalysing the donating of $2H^+$ to convert H_2O_2 into $2H_2O$ (205). This increased susceptibility highlights the importance of catalase activity and supports the evidence for H_2O_2 production, either directly from photoactivation or as a byproduct of SOD activity. Overall, these results support the prediction that Compound **2** activation leads to the production of intracellular ROS and significant cytotoxicity if appropriate detoxification pathways are unavailable.

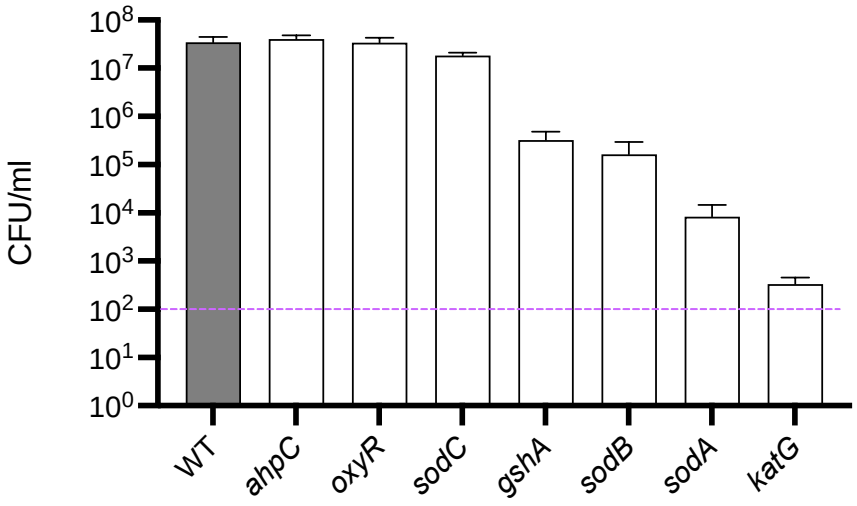

Figure 30. Susceptibility of *E. coli* strains deficient in ROS detoxification pathways. *E. coli* strains were exposed to Compound **2** (8 µM) and exposed to 365 nm light. Serial dilutions of bacteria were spotted onto LB agar plates, incubated at 37°C for 16 h and colonies counted to determine CFU/mL. Values represent the mean and standard error of three independent experiments.

5.2.5 Effect of Compound 2 on *E. coli* mutants defective in DNA repair pathways

To further establish that the photoactivation of Compound **2** leads to DNA damage, I assayed a small number of additional *E. coli* mutants with specific defects in oxidative damage repair (Δ*mutT* and Δ*mutM*) and recombinational repair of DNA breaks (Δ*recA*).

The genes *mutT* and *mutM* prevent GC to AT transversions by avoidance or repair of oxidatively damaged guanine bases, notably 8-oxo-7,8-dihydro-2'-deoxyguanine (8-OxodG). MutT hydrolyses 8-oxo-dGTP to 8-oxo-dGMP, preventing its misincorporation by DNA polymerases by removal from the nucleotide pool (206), while the DNA glycosylase MutM recognises and removes any incorporated 8-oxo-dG before it can mispair with adenosine (207). Meanwhile, RecA is required for homologous recombination and is necessary for double-stranded DNA break repair arising from single and double-strand breaks generated by oxygen radicals (208).

The Δ*recA* strain displayed a 10^4-fold reduction in viability following treatment with Compound **2**, confirming that chromosomal DNA breaks must be generated following photoactivation (figure 31). Δ*mutT* and Δ*mutM* both displayed a 10^5-fold reduction when exposed to light with Compound **2** (figure 31). The results again support the production of significant amounts of ROS following compound activation that drives the oxidation of guanine to 8-OxodG. The susceptibility of these knockouts suggests cytosolic ROS production by the activated compound causes significant oxidative damage to both nucleotides and chromosomal DNA.

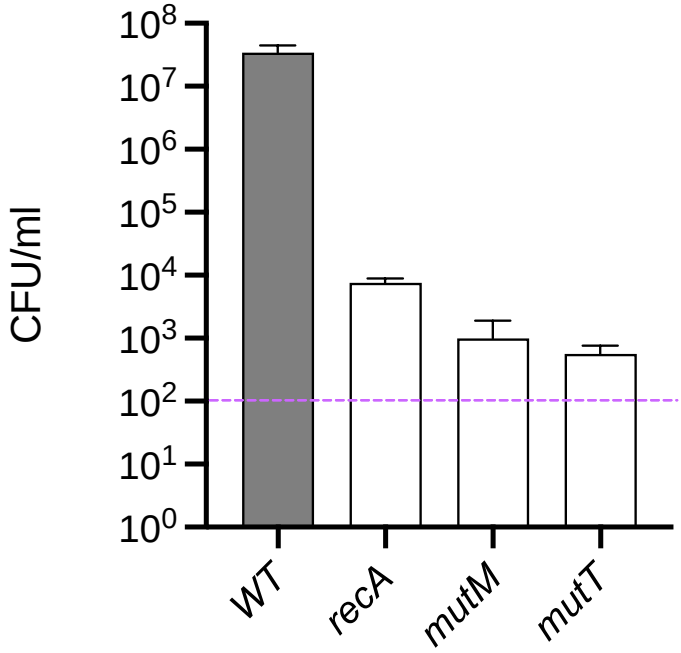

Figure 31. Susceptibility of *E. coli* strains deficient in DNA repair pathways. *E. coli* strains were exposed to Compound **2** (8 µM) and exposed to 365 nm light. Serial dilutions of bacteria were spotted onto LB agar plates, incubated at 37°C for 16 h and colonies counted to determine CFU/mL. Values represent the mean and standard error of three independent experiments.

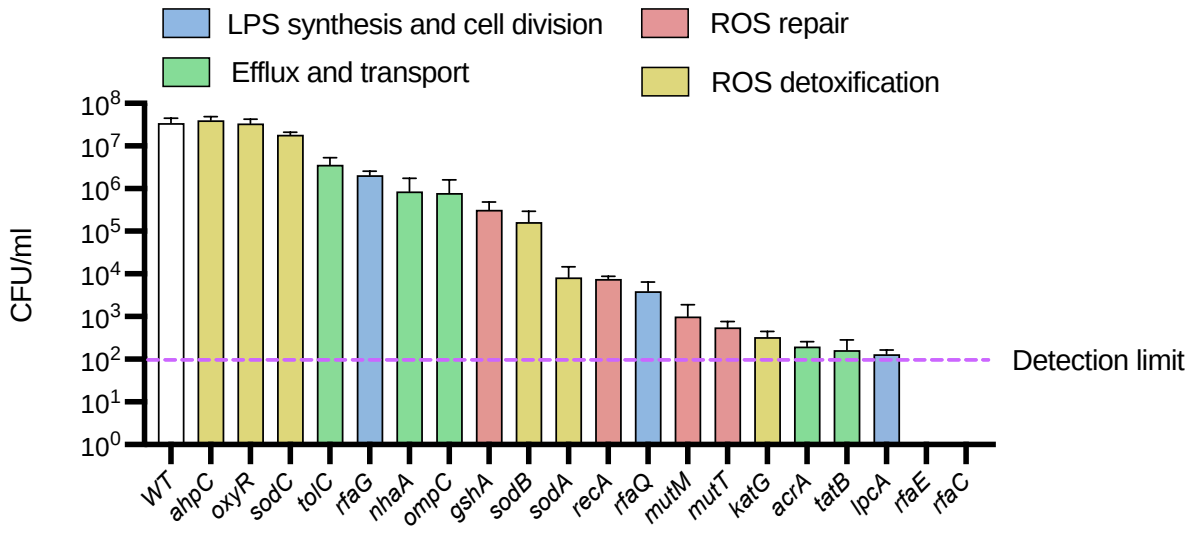

Figure 32. Summary of all *E. coli* knockout mutants. *E. coli* strains were incubated with 8 µM Compound **2** and exposed to 365 nm light for 5 min, with serial (ten-fold) dilutions applied to agar plates and CFU/ml calculated. Viability of each strain was plotted from least to most susceptible and each strain colour coded based on function

5.2.6 Intracellular oxidative stress detection in *E. coli* cells lacking catalase activity

The experiments described above provide strong evidence for the entry of Compound **2** into the *E. coli* cytosol even in cells with an intact outer membrane. They also support the notion that large amounts of ROS are produced upon compound excitation with light at 365 nm. To further confirm the presence of cytosolic oxidative stress following compound activation, CellRox fluorescence as a redox indicator was visualised by confocal microscopy. *E. coli* WT and *ΔkatG* strains were grown to mid-log phase and treated with Compound **2** in the presence of the CellRox dye, as described in the materials and methods, and then imaged.

Cells lacking KatG displayed a dramatic increase in fluorescence following activation in the presence of Compound **2**, while no such increase was detected in a DMSO control exposed to light (figure 33A). This suggests that both the compound and light are necessary for ROS production detected by the CellRox dye. In addition, the Δ*katG* mutant displayed a significant increase in CellRox fluorescence relative to the WT upon compound activation (figure 33B), indicative of the production of H_2O_2 following activation and sugesting a critical role for catalase in detoxifying these species. Together with the viability data, these experiments indicate that a surge of ROS, probably H_2O_2, is released following activation, which generates oxidative stress if not detoxified or the damage repaired.

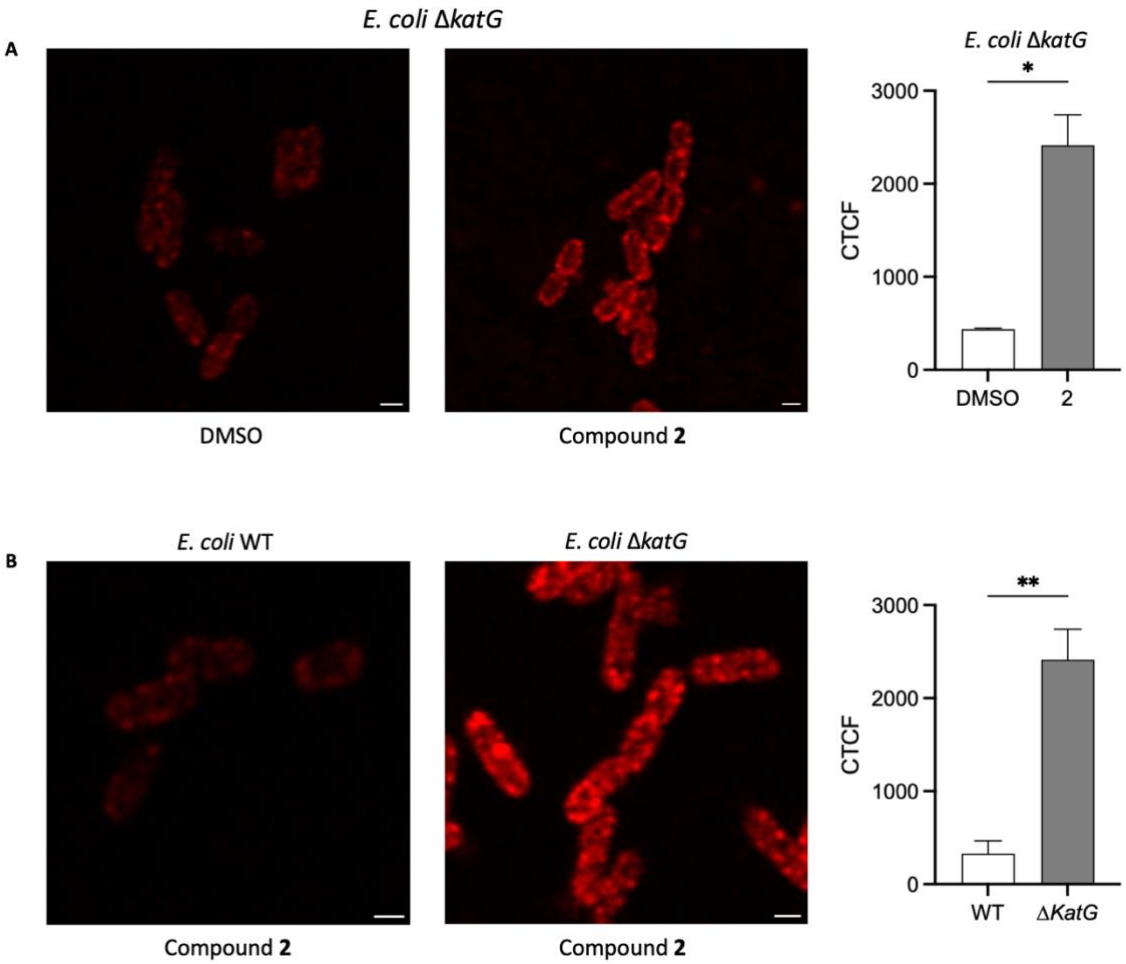

Figure 33. Production of intracellular oxidative stress in bacteria lacking catalase activity. *E. coli* WT and Δ*katG* strains were grown to mid-log phase in the presence or absence of Compound **2** and CellRox, exposed to 365 nm light then fixed and imaged via confocal microscopy, with fluorescence from 3 technical replicates captured before the background fluorescence was removed to give the CTCF, an unpaired t-test was performed to quantify CTCF significance between samples **A.** CellRox fluorescence of Δ*katG* in the presence of 0.8% DMSO or 8 µM Compound **2**, both exposed to 365 nm light before fluorescence was quantified **B.** Comparison of CellRox fluorescence of *E. coli* WT and Δ*katG* cells upon treatment with light-activated Compound **2** (8 µM).

5.4 Discussion

The primary objective of the experiments described in this chapter was to clarify the role of LPS as a permeability barrier to the entry of Compound **2**. As components of the LPS structure are removed by specific mutations, the permeability of the outer membrane to hydrophobic compounds is known to increased be increased (190). Enhanced compound **2** penetration and greater susceptibility, was notably apparent with Δ*rfaE*, Δ*rfaC*, and Δ*lpcA* mutant strains, which correlates with the greatest truncations in the LPS structure and, consequently, the highest permeability (figure 28A).

Despite the increased susceptibility in the LPS defective strains, cells with a fully intact outer membrane also showed enhanced vulnerability when other critical cellular functions were compromised. While the outer membrane serves as a barrier, efflux pumps such as AcrAB-TolC are crucial for actively expelling hydrophobic antimicrobial compounds from the cytoplasm (209) and this was also true of sensitivity to the photoactivated Compound **2** (figure 29). The findings here are supportive of entry of Compound **2** into the *E. coli* cytosol. The hypersusceptibility of both the Δ*acrA* and Δ*tatB* knockouts indicates a fine balance between the cell's ability to restrict compound entry and its capacity to remove accumulated compound once it has gained entry. Mutants deficient in either pathway showed a significantly increased susceptibility (figure 28, 29), highlighting a tolerance that is precariously balanced at this concentration. This observation also accounts for the increased susceptibility at 16 µM, where wild-type *E. coli* cannot effectively remove the compound that accumulated in the cytoplasm.

In addition to maintaining an appropriate level of Compound **2** export that allows tolerance, there is an additional requirement for capacity to detoxify ROS released upon activation,

particularly superoxide and hydrogen peroxide (figure 30). Once photoactivated, cytoplasmic ROS is generated by the compound that leads to significant oxidation of free nucleotides and those incorporated in the genome. Cells deficient in the repair the resultant DNA damage exhibit dramatically increased susceptibility and are consistent with chromosomal breaks and oxidatively damaged bases (figure 31).

Taken together, the susceptibility of the *E. coli* mutants reveals a mechanism where Compound **2** enters the cytoplasm, possibly circumventing the LPS barrier using non-specific outer membrane porins. If sufficient compound accumulates, subsequent photoactivation leads to the production of ROS. This generates substantial DNA damage, and presumably also oxidative damage to nearby proteins and lipids, that can be lethal if left unrepaired. *E. coli* relies on a complex array of defence mechanisms to tolerate activated Compound **2**, with the removal of any single function resulting in a substantial reduction in viability.

Chapter 6 Discussion

6.1 Introduction

This study aimed to determine which, if any, of LightOx's novel photosensitisers have antimicrobial activity in a range of species and to investigate the mechanisms of action by which selected compounds work. This work focused in particular on Compound **2** that was effective in inhibiting growth and eliminating a range of species, including some of the clinically relevant ESKAPE pathogens and bacteria resistant to common antibiotics. The study also investigated if *S. aureus* develops resistance to photoactivated Compound **2** after repeated subculturing with a sub-lethal treatment concentration. Additionally, the study explored the mechanism of action of Compound **2** upon photoactivation, focusing on the production of ROS and the differing susceptibilities of Gram-positive and Gram-negative bacteria in relation to the localisation of Compound **2**. The findings demonstrated the potential of Compound **2** as a therapeutic agent against clinically relevant Gram-positive bacteria and provided insights into its mechanism of action of ROS production leading to DNA damage.

6.2 Summary of Key Findings

The first results chapter screened a library of LightOx compounds, establishing the efficacy of Compound **2** against various Gram-positive bacteria, including those resistant to conventional antibiotics. Notably, no resistance developed after repeated subculturing, suggesting that compound **2** has potential as a therapeutic agent against clinically relevant pathogens. The majority of the work is published in *Frontiers in Microbiology.*

The second results chapter focused on the production of ROS upon activation of Compound **2** with 365 nm light, indicating that a type I or type III photoreaction is the most likely mechanism for ROS generation. It was suggested that internalisation of the compound is necessary for susceptibility in Gram-positive bacteria, with internalisation of compound bound membrane suggested as a mechanism by which Compound **2** is internalised in *B. subtilis*.

Finally, the third results chapter highlighted the differential susceptibility of Gram-positive versus Gram-negative bacteria and confirmed the role of LPS in tolerance to Compound **2**, Gene knockout studies were also employed to elucidate the roles of compound efflux and the balance between ROS detoxification and repair of subsequent DNA damage following activation.

6.3 Compound 2 effectively eliminated clinically relevant Gram–positive bacteria

Compound **2** was identified as the most effective compound screened, capable of inhibiting the growth of Gram-positive bacteria at concentrations as low as 0.1 µM (Figure 5). Activation at 2 µM resulted in a 10^6-fold decrease in viable cells of *S. epidermidis* and *B. subtilis* (Figure 12). Cell killing occurred rapidly, with full PI uptake within 10 minutes of activation (Figure 15), indicating a rapid cytotoxic effect likely due to an overwhelming surge of ROS produced following photoactivation.

Additionally, the ESKAPE pathogen *E. faecalis* exhibited the same susceptibility as *S. epidermidis* and *B. subtilis*, with MBC values of 0.25 µM (Table 4). Typically, pathogenic bacteria are more resilient to oxidative stress than their non-pathogenic counterparts (210), as noted in the case of *S. aureus*, which had an MBC value of 1 µM (Table 4). This increased

tolerance in *S. aureus*, that was not mirrored in *E. faecalis*, may be attributed to the presence of staphyloxanthin (STX), a carotenoid that gives the bacterium its golden colour and serves as a virulence factor by functioning as an antioxidant (211).

Research has shown that STX confers resistance to oxidative stress and protects against ROS-mediated killing by host neutrophils (212). Therefore, the presence of STX may mitigate oxidative stress following the photoactivation of Compound **2** by scavenging some of the ROS produced, thereby increasing tolerance to the compound. Experiments with strains lacking this biosynthetic pathway could provide further insight into the protective role of pigments and the mechanism of action of Compound **2**.

6.4 Compound 2 displayed no difference in susceptibility against MRSA and tolerance did not develop following sub-lethal treatment

Unlike conventional antibiotics, which target specific sites, PDT operates through a non-specific mechanism. As a result, it was anticipated that Compound **2** could effectively overcome various resistance mechanisms. This was confirmed in assays with MRSA and MSSA, where no significant difference in susceptibility was observed following the photoactivation of Compound **2** (Figure 16A). Since the methicillin resistance in the USA300 strain is due to a modified PBP, this alteration was unlikely to impact the efficacy of Compound **2** as the PS does not require tight binding to an enzyme to produce ROS, allowing it to function effectively despite the modification.

While the potential of Compound **2** to eliminate resistant pathogens is promising, studying resistant mutants that significantly reduce bacterial susceptibility—such as those with a

multidrug-resistant (MDR) efflux pump—could offer valuable insights into its effectiveness against relevant resistance mechanisms.

Additionally, after 15 cycles of subculturing with 0.1 µM of activated Compound **2**, no increased tolerance was observed (Figure 17 A,B). In contrast, the ampicillin control exhibited significant resistance after just 9 cycles of treatment (Figure 17,D). This suggests that Compound **2** holds promise in preventing tolerance development in Staphylococcus aureus. However, it's important to note that tolerance to PDT can occur. For instance, Rapacka-Zdonczyk et al. demonstrated significant tolerance to the PS Rose Bengal when activated with 515 nm light after 10 cycles of treatment. Moreover, DNA damage resulting from ROS production can lead to an increased mutation rate due to the stimulation of the mutagenic SOS response (109). Gene knockouts in *E. coli* indicated that photoactivated Compound **2** caused DNA damage, as strains unable to repair this damage showed significantly increased susceptibility (Figure 31).

The apparent lack of DNA damage in *S. aureus* may be due to two possible factors: either the mechanism of action differs from that in *E. coli*, resulting in no DNA damage after photoactivation, or the concentration used during sub-lethal subculturing was not sufficient to induce mutations. Sub-lethal treatment is defined as a concentration that leads to a 10^1 to 10^3 fold reduction in cell viability (157). To explore this further, future assays should utilise a concentration of 0.25 µM, which has been shown to reduce cell viability by 10^2-fold following photoactivation (Figure 16A). This adjustment may increase the selection pressure and provide insights into whether tolerance develops.

6.5 Growth assays are not an effective method of assessing Compound 2 activity.

Growth assays, particularly MIC assays, are commonly used to evaluate the effectiveness of antimicrobial compounds and assess resistance. In contrast to typical antibiotics, which exert a continuous effect on bacteria, PS operate differently, exhibiting two distinct toxicity profiles, dark toxicity and light toxicity.

In the case of Compound **2**, there was a notable difference between the dark and light toxicity profiles (Figure 12). Compound **2** was only active for the first 5 minutes during growth assays. ROS, which cause damage upon activation, are inherently short-lived, meaning that any damage likely occurs shortly after activation before the ROS dissipate. As a result, cells that survive this initial exposure then contend only with the compound's dark toxicity. Since this dark toxicity is significantly lower, surviving cells can repair damage and grow in a relatively non-toxic environment.

Once these cells resume logarithmic growth, they can re-seed the population and rapidly increase in number. This led to a situation where MIC values were considerably higher than MBC values for Gram–positive bacteria following Compound **2** activation (figures 13,16). Given that photoactivation of Compound **2** led to rapid cell death, measuring cell death using MBC assays provided a more effective method for quantifying the effects of Compound **2** on bacteria.

6.6 Internalisation of Compound 2 is required for effective toxicity

Upon visualisation of Compound **2**, membrane fluorescence was observed exclusively in Gram-negative bacteria, while internal aggregates were detected in Gram-positive bacteria,

indicating internalisation. This difference in susceptibility suggested that increased internalisation of Compound **2** occurred in Gram-positive bacteria. The LPS layer of the outer membrane served as a barrier to hydrophobic molecules, limiting their entry into the cytoplasm (155). In *E. coli*, the removal of LPS components demonstrated a direct correlation between membrane permeability and susceptibility (Figure 28), highlighting the protective role of the outer membrane against the toxicity of Compound **2**.

Notably, the removal of AcrA, an essential component of the tripartite ArcAB-TolC efflux pump, resulted in a significant increase in susceptibility, indicating that Compound **2** penetrated the cell cytoplasm even in the presence of intact LPS. However, the removal of LPS greatly enhanced internalisation. Furthermore, cytosolic ROS detoxification pathways, such as KatG, SodA, and SodB, exhibited increased susceptibility at 8 µM (figure 30), suggesting that the accumulation of Compound **2** in the cell cytosol was a critical factor for toxicity. Internalised Compound **2** likely generated ROS, leading to the formation of lethal DNA lesions upon photoactivation. This was supported by proteomic data in *S. aureus*, which showed increased expression of DNA repair enzymes and cytosolic antioxidative systems following activation with 1 µM Compound **2** (Table 6).

While lipid peroxidation is a well-documented target of PDT in eukaryotes (213), the presence of poorly oxidisable saturated and monounsaturated lipids, which predominantly characterise bacterial membranes (93), raised questions about its occurrence in bacteria. Future experiments investigating lipid peroxidation following the photoactivation of Compound **2** would be valuable for determining whether the compound causes damage at the membrane level or if cellular damage is primarily confined to cytosolic components.

6.7 Membrane bound compound is internalised in *B. subtilis*

In *B. subtilis*, Nile red, known to fluoresce strongly in the presence of membranes and lipid droplets (176), was shown to strongly colocalise with Compound **2** (figure 23), providing evidence that Compound **2** localised to bacterial lipids. Furthermore, *B. subtilis* grown in a low-stress environment with ample oxygen and nutrients showed no lipid aggregates when imaged with Nile red. However, the addition of Compound **2** resulted in the formation of aggregates (figure 24). *B. subtilis* produces these irregular membrane domains in response to stress (178).

The fluorescently tagged membrane-bound protein WALP-23 exhibited strong colocalisation with Compound **2** after incubation, displaying intracellular fluorescence (figure 25). This suggested that the adherence of Compound **2** to the membrane of Gram-positive bacteria leads to membrane depolarisation, resulting in the formation of aggregates that pull portions of the membrane, along with Compound **2**, into the cytosol, this proposes a mechanism by which compound is internalised in Gram–positive bacteria.

6.8 Bacteria are eliminated by a type 1 or type 3 ROS based mechanism following photoactivation

The knockout studies revealed that strains deficient in ROS detoxification pathways exhibited increased susceptibility to photoactivated Compound **2** (figure 30). Both *S. aureus* and *E. coli* lacking SOD activity showed heightened sensitivity to Compound **2**, providing evidence of $O^{2\bullet-}$ production following its photoactivation. $O^{2\bullet-}$ is a key component of both type 1 and type 3

photoreactions , involving electron transfer to oxygen. The primary distinction between type 1 and type 3 reactions lies in their dependency on oxygen. Type 1 reactions are oxygen-dependent, involving the transfer of electrons or hydrogen to molecular oxygen. In contrast, type 3 reactions facilitate the direct transfer of electrons or hydrogen to the target substrate, removing the requirement for molecular oxygen (77, 214). Additionally, *E. coli* deficient in catalase activity demonstrated a dramatic increase in susceptibility and elevated intracellular oxidative stress after photoactivation (figure 30). This suggested the presence of H_2O_2, although it remains unclear whether H_2O_2 is produced directly through hydrogen donation to molecular oxygen upon activation or solely as a byproduct of superoxide dismutation. Regardless, these findings are consistent with a type 1 or type 3 mechanism of ROS production leading to superoxide formation following activation.

The observed DNA damage indicated the production of •OH radicals, which are known to damage DNA (84). The upregulation of catalase and the thioredoxin system in *S. aureus* after treatment with Compound **2** suggests that the bacteria attempted to detoxify H_2O_2, as H_2O_2 reacts with free iron in the cell to produce •OH radicals, resulting in widespread damage to vital cellular components (215).

Further experiments aimed at identifying the specific reactive species generated would be valuable. The mechanism of DNA damage implies •OH radical production; thus, using dyes to detect these radicals could confirm their presence. Additionally, employing chelators to scavenge free iron may help reduce the rate of the Fenton reaction, providing further insight into •OH radical production following the photoactivation of Compound **2**. Finally, viability experiments with Compound **2** conducted in the absence of oxygen will help clarify whether

Compound **2** operates through an oxygen-dependent type 1 mechanism, an oxygen-independent type 3 mechanism, or a combination of both.

6.9 Implications for Clinical Applications

The successful demonstration of Compound **2**'s efficacy against resistant Gram-positive strains has significant clinical implications. As antibiotic resistance becomes an increasingly pressing global health issue, alternative therapeutic strategies like PDT offer effective solutions. The ability of Compound **2** to eliminate resistant bacteria while minimising the spread of resistance is particularly advantageous in the fight against infectious diseases.

Given the requirement for light activation, most photosensitisers are primarily used for treating wounds or dental plaque. Compound **2** could serve this purpose, given its effectiveness at eliminating *S. aureus*, the most common coloniser of wounds (216). Therefore, future work should include the development of wound models, utilising either synthetic skin models capable of supporting bacterial growth or animal models to better assess the therapeutic potential of Compound **2**.

Additionally, Compound **2** can be modified through the attachment of a targeting molecule to the free amine group. By attaching an antibody that specifically targets protein A of *S. aureus*, it may be possible to develop a derivative of Compound **2** with improved specificity for *S. aureus*, thereby enhancing its efficacy as a wound treatment. It may also be feasible to include an excipient when applying Compound **2**, such as EDTA, which has been shown to increase the permeability of cell membranes. This could improve the efficacy of Compound **2**

6.10 Future work – elucidation of the mechanism

This thesis offered insights into the mechanism of Compound **2**, particularly highlighting the roles of compound internalisation and the subsequent production of ROS, likely through a type 1 reaction, upon activation. However, the exact mode of action remains unclear. Due to the non-specific nature of PDT, it is improbable that a single cellular target can be pinpointed. However, Further research could elucidate which ROS are generated during photoactivation and the cellular targets.

The only dye used to measure ROS in this thesis focused on oxidative stress rather than identifying specific species. To better characterise the ROS produced, employing dyes such as hydroethidine (HE) for detecting superoxide radicals (217) or hydroxyphenyl fluorescein (HPF) for hydroxyl radicals (218) may be beneficial. However, these dyes have specificity issues, other radicals and high-valence metal ions can oxidise them, potentially leading to misidentification of the radicals involved (219).

While DNA repair knockouts have shed light on DNA damage caused by activation of Compound **2** (figure 30), it remains uncertain whether Compound **2** also inflicts damage on proteins or lipids. Dyes like BODIPY could be utilised to assess lipid peroxidation (220), while 2,4-dinitrophenylhydrazine (DNPH) has proven effective in measuring protein carbonylation (221), and could help evaluate protein oxidation following the activation of Compound **2**.

6.11 Future work – Biofilms

While Compound **2** has shown effectiveness against various bacterial species, the experiments conducted used cells in the logarithmic growth phase cultivated in fresh media. In natural environments, however, bacteria do not continuously exist in nutrient-rich conditions. Instead, they often form biofilms, which are clusters of connected cells adhered to each other or to surfaces, encased in an extracellular matrix composed of proteins, carbohydrates, and extracellular DNA (eDNA) (222).

Biofilm-associated infections are prevalent and exhibit increased tolerance to antimicrobials (223). This tolerance arises from the EPS that limits drug access and the varied metabolic states of cells within the biofilm. In nutrient-depleted zones, dormant cells emerge that are less susceptible to antibiotics which target actively dividing cells (224).

Future experiments should investigate the effects of Compound **2** photoactivation on biofilm formation and disruption. It is crucial to determine whether biofilm infections demonstrate greater tolerance to Compound **2**. Additionally, studies could explore the potential of Compound **2** to disrupt the EPS, facilitating antibiotic penetration and allowing for possible co-treatment strategies. This approach has previously been shown to effectively clear biofilm infections caused by *S. aureus* and *P. aeruginosa* using amoxicillin coated gold nanoparticles (225)

6.12 Future work – elimination of cutaneous mycobacteria

Given its potential as a wound care treatment, Compound **2** could effectively address challenging *mycobacterial* infections, particularly cutaneous infections caused by *M.*

tuberculosis and *M. leprae*. *Mycobacteria* exhibit intrinsic resistance to many antibiotics due to their thick, lipid-rich cell envelope, enzymatic inactivation systems, and the presence of multi-drug efflux pumps (226). Moreover, *M. tuberculosis* can rapidly develop resistance to antibiotics designed to target it (227), highlighting the urgent need for alternative treatments.

Photodynamic therapy (PDT) has demonstrated effectiveness against *mycobacteria* (228). The lipophilic nature of Compound **2** suggests that it can readily adhere to the lipid rich *mycobacterial* membrane. Additionally, attaching trehalose—a sugar that is actively incorporated into the inner membrane of *mycobacteria* (229), to the amine moiety of Compound **2** could enable selective targeting of these pathogens. The attachment of trehalose has been shown to enhance the efficacy of photosensitisers (PS) against *M. tuberculosis* (229), suggesting that Compound **2** could be developed into an effective PS for treating *mycobacterial* infections, addressing a significant medical challenge.

6.13 Concluding Remarks

In conclusion, this research described a novel photosensitiser, Compound **2**, capable of eliminating clinically relevant Gram–positive infections via the production of ROS following photoactivation. Key aspects of the mechanisms of action and differences in susceptibility between bacterial groups were determined, this study lays the groundwork for the development of Compound 2 as an effective wound treatment, particularly in the face of rising antimicrobial resistance

Appendix

Gene name	Name	fold change	P value
Q2FZC2_STAA8	Fibrinogen-binding protein	0.78	4.92
RL21_STAA8	Large ribosomal subunit protein bL21	0.64	3.69
RL3_STAA8	Large ribosomal subunit protein uL3	0.63	3.78
RL35_STAA8	Large ribosomal subunit protein bL35	0.59	4.22
RS12_STAA8	Small ribosomal subunit protein uS12	0.59	4.85
RL2_STAA8	Large ribosomal subunit protein uL2 1	0.57	3.40
RS16_STAA8	Small ribosomal subunit protein bS16	0.56	3.61
RS17_STAA8	Small ribosomal subunit protein uS17	0.53	2.98
RS3_STAA8	Small ribosomal subunit protein uS3	0.52	4.27
RL4_STAA8	Large ribosomal subunit protein uL4	0.52	3.56
RL28_STAA8	Large ribosomal subunit protein bL28	0.51	4.29
RL16_STAA8	Large ribosomal subunit protein uL16	0.50	3.11
RS13_STAA8	Small ribosomal subunit protein uS13	0.49	4.48
RS14Z_STAA8	Small ribosomal subunit protein uS14B	0.48	3.72
RL19_STAA8	Large ribosomal subunit protein bL19	0.48	2.64
RL15_STAA8	Large ribosomal subunit protein uL15	0.46	3.11
RL1_STAA8	Large ribosomal subunit protein uL1	0.45	3.71
RL20_STAA8	Large ribosomal subunit protein bL20	0.45	3.57
RL24_STAA8	Large ribosomal subunit protein uL24	0.45	3.00
ENO_STAA8	Enolase	0.44	4.44
RS11_STAA8	Small ribosomal subunit protein uS11	0.44	7.57
CATA_STAA8	Catalase	0.43	4.26
RL13_STAA8	Large ribosomal subunit protein uL13	0.43	2.94
RS18_STAA8	Small ribosomal subunit protein bS18	0.41	3.31
RL6_STAA8	Large ribosomal subunit protein uL6	0.41	3.49
RS5_STAA8	Small ribosomal subunit protein uS5	0.41	4.34
RS15_STAA8	Small ribosomal subunit protein uS15	0.41	1.99
RL23_STAA8	Large ribosomal subunit protein uL23	0.41	3.82
RS20_STAA8	Small ribosomal subunit protein bS20	0.37	2.78
Q2FZT7_STAA8	Signal peptidase I	0.37	3.72
RS21_STAA8	Small ribosomal subunit protein bS21	0.36	2.82
RS19_STAA8	Small ribosomal subunit protein uS19	0.35	4.22
GCSPB_STAA8	Probable glycine dehydrogenase (decarboxylating) subunit 2	0.32	2.09
RL17_STAA8	Large ribosomal subunit protein bL17	0.32	2.64
RNJ2_STAA8	Ribonuclease J 2	0.31	4.24
Q2FYT8_STAA8	Transketolase	0.30	3.29
Q2FXT7_STAA8	Preprotein translocase, YajC subunit	0.30	1.98
RS7_STAA8	Small ribosomal subunit protein uS7	0.30	2.44

Q2G046_STAA8	UvrABC system protein A	0.29	2.87
AHPF_STAA8	Alkyl hydroperoxide reductase subunit F	0.29	2.83
RL30_STAA8	Large ribosomal subunit protein uL30	0.28	2.05
RS4_STAA8	Small ribosomal subunit protein uS4	0.28	2.59
Q2G2A3_STAA8	Dihydrolipoyl dehydrogenase	0.28	5.87
RL14_STAA8	Large ribosomal subunit protein uL14	0.28	3.02
Q2FYY6_STAA8	Glutamine synthetase	0.27	3.43
Q2G2H4_STAA8	Beta sliding clamp	0.27	3.52
IF3_STAA8	Translation initiation factor IF-3	0.26	3.70
Q2G2A4_STAA8	Dihydrolipoamide acetyltransferase pyruvate dehydrogenase complex	0.26	4.36
RS9_STAA8	Small ribosomal subunit protein uS9	0.26	2.37
G6PI_STAA8	Glucose-6-phosphate isomerase	0.26	3.54
RPOB_STAA8	DNA-directed RNA polymerase subunit beta	0.25	5.94
RS2_STAA8	Small ribosomal subunit protein uS2	0.25	4.09
FABI_STAA8	Enoyl-[acyl-carrier-protein] reductase [NADPH] FabI	0.25	1.73
RL27_STAA8	Large ribosomal subunit protein bL27	0.25	3.07
RPOC_STAA8	DNA-directed RNA polymerase subunit beta	0.24	6.12
Q2FVW9_STAA8	Fe/B12 periplasmic-binding domain-containing protein	0.24	2.70
ARCA_STAA8	Arginine deiminase	0.23	1.73
Q2G2A5_STAA8	Pyruvate dehydrogenase complex, E1 component	0.23	3.35
Q2G1H0_STAA8	Indolepyruvate decarboxylase, putative	0.23	1.40
Q2G032_STAA8	Glyceraldehyde-3-phosphate dehydrogenase	0.23	3.66
RL18_STAA8	Large ribosomal subunit protein uL18	0.23	2.82
FTN_STAA8	Bacterial non-heme ferritin	0.23	2.24
RL11_STAA8	Large ribosomal subunit protein uL11	0.23	2.80
NDH_STAA8	Type II NADH:quinone oxidoreductase	0.22	1.90
Q2FZY6_STAA8	SUF system FeS cluster assembly SufBD N-terminal domain	0.22	2.13
FTHS_STAA8	Formate--tetrahydrofolate ligase	0.22	1.49
Q2FWD7_STAA8	Transcription termination factor Rho	0.22	2.99
Q2FWJ5_STAA8	S1 RNA binding domain protein	0.21	3.03
IF2_STAA8	Translation initiation factor IF-2	0.21	4.64
Q2FWB8_STAA8	Purine nucleoside phosphorylase DeoD-type	0.21	4.21
NDK_STAA8	Nucleoside diphosphate kinase	0.20	1.47
GYRA_STAA8	DNA gyrase subunit A	0.20	2.96
Q2G274_STAA8	DNA gyrase subunit B	0.20	2.44
RS8_STAA8	Small ribosomal subunit protein uS8	0.20	2.76
AHPC_STAA8	Alkyl hydroperoxide reductase C	0.20	3.80
RL9_STAA8	Large ribosomal subunit protein bL9	0.20	2.71
Q2FZG4_STAA8	Pyruvate dehydrogenase E1 component subunit alpha	0.19	3.00
Q2G041_STAA8	Thioredoxin reductase	0.19	2.34
Q2FXM1_STAA8	UspA domain-containing protein	0.19	2.22
Y851_STAA8	UPF0051 protein SAOUHSC_00851	0.18	2.97
DER_STAA8	GTPase Der	0.18	1.41
Q2G1R9_STAA8	Methionine--tRNA ligase	0.18	1.49
DHA2_STAA8	Alanine dehydrogenase 2	0.18	1.77

RL29_STAA8	Large ribosomal subunit protein uL29	0.17	1.32
ODO1_STAA8	2-oxoglutarate dehydrogenase E1 component	0.17	1.41
ACCA_STAA8	Acetyl-coenzyme A carboxylase carboxyl transferase subunit alpha	0.16	1.45
ATPF_STAA8	ATP synthase subunit b	0.16	2.66
GLPD_STAA8	Aerobic glycerol-3-phosphate dehydrogenase	0.15	1.55
IMDH_STAA8	Inosine-5'-monophosphate dehydrogenase	0.14	3.34
ADH_STAA8	Alcohol dehydrogenase	0.14	1.40
HCHA_STAA8	Protein/nucleic acid deglycase HchA	0.14	1.76
SYP_STAA8	Proline--tRNA ligase	0.14	2.43
FTSZ_STAA8	Cell division protein FtsZ	0.12	1.59
HSLU_STAA8	ATP-dependent protease ATPase subunit HslU	0.12	1.90
ALDH_STAA8	Putative aldehyde dehydrogenase	0.11	1.43
LDH2_STAA8	L-lactate dehydrogenase 2	0.10	2.26
KPYK_STAA8	Pyruvate kinase	0.10	3.06
ATPA_STAA8	ATP synthase subunit alpha	0.08	2.37

Appendix table 1. List of gene names, protein names and the relative upregulation and P value to the untreated control expressed as Log10 and -Log10 for fold change and P value respectively

gene name	Name	fold change	P value
ISAA_STAA8	Probable transglycosylase	-2.66	5.15
Q2FXI6_STAA8	Thioredoxin domain-containing protein	-2.58	4.38
IF1_STAA8	Translation initiation factor IF-1	-2.26	4.82
Q2G2M0_STAA8	Tautomerase	-2.06	4.11
Q2FZY4_STAA8	NIF system FeS cluster assembly NifU N-terminal domain	-1.97	4.61
Y444_STAA8	Nucleoid-associated protein SAOUHSC_00444	-1.92	3.59
Y845_STAA8	UPF0337 protein SAOUHSC_00845	-1.63	3.93
Q2G000_STAA8	Thioredoxin	-1.55	4.36
RSBW_STAA8	Serine-protein kinase RsbW	-1.54	3.30
RPOE_STAA8	Probable DNA-directed RNA polymerase subunit delta	-1.50	3.66
Q2G298_STAA8	Ribosomal silencing factor RsfS	-1.46	3.38
YQGF_STAA8	Putative pre-16S rRNA nuclease	-1.36	4.31
LUKL2_STAA8	Uncharacterized leukocidin-like protein 2	-1.34	2.63
Q2G029_STAA8	2,3-bisphosphoglycerate-independent phosphoglycerate mutase	-1.26	5.93
Q2FX90_STAA8	Glucosamine-6-phosphate isomerase	-1.25	3.39
Q2FV27_STAA8	PhnB-like domain-containing protein	-1.21	4.81
HPS_STAA8	3-hexulose-6-phosphate synthase	-1.15	4.22
XPT_STAA8	Xanthine phosphoribosyltransferase	-1.14	3.85
THIO_STAA8	Thioredoxin	-1.12	4.08
PYRR_STAA8	Bifunctional protein PyrR	-0.91	3.02
Q2FZG6_STAA8	Peptide deformylase	-0.90	1.95
SSAA2_STAA8	Staphylococcal secretory antigen ssaA2	-0.90	3.90
CODY_STAA8	Global transcriptional regulator CodY	-0.84	4.72
Y675_STAA8	Probable transcriptional regulatory protein SAOUHSC_00675	-0.84	2.96
Q2G276_STAA8	Uncharacterized protein	-0.82	1.54
PPI1_STAA8	Putative peptidyl-prolyl cis-trans isomerase	-0.81	3.96
RL332_STAA8	Large ribosomal subunit protein bL33B	-0.80	4.72
EFP_STAA8	Elongation factor P	-0.78	3.08
Q2G077_STAA8	ribonucleoside-diphosphate reductase	-0.75	1.93
Q2G2D2_STAA8	Transcription termination/antitermination protein NusA	-0.74	2.64
Q2FYF5_STAA8	(d)CMP kinase	-0.63	1.91
Q2G0Z0_STAA8	General stress protein 17M-like domain-containing protein	-0.62	3.63
PDXT_STAA8	Pyridoxal 5'-phosphate synthase subunit PdxT	-0.61	1.97
RL36_STAA8	Large ribosomal subunit protein bL36	-0.61	2.21
DEOB_STAA8	Phosphopentomutase	-0.60	2.65
Q2FX98_STAA8	HTH cro/C1-type domain-containing protein	-0.57	2.80
Q2FZL5_STAA8	1,4-dihydroxy-2-naphthoyl-CoA synthase	-0.54	1.71
Q2FXP2_STAA8	Glyceraldehyde-3-phosphate dehydrogenase	-0.50	1.44
Q2FZY7_STAA8	ABC transporter, ATP-binding protein, putative	-0.50	2.49
ATPD_STAA8	ATP synthase subunit delta	-0.50	2.44
Q2G0R0_STAA8	ATP-dependent zinc metalloprotease FtsH	-0.48	1.65
Y906_STAA8	Uncharacterized protein SAOUHSC_00906	-0.48	1.34
TARI1_STAA8	Ribitol-5-phosphate cytidylyltransferase 1	-0.45	2.00

Q2FW27_STAA8	Adenylate kinase	-0.40	1.38
SUCC_STAA8	Succinate--CoA ligase [ADP-forming] subunit beta	-0.38	1.58
Q2FV76_STAA8	HMG-CoA synthase, putative	-0.37	2.53
Q2G0Q8_STAA8	Cysteine synthase	-0.36	2.09
CLPP_STAA8	ATP-dependent Clp protease proteolytic subunit	-0.36	2.59
KGUA_STAA8	Guanylate kinase	-0.34	1.73
Q2FXM5_STAA8	NADP-dependent malic enzyme, putative	-0.32	1.57
Q2FXM5_STAA8	NADP-dependent malic enzyme, putative	-0.32	1.57
SYS_STAA8	Serine--tRNA ligase	-0.31	1.42
SYS_STAA8	Serine--tRNA ligase	-0.31	1.42
Q2G0S2_STAA8	Ribose-phosphate pyrophosphokinase	-0.28	1.27
Q2G0S2_STAA8	Ribose-phosphate pyrophosphokinase	-0.28	1.27

Appendix table 2. List of gene names, protein names and the relative downregulation and P value to the untreated control expressed as Log10 and -Log10 for fold change and P value respectively

References

1. Hutchings MI, Wilkinson AWTaB. Antibiotics: past, present and future. Current Opinion in Microbiology. 2019
;51:72-80.
2. Murray CJ, Ikuta KS, Sharara F, Swetschinski L, Robles Aguilar G, Gray A, et al. Global burden of bacterial antimicrobial resistance in 2019: a systematic analysis. The Lancet. 2022;399(10325):629-55.
3. Adedeji WA. THE TREASURE CALLED ANTIBIOTICS. Ann Ib Postgrad Med. 2016;14(2):56-7.
4. Ahmed SK, Hussein S, Qurbani K, Ibrahim RH, Fareeq A, Mahmood KA, et al. Antimicrobial resistance: Impacts, challenges, and future prospects. Journal of Medicine, Surgery, and Public Health. 2024;2:100081.
5. Qurbani K, Ali S, Hussein S, Hamzah H. Antibiotic resistance in Kurdistan, Iraq: A growing concern. New Microbes and New Infections. 2024;57:101221.
6. Patangia DV, Ryan CA, Dempsey E, Stanton C, Ross RP. Vertical transfer of antibiotics and antibiotic resistant strains across the mother/baby axis. Trends Microbiol. 2022;30(1):47-56.
7. Liu J, Chang W, Pan L, Liu X, Su L, Zhang W, et al. An Improved Method of Preparing High Efficiency Transformation Escherichia coli with Both Plasmids and Larger DNA Fragments. Indian J Microbiol. 2018;58(4):448-56.
8. Colavecchio A, Cadieux B, Lo A, Goodridge LD. Bacteriophages Contribute to the Spread of Antibiotic Resistance Genes among Foodborne Pathogens of the Enterobacteriaceae Family – A Review. Frontiers in Microbiology. 2017;8.
9. Reygaert WC. An overview of the antimicrobial resistance mechanisms of bacteria. AIMS Microbiol. 2018;4(3):482-501.
10. Virolle C, Goldlust K, Djermoun S, Bigot S, Lesterlin C. Plasmid Transfer by Conjugation in Gram-Negative Bacteria: From the Cellular to the Community Level. Genes (Basel). 2020;11(11).
11. Goldlust K, Ducret A, Halte M, Dedieu-Berne A, Erhardt M, Lesterlin C. The F pilus serves as a conduit for the DNA during conjugation between physically distant bacteria. Proceedings of the National Academy of Sciences. 2023;120(47).
12. Wong JJW, Lu J, Glover JNM. Relaxosome function and conjugation regulation in F-like plasmids – a structural biology perspective. Molecular Microbiology. 2012;85(4):602-17.
13. Shen Z, Tang CM, Liu G-Y. Towards a better understanding of antimicrobial resistance dissemination: what can be learnt from studying model conjugative plasmids? Military Medical Research. 2022;9(1):3.
14. Lima LM, Silva BNMd, Barbosa G, Barreiro EJ. β-lactam antibiotics: An overview from a medicinal chemistry perspective. European Journal of Medicinal Chemistry. 2020;208:112829.
15. Drlica K. Mechanism of fluoroquinolone action. Curr Opin Microbiol. 1999;2(5):504-8.

16. Chopra I, Roberts M. Tetracycline antibiotics: mode of action, applications, molecular biology, and epidemiology of bacterial resistance. Microbiol Mol Biol Rev. 2001;65(2):232-60 ; second page, table of contents.
17. Spratt BG. Resistance to Antibiotics Mediated by Target Alterations. Science. 1994;264(5157):388-93.
18. Kareem SM, Al-Kadmy IMS, Kazaal SS, Mohammed Ali AN, Aziz SN, Makharita RR, et al. Detection of gyrA and parC Mutations and Prevalence of Plasmid-Mediated Quinolone Resistance Genes in Klebsiella pneumoniae. Infect Drug Resist. 2021;14:555-63.
19. Rudkin JK, Edwards AM, Bowden MG, Brown EL, Pozzi C, Waters EM, et al. Methicillin resistance reduces the virulence of healthcare-associated methicillin-resistant Staphylococcus aureus by interfering with the agr quorum sensing system. J Infect Dis. 2012;205(5):798-806.
20. Lin J, Lv H, Wang T, Tao H, Zhong Y, Zhou Y, et al. The global distribution of the macrolide esterase EstX from the alpha/beta hydrolase superfamily. Communications Biology. 2024;7(1):781.
21. Morar M, Pengelly K, Koteva K, Wright GD. Mechanism and Diversity of the Erythromycin Esterase Family of Enzymes. Biochemistry. 2012;51(8):1740-51.
22. Taniguchi K, Nakamura A, Tsurubuchi K, Ishii A, O'Hara K, Sawai T. Identification of functional amino acids in the macrolide 2'-phosphotransferase II. Antimicrob Agents Chemother. 1999;43(8):2063-5.
23. Fyfe C, Grossman TH, Kerstein K, Sutcliffe J. Resistance to Macrolide Antibiotics in Public Health Pathogens. Cold Spring Harb Perspect Med. 2016;6(10).
24. Blair JM, Richmond GE, Piddock LJ. Multidrug efflux pumps in Gram-negative bacteria and their role in antibiotic resistance. Future Microbiol. 2014;9(10):1165-77.
25. Kumar A, Schweizer HP. Bacterial resistance to antibiotics: Active efflux and reduced uptake. Advanced Drug Delivery Reviews. 2005;57(10):1486-513.
26. Li XZ, Nikaido H. Efflux-mediated drug resistance in bacteria: an update. Drugs. 2009;69(12):1555-623.
27. Jang S. AcrAB-TolC, a major efflux pump in Gram negative bacteria: toward understanding its operation mechanism. BMB Rep. 2023;56(6):326-34.
28. Lekshmi M, Ortiz-Alegria A, Kumar S, Varela MF. Major facilitator superfamily efflux pumps in human pathogens: Role in multidrug resistance and beyond. Current Research in Microbial Sciences. 2024;7:100248.
29. Tait-Kamradt A, Clancy J, Cronan M, Dib-Hajj F, Wondrack L, Yuan W, et al. mefE is necessary for the erythromycin-resistant M phenotype in Streptococcus pneumoniae. Antimicrobial Agents and Chemotherapy. 1997;41(10):2251-5.
30. Cui L, Murakami H, Kuwahara-Arai K, Hanaki H, Hiramatsu K. Contribution of a thickened cell wall and its glutamine nonamidated component to the vancomycin resistance expressed by Staphylococcus aureus Mu50. Antimicrob Agents Chemother. 2000;44(9):2276-85.
31. Yin W, Wang Y, Liu L, He J. Biofilms: The Microbial "Protective Clothing" in Extreme Environments. Int J Mol Sci. 2019;20(14).
32. Zhao A, Sun J, Liu Y. Understanding bacterial biofilms: From definition to treatment strategies. Front Cell Infect Microbiol. 2023;13:1137947.
33. Petrova OE, Sauer K. Sticky situations: key components that control bacterial surface attachment. J Bacteriol. 2012;194(10):2413-25.

34. Rather MA, Gupta K, Mandal M. Microbial biofilm: formation, architecture, antibiotic resistance, and control strategies. Braz J Microbiol. 2021;52(4):1701-18.
35. Mah T-F. Biofilm-Specific Antibiotic Resistance. Future Microbiology. 2012;7(9):1061-72.
36. Sharma D, Misba L, Khan AU. Antibiotics versus biofilm: an emerging battleground in microbial communities. Antimicrobial Resistance & Infection Control. 2019;8(1):76.
37. Brauner A, Fridman O, Gefen O, Balaban NQ. Distinguishing between resistance, tolerance and persistence to antibiotic treatment. Nature Reviews Microbiology. 2016;14(5):320-30.
38. Levin-Reisman I, Brauner A, Ronin I, Balaban NQ. Epistasis between antibiotic tolerance, persistence, and resistance mutations. Proceedings of the National Academy of Sciences. 2019;116(29):14734-9.
39. Levin-Reisman I, Ronin I, Gefen O, Braniss I, Shoresh N, Balaban NQ. Antibiotic tolerance facilitates the evolution of resistance. Science. 2017;355(6327):826-30.
40. Fisher RA, Gollan B, Helaine S. Persistent bacterial infections and persister cells. Nature Reviews Microbiology. 2017;15(8):453-64.
41. Kussell E, Kishony R, Balaban NQ, Leibler S. Bacterial Persistence. Genetics. 2005;169(4):1807-14.
42. Friedman ND, Temkin E, Carmeli Y. The negative impact of antibiotic resistance. Clinical Microbiology and Infection. 2016;22(5):416-22.
43. Llor C, Bjerrum L. Antimicrobial resistance: risk associated with antibiotic overuse and initiatives to reduce the problem. Ther Adv Drug Saf. 2014;5(6):229-41.
44. Birgand G, Dhar P, Holmes A. The threat of antimicrobial resistance in surgical care: the surgeon's role and ownership of antimicrobial stewardship. British Journal of Surgery. 2023;110(12):1567-9.
45. Dadgostar P. Antimicrobial Resistance: Implications and Costs. Infect Drug Resist. 2019;12:3903-10.
46. Miller WR, Arias CA. ESKAPE pathogens: antimicrobial resistance, epidemiology, clinical impact and therapeutics. Nature Reviews Microbiology. 2024.
47. Cetinkaya Y, Falk P, Mayhall CG. Vancomycin-resistant enterococci. Clin Microbiol Rev. 2000;13(4):686-707.
48. Navidinia M. The clinical importance of emerging ESKAPE pathogens in nosocomial infections. Archives of Advances in Biosciences,. 2016;7:43–57.
49. Nordmann P, Cuzon G, Naas T. The real threat of Klebsiella pneumoniae carbapenemase-producing bacteria. Lancet Infect Dis. 2009;9(4):228-36.
50. Al-Harmoosh R, Jarallah E. FIRST DETECTION OF THE blaNDM-1 and blaNDM-2 GENES IN A CLINICAL ISOLATES OF Acinetobacter baumannii IN HILLAH HOSPITALS-IRAQ. International Journal of Advanced Research. 2015;3:1407-16.
51. Pang Z, Raudonis R, Glick BR, Lin T-J, Cheng Z. Antibiotic resistance in Pseudomonas aeruginosa: mechanisms and alternative therapeutic strategies. Biotechnology Advances. 2019;37(1):177-92.
52. Pitout JDD, Nordmann P, Laupland KB, Poirel L. Emergence of Enterobacteriaceae producing extended-spectrum β-lactamases (ESBLs) in the community. Journal of Antimicrobial Chemotherapy. 2005;56(1):52-9.
53. Minssen T, Outterson K, Rogers Van Katwyk S, Batista PHD, Chandler CIR, Ciabuschi F, et al. Social, cultural and economic aspects of antimicrobial resistance. Bull World Health Organ. 2020;98(12):823-a.

54. Cooper LN, Beauchamp AM, Ingle TA, Diaz MI, Wakene AD, Katterpalli C, et al. Socioeconomic Disparities and the Prevalence of Antimicrobial Resistance. Clin Infect Dis. 2024.
55. Tanday S. Resisting the use of antibiotics for viral infections. The Lancet Respiratory Medicine. 2016;4(3):179.
56. Almutairi KS, Okmi EA, Alnofaiei SS, Alshamari WK, Almutairi SH, Alsuwailem SI, et al. The Effects of Health Education on the Awareness of Antimicrobial Resistance Among High School Students in Riyadh, Saudi Arabia During 2023: A Quasi-experimental Study. Cureus. 2023;15(7):e41639.
57. Towse A, Hoyle CK, Goodall J, Hirsch M, Mestre-Ferrandiz J, Rex JH. Time for a change in how new antibiotics are reimbursed: Development of an insurance framework for funding new antibiotics based on a policy of risk mitigation. Health Policy. 2017;121(10):1025-30.
58. Plackett B. Why big pharma has abandoned antibiotics. Nature. 2020;586(7830):S50-S2.
59. Ciabuschi F, Baraldi E, Lindahl O, Callegari S. Supporting innovation against the threat of antibiotic resistance: Exploring the impact of public incentives on firm performance and entrepreneurial orientation. Journal of Business Research. 2020;112:271-80.
60. England N. NHS steps up battle against life-threatening infections following successful world-first pilot. NHS England https://www england nhs uk/2023/07/nhs-steps-up-battle-against-life-threatening-infections-following-successful-world-first-pilot/(11 July 2023). 2023.
61. Glover RE, Singer AC, Roberts AP, Kirchhelle C. The antibiotic subscription model: fostering innovation or repackaging old drugs? The Lancet Microbe. 2023;4(1):e2-e3.
62. Wouters OJ, McKee M, Luyten J. Estimated research and development investment needed to bring a new medicine to market, 2009-2018. Jama. 2020;323(9):844-53.
63. Lin DM, Koskella B, Lin HC. Phage therapy: An alternative to antibiotics in the age of multi-drug resistance. World J Gastrointest Pharmacol Ther. 2017;8(3):162-73.
64. Lin J, Du F, Long M, Li P. Limitations of Phage Therapy and Corresponding Optimization Strategies: A Review. Molecules. 2022;27(6).
65. Dickey SW, Cheung GYC, Otto M. Different drugs for bad bugs: antivirulence strategies in the age of antibiotic resistance. Nature Reviews Drug Discovery. 2017;16(7):457-71.
66. Bhandari V, Suresh A. Next-Generation Approaches Needed to Tackle Antimicrobial Resistance for the Development of Novel Therapies Against the Deadly Pathogens. Frontiers in Pharmacology. 2022;13.
67. Migone TS, Subramanian GM, Zhong J, Healey LM, Corey A, Devalaraja M, et al. Raxibacumab for the treatment of inhalational anthrax. N Engl J Med. 2009;361(2):135-44.
68. Hu X, Huang Y-Y, Wang Y, Wang X, Hamblin MR. Antimicrobial Photodynamic Therapy to Control Clinically Relevant Biofilm Infections. Frontiers in Microbiology. 2018;9.
69. Robertson CA, Evans DH, Abrahamse H. Photodynamic therapy (PDT): A short review on cellular mechanisms and cancer research applications for PDT. Journal of Photochemistry and Photobiology B: Biology. 2009;96(1):1-8.
70. Kwiatkowski S, Knap B, Przystupski D, Saczko J, Kędzierska E, Knap-Czop K, et al. Photodynamic therapy – mechanisms, photosensitizers and combinations. Biomedicine & Pharmacotherapy. 2018;106:1098-107.

71. Abrahamse H, Michael. New photosensitizers for photodynamic therapy. Biochemical Journal. 2016;473(4):347-64.
72. Waite R, Adams CT, Chisholm DR, Sims CHC, Hughes JG, Dias E, et al. The antibacterial activity of a photoactivatable diarylacetylene against Gram-positive bacteria. Frontiers in Microbiology. 2023;14.
73. Baptista MS, Cadet J, Di Mascio P, Ghogare AA, Greer A, Hamblin MR, et al. Type I and Type II Photosensitized Oxidation Reactions: Guidelines and Mechanistic Pathways. Photochemistry and Photobiology. 2017;93(4):912-9.
74. Aldred EM, Buck C, Vall K. Chapter 7 - Free radicals. In: Aldred EM, Buck C, Vall K, editors. Pharmacology. Edinburgh: Churchill Livingstone; 2009. p. 41-52.
75. Gunaydin G, Gedik ME, Ayan S. Photodynamic Therapy—Current Limitations and Novel Approaches. Frontiers in Chemistry. 2021;9.
76. Yao Q, Fan J, Long S, Zhao X, Li H, Du J, et al. The concept and examples of type-III photosensitizers for cancer photodynamic therapy. Chem. 2022;8(1):197-209.
77. Scherer KM, Bisby RH, Botchway SW, Parker AW. New Approaches to Photodynamic Therapy from Types I, II and III to Type IV Using One or More Photons. Anticancer Agents Med Chem. 2017;17(2):171-89.
78. Memar MY, Ghotaslou R, Samiei M, Adibkia K. Antimicrobial use of reactive oxygen therapy: current insights. Infect Drug Resist. 2018;11:567-76.
79. Sabino CP, Wainwright M, Ribeiro MS, Sellera FP, Dos Anjos C, Baptista MDS, et al. Global priority multidrug-resistant pathogens do not resist photodynamic therapy. Journal of Photochemistry and Photobiology B: Biology. 2020;208:111893.
80. Toyoshima K, Ohsugi Y, Lin P, Komatsu K, Shiba T, Takeuchi Y, et al. Blue Light-Emitting Diode Irradiation Without a Photosensitizer Alters Oral Microbiome Composition of Ligature-Induced Periodontitis in Mice. Photobiomodulation, Photomedicine, and Laser Surgery. 2023;41(10):549-59.
81. Schastak S, Ziganshyna S, Gitter B, Wiedemann P, Claudepierre T. Efficient photodynamic therapy against gram-positive and gram-negative bacteria using THPTS, a cationic photosensitizer excited by infrared wavelength. PLoS One. 2010;5(7):e11674.
82. Surur AK, de Oliveira AB, De Annunzio SR, Ferrisse TM, Fontana CR. Bacterial resistance to antimicrobial photodynamic therapy: A critical update. Journal of Photochemistry and Photobiology B: Biology. 2024;255:112905.
83. Liu Y, Qin R, Zaat SAJ, Breukink E, Heger M. Antibacterial photodynamic therapy: overview of a promising approach to fight antibiotic-resistant bacterial infections. J Clin Transl Res. 2015;1(3):140-67.
84. Imlay JA. Pathways of Oxidative Damage. Annual Review of Microbiology. 2003;57(1):395-418.
85. Vasquez-Medrano R, Prato-Garcia D, Vedrenne M. Chapter 4 - Ferrioxalate-Mediated Processes. In: Ameta SC, Ameta R, editors. Advanced Oxidation Processes for Waste Water Treatment: Academic Press; 2018. p. 89-113.
86. Shacter E. Quantification and significance of protein oxidation in biological samples. Drug Metab Rev. 2000;32(3-4):307-26.
87. Ezraty B, Gennaris A, Barras F, Collet J-F. Oxidative stress, protein damage and repair in bacteria. Nature Reviews Microbiology. 2017;15(7):385-96.
88. Nayak J, Jena SR, Samanta L. Chapter 4.3 - Oxidative Stress and Sperm Dysfunction: An Insight Into Dynamics of Semen Proteome. In: Henkel R, Samanta L, Agarwal A, editors.

Oxidants, Antioxidants and Impact of the Oxidative Status in Male Reproduction: Academic Press; 2019. p. 261-75.
89. Stadtman ER. Oxidation of free amino acids and amino acid residues in proteins by radiolysis and by metal-catalyzed reactions. Annu Rev Biochem. 1993;62:797-821.
90. Fasnacht M, Polacek N. Oxidative Stress in Bacteria and the Central Dogma of Molecular Biology. Frontiers in Molecular Biosciences. 2021;8.
91. Imlay JA. Iron-sulphur clusters and the problem with oxygen. Molecular Microbiology. 2006;59(4):1073-82.
92. Keyer K, Imlay JA. Superoxide accelerates DNA damage by elevating free-iron levels. Proc Natl Acad Sci U S A. 1996;93(24):13635-40.
93. Strahl H, Errington J. Bacterial Membranes: Structure, Domains, and Function. Annu Rev Microbiol. 2017;71:519-38.
94. Naguib M, Feldman N, Zarodkiewicz P, Shropshire H, Biamis C, El-Halfawy OM, et al. An evolutionary conserved detoxification system for membrane lipid-derived peroxyl radicals in Gram-negative bacteria. PLoS Biol. 2022;20(5):e3001610.
95. Cabiscol E, Tamarit J, Ros J. Oxidative stress in bacteria and protein damage by reactive oxygen species. Int Microbiol. 2000;3(1):3-8.
96. Juan CA, Pérez de la Lastra JM, Plou FJ, Pérez-Lebeña E. The Chemistry of Reactive Oxygen Species (ROS) Revisited: Outlining Their Role in Biological Macromolecules (DNA, Lipids and Proteins) and Induced Pathologies. Int J Mol Sci. 2021;22(9).
97. Imlay JA. The molecular mechanisms and physiological consequences of oxidative stress: lessons from a model bacterium. Nature Reviews Microbiology. 2013;11(7):443-54.
98. Henle ES, Han Z, Tang N, Rai P, Luo Y, Linn S. Sequence-specific DNA cleavage by Fe2+-mediated fenton reactions has possible biological implications. J Biol Chem. 1999;274(2):962-71.
99. Candeias LP, Steenken S. Electron transfer in di (deoxy) nucleoside phosphates in aqueous solution: rapid migration of oxidative damage (via adenine) to guanine. Journal of the American Chemical Society. 1993;115(6):2437-40.
100. Henrikus SS, Henry C, McDonald JP, Hellmich Y, Wood EA, Woodgate R, et al. DNA double-strand breaks induced by reactive oxygen species promote DNA polymerase IV activity in Escherichia coli. bioRxiv. 2019:533422.
101. Gruber CC, Walker GC. Incomplete base excision repair contributes to cell death from antibiotics and other stresses. DNA Repair. 2018;71:108-17.
102. Broxton CN, Culotta VC. SOD Enzymes and Microbial Pathogens: Surviving the Oxidative Storm of Infection. PLoS Pathog. 2016;12(1):e1005295.
103. Steimbrüch BA, Sartorio MG, Cortez N, Albanesi D, Lisa M-N, Repizo GD. The distinctive roles played by the superoxide dismutases of the extremophile Acinetobacter sp. Ver3. Scientific Reports. 2022;12(1):4321.
104. Yuan F, Yin S, Xu Y, Xiang L, Wang H, Li Z, et al. The Richness and Diversity of Catalases in Bacteria. Front Microbiol. 2021;12:645477.
105. Zhao X, Drlica K. Reactive oxygen species and the bacterial response to lethal stress. Current Opinion in Microbiology. 2014;21:1-6.
106. Zeller T, Klug G. Thioredoxins in bacteria: functions in oxidative stress response and regulation of thioredoxin genes. Naturwissenschaften. 2006;93(6):259-66.
107. Spector A, Yan GZ, Huang RR, McDermott MJ, Gascoyne PR, Pigiet V. The effect of H2O2 upon thioredoxin-enriched lens epithelial cells. Journal of Biological Chemistry. 1988;263(10):4984-90.

108. Das KC, Das CK. Thioredoxin, a singlet oxygen quencher and hydroxyl radical scavenger: redox independent functions. Biochem Biophys Res Commun. 2000;277(2):443-7.
109. Maslowska KH, Makiela-Dzbenska K, Fijalkowska IJ. The SOS system: A complex and tightly regulated response to DNA damage. Environ Mol Mutagen. 2019;60(4):368-84.
110. Patel M, Jiang Q, Woodgate R, Cox MM, Goodman MF. A new model for SOS-induced mutagenesis: how RecA protein activates DNA polymerase V. Crit Rev Biochem Mol Biol. 2010;45(3):171-84.
111. Wozniak KJ, Simmons LA. Bacterial DNA excision repair pathways. Nat Rev Microbiol. 2022;20(8):465-77.
112. Friedberg EC, Walker GC, Siede W, Wood RD. DNA repair and mutagenesis: American Society for Microbiology Press; 2005.
113. Goodman MF. Error-prone repair DNA polymerases in prokaryotes and eukaryotes. Annu Rev Biochem. 2002;71:17-50.
114. Tang M, Pham P, Shen X, Taylor JS, O'Donnell M, Woodgate R, et al. Roles of E. coli DNA polymerases IV and V in lesion-targeted and untargeted SOS mutagenesis. Nature. 2000;404(6781):1014-8.
115. Collins TL, Markus EA, Hassett DJ, Robinson JB. The effect of a cationic porphyrin on Pseudomonas aeruginosa biofilms. Curr Microbiol. 2010;61(5):411-6.
116. Di Poto A, Sbarra MS, Provenza G, Visai L, Speziale P. The effect of photodynamic treatment combined with antibiotic action or host defence mechanisms on Staphylococcus aureus biofilms. Biomaterials. 2009;30(18):3158-66.
117. Cieplik F, Späth A, Regensburger J, Gollmer A, Tabenski L, Hiller KA, et al. Photodynamic biofilm inactivation by SAPYR--an exclusive singlet oxygen photosensitizer. Free Radic Biol Med. 2013;65:477-87.
118. Bertoloni G, Rossi F, Valduga G, Jori G, Ali H, van Lier JE. Photosensitizing activity of water- and lipid-soluble phthalocyanines on prokaryotic and eukaryotic microbial cells. Microbios. 1992;71(286):33-46.
119. Najafi S, Khayamzadeh M, Paknejad M, Poursepanj G, Kharazi Fard MJ, Bahador A. An In Vitro Comparison of Antimicrobial Effects of Curcumin-Based Photodynamic Therapy and Chlorhexidine, on Aggregatibacter actinomycetemcomitans. J Lasers Med Sci. 2016;7(1):21-5.
120. Dahl TA, McGowan WM, Shand MA, Srinivasan VS. Photokilling of bacteria by the natural dye curcumin. Arch Microbiol. 1989;151(2):183-5.
121. García I, Ballesta S, Gilaberte Y, Rezusta A, Pascual Á. Antimicrobial photodynamic activity of hypericin against methicillin-susceptible and resistant Staphylococcus aureus biofilms. Future Microbiol. 2015;10(3):347-56.
122. Yow CM, Tang HM, Chu ES, Huang Z. Hypericin-mediated photodynamic antimicrobial effect on clinically isolated pathogens. Photochem Photobiol. 2012;88(3):626-32.
123. Pérez-Laguna V, García-Luque I, Ballesta S, Pérez-Artiaga L, Lampaya-Pérez V, Rezusta A, et al. Photodynamic therapy using methylene blue, combined or not with gentamicin, against Staphylococcus aureus and Pseudomonas aeruginosa. Photodiagnosis Photodyn Ther. 2020;31:101810.
124. Shrestha A, Kishen A. Polycationic chitosan-conjugated photosensitizer for antibacterial photodynamic therapy. Photochem Photobiol. 2012;88(3):577-83.

125. Wang M, Huang L, Sharma SK, Jeon S, Thota S, Sperandio FF, et al. Synthesis and photodynamic effect of new highly photostable decacationically armed [60]- and [70]fullerene decaiodide monoadducts to target pathogenic bacteria and cancer cells. J Med Chem. 2012;55(9):4274-85.
126. Spesia MB, Milanesio ME, Durantini EN. Synthesis, properties and photodynamic inactivation of Escherichia coli by novel cationic fullerene C60 derivatives. European Journal of Medicinal Chemistry. 2008;43(4):853-61.
127. Maness PC, Smolinski S, Blake DM, Huang Z, Wolfrum EJ, Jacoby WA. Bactericidal activity of photocatalytic TiO(2) reaction: toward an understanding of its killing mechanism. Appl Environ Microbiol. 1999;65(9):4094-8.
128. Amos-Tautua B, Songca S, Oluwafemi O. Application of Porphyrins in Antibacterial Photodynamic Therapy. Molecules. 2019;24(13):2456.
129. Kou J, Dou D, Yang L. Porphyrin photosensitizers in photodynamic therapy and its applications. Oncotarget. 2017;8(46):81591-603.
130. Baigorria E, Durantini JE, Di Palma MA, Gsponer NS, Milanesio ME, Durantini EN. Amphiphilic tricationic Zn(II)phthalocyanine provides effective photodynamic action to eradicate broad-spectrum microorganisms. Photochem Photobiol Sci. 2021;20(7):939-53.
131. Zdubek A, Maliszewska I. On the Possibility of Using 5-Aminolevulinic Acid in the Light-Induced Destruction of Microorganisms. Int J Mol Sci. 2024;25(7).
132. Harris F, Pierpoint L. Photodynamic therapy based on 5-aminolevulinic acid and its use as an antimicrobial agent. Med Res Rev. 2012;32(6):1292-327.
133. Leite DPV, Paolillo FR, Parmesano TN, Fontana CR, Bagnato VS. Effects of Photodynamic Therapy with Blue Light and Curcumin as Mouth Rinse for Oral Disinfection: A Randomized Controlled Trial. Photomedicine and Laser Surgery. 2014;32(11):627-32.
134. Babalola BA, Malik M, Sharma L, Olowokere O, Folajimi O. Exploring the therapeutic potential of phenothiazine derivatives in medicinal chemistry. Results in Chemistry. 2024;8:101565.
135. Boltes Cecatto R, Siqueira de Magalhães L, Fernanda Setúbal Destro Rodrigues M, Pavani C, Lino-dos-Santos-Franco A, Teixeira Gomes M, et al. Methylene blue mediated antimicrobial photodynamic therapy in clinical human studies: The state of the art. Photodiagnosis and Photodynamic Therapy. 2020;31:101828.
136. Nicolas G. Loebel, Carolyn M. Cross, David M. Meller, Jason Hickok, Roger Andersen, Michael Wilson. Antimicrobial Photodisinfection Therapy:
Essential Technology for Infection Control. 2020.
137. Pérez-Laguna V, García-Luque I, Ballesta S, Pérez-Artiaga L, Lampaya-Pérez V, Samper S, et al. Antimicrobial photodynamic activity of Rose Bengal, alone or in combination with Gentamicin, against planktonic and biofilm Staphylococcus aureus. Photodiagnosis and Photodynamic Therapy. 2018;21:211-6.
138. Chen L, Huang J, Li X, Huang M, Zeng S, Zheng J, et al. Progress of Nanomaterials in Photodynamic Therapy Against Tumor. Front Bioeng Biotechnol. 2022;10:920162.
139. Mahmoudi K, Garvey KL, Bouras A, Cramer G, Stepp H, Jesu Raj JG, et al. 5-aminolevulinic acid photodynamic therapy for the treatment of high-grade gliomas. J Neurooncol. 2019;141(3):595-607.
140. Chisholm DR, Lamb R, Pallett T, Affleck V, Holden C, Marrison J, et al. Photoactivated cell-killing involving a low molecular weight, donor–acceptor diphenylacetylene. Chemical Science. 2019;10(17):4673-83.

141. Park J, Lee YK, Park IK, Hwang SR. Current Limitations and Recent Progress in Nanomedicine for Clinically Available Photodynamic Therapy. Biomedicines. 2021;9(1).
142. Chisholm DR, Hughes JG, Blacker TS, Humann R, Adams C, Callaghan D, et al. Cellular localisation of structurally diverse diphenylacetylene fluorophores. Organic & Biomolecular Chemistry. 2020;18(45):9231-45.
143. Gala De Pablo J, Chisholm DR, Steffen A, Nelson AK, Mahler C, Marder TB, et al. Tandem fluorescence and Raman (fluoRaman) characterisation of a novel photosensitiser in colorectal cancer cell line SW480. The Analyst. 2018;143(24):6113-20.
144. Würth C, Grabolle M, Pauli J, Spieles M, Resch-Genger U. Relative and absolute determination of fluorescence quantum yields of transparent samples. Nature Protocols. 2013;8(8):1535-50.
145. Wainwright M, Maisch T, Nonell S, Plaetzer K, Almeida A, Tegos GP, et al. Photoantimicrobials—are we afraid of the light? The Lancet Infectious Diseases. 2017;17(2):e49-e55.
146. Singh M, Sasaki T, Matsuo M, Morimoto Y, Aiba Y, Hiramatsu K. Complete Genome Sequence of the Drug-Naive Classical Staphylococcus aureus Strain FDA209P. Genome Announc. 2015;3(6).
147. Horsburgh MJ, Aish JL, White IJ, Shaw L, Lithgow JK, Foster SJ. sigmaB modulates virulence determinant expression and stress resistance: characterization of a functional rsbU strain derived from Staphylococcus aureus 8325-4. J Bacteriol. 2002;184(19):5457-67.
148. Baba T, Ara T, Hasegawa M, Takai Y, Okumura Y, Baba M, et al. Construction of Escherichia coli K-12 in-frame, single-gene knockout mutants: the Keio collection. Molecular Systems Biology. 2006;2(1).
149. Cardozo APM, da Silva DdFT, Fernandes KPS, Ferreira RdC, Lino-dos-Santos-Franco A, Rodrigues MFSD, et al. Antimicrobial photodynamic therapy with methylene blue and its derivatives in animal studies: Systematic review. Photodermatology, Photoimmunology & Photomedicine. 2024;40(4):e12978.
150. Ambler Aa. Unpublished.
151. Barák I. Special Issue "Bacillus subtilis as a Model Organism to Study Basic Cell Processes". Microorganisms. 2021;9(12).
152. Netuschil L, Auschill TM, Sculean A, Arweiler NB. Confusion over live/dead stainings for the detection of vital microorganisms in oral biofilms - which stain is suitable? BMC Oral Health. 2014;14(1):2.
153. Stocks SM. Mechanism and use of the commercially available viability stain,BacLight. Cytometry. 2004;61A(2):189-95.
154. Tsonis I, Karamani L, Xaplanteri P, Kolonitsiou F, Zampakis P, Gatzounis G, et al. Spontaneous cerebral abscess due to Bacillus subtilis in an immunocompetent male patient: A case report and review of literature. World J Clin Cases. 2018;6(16):1169-74.
155. Tang Y-W, Y. Hindiyeh M, Liu D, Sails A, Spearman P, Zhang J-R. Chapter 1 - Molecular medical microbiology—from bench to bedside. In: Tang Y-W, Hindiyeh MY, Liu D, Sails A, Spearman P, Zhang J-R, editors. Molecular Medical Microbiology (Third Edition): Academic Press; 2024. p. 1-6.
156. Khan HA, Baig FK, Mehboob R. Nosocomial infections: Epidemiology, prevention, control and surveillance. Asian Pacific Journal of Tropical Biomedicine. 2017;7(5):478-82.
157. Rapacka-Zdonczyk A, Wozniak A, Pieranski M, Woziwodzka A, Bielawski KP, Grinholc M. Development of Staphylococcus aureus tolerance to antimicrobial photodynamic

inactivation and antimicrobial blue light upon sub-lethal treatment. Scientific Reports. 2019;9(1).
158. Chaudhuri RR, Allen AG, Owen PJ, Shalom G, Stone K, Harrison M, et al. Comprehensive identification of essential Staphylococcus aureus genes using Transposon-Mediated Differential Hybridisation (TMDH). BMC Genomics. 2009;10:291.
159. Vaish M, Jereen A, Ali A, Krulwich TA. The alkaliphilic side of Staphylococcus aureus. bioRxiv. 2019:735191.
160. Dikalov SI, Harrison DG. Methods for detection of mitochondrial and cellular reactive oxygen species. Antioxid Redox Signal. 2014;20(2):372-82.
161. Tavares A, Carvalho CM, Faustino MA, Neves MG, Tomé JP, Tomé AC, et al. Antimicrobial photodynamic therapy: study of bacterial recovery viability and potential development of resistance after treatment. Mar Drugs. 2010;8(1):91-105.
162. Amin RM, Bhayana B, Hamblin MR, Dai T. Antimicrobial blue light inactivation of Pseudomonas aeruginosa by photo-excitation of endogenous porphyrins: In vitro and in vivo studies. Lasers Surg Med. 2016;48(5):562-8.
163. Painter KL, Strange E, Parkhill J, Bamford KB, Armstrong-James D, Edwards AM. Staphylococcus aureus adapts to oxidative stress by producing H2O2-resistant small-colony variants via the SOS response. Infect Immun. 2015;83(5):1830-44.
164. Gottenbos B, Grijpma DW, van der Mei HC, Feijen J, Busscher HJ. Antimicrobial effects of positively charged surfaces on adhering Gram-positive and Gram-negative bacteria. Journal of Antimicrobial Chemotherapy. 2001;48(1):7-13.
165. Fonseca SM, Pina J, Arnaut LG, Seixas De Melo J, Burrows HD, Chattopadhyay N, et al. Triplet-State and Singlet Oxygen Formation in Fluorene-Based Alternating Copolymers. The Journal of Physical Chemistry B. 2006;110(16):8278-83.
166. Joyce LR, Doran KS. Gram-positive bacterial membrane lipids at the host-pathogen interface. PLoS Pathog. 2023;19(1):e1011026.
167. Bertani B, Ruiz N. Function and Biogenesis of Lipopolysaccharides. EcoSal Plus. 2018;8(1).
168. Karavolos MH, Horsburgh MJ, Ingham E, Foster SJ. Role and regulation of the superoxide dismutases of Staphylococcus aureus. Microbiology (Reading). 2003;149(Pt 10):2749-58.
169. Gaupp R, Ledala N, Somerville GA. Staphylococcal response to oxidative stress. Front Cell Infect Microbiol. 2012;2:33.
170. Manoil D, Bouillaguet S. Oxidative stress in bacteria measured by flow cytometry. Adv Biotechnol Microbiol. 2018;8(1):555726.
171. Wong F, Amir A. Mechanics and Dynamics of Bacterial Cell Lysis. Biophys J. 2019;116(12):2378-89.
172. Dwyer DJ, Kohanski MA, Hayete B, Collins JJ. Gyrase inhibitors induce an oxidative damage cellular death pathway in Escherichia coli. Mol Syst Biol. 2007;3:91.
173. Cirz RT, Jones MB, Gingles NA, Minogue TD, Jarrahi B, Peterson SN, et al. Complete and SOS-mediated response of Staphylococcus aureus to the antibiotic ciprofloxacin. J Bacteriol. 2007;189(2):531-9.
174. Kamariah N, Eisenhaber B, Eisenhaber F, Grüber G. Molecular mechanism of the Escherichia coli AhpC in the function of a chaperone under heat-shock conditions. Scientific Reports. 2018;8(1).
175. Ballal A, Manna AC. Control of thioredoxin reductase gene (trxB) transcription by SarA in Staphylococcus aureus. J Bacteriol. 2010;192(1):336-45.

176. Greenspan P, Mayer EP, Fowler SD. Nile red: a selective fluorescent stain for intracellular lipid droplets. J Cell Biol. 1985;100(3):965-73.
177. Mozaheb N, Mingeot-Leclercq MP. Membrane Vesicle Production as a Bacterial Defense Against Stress. Front Microbiol. 2020;11:600221.
178. Abe K, Toyofuku M, Nomura N, Obana N. Autolysis-mediated membrane vesicle formation in Bacillus subtilis. Environmental Microbiology. 2021;23(5):2632-47.
179. Peterson BW, Sharma PK, van der Mei HC, Busscher HJ. Bacterial cell surface damage due to centrifugal compaction. Appl Environ Microbiol. 2012;78(1):120-5.
180. Matalon E, Kaminker I, Zimmermann H, Eisenstein M, Shai Y, Goldfarb D. Topology of the Trans-Membrane Peptide WALP23 in Model Membranes under Negative Mismatch Conditions. The Journal of Physical Chemistry B. 2013;117(8):2280-93.
181. Missiakas DM, Schneewind O. Growth and laboratory maintenance of Staphylococcus aureus. Curr Protoc Microbiol. 2013;Chapter 9:Unit 9C.1.
182. Andreou C, Gregoriou Y, Ali A, Pal S. Chapter 7 - In vivo imaging with SERS nanoprobes. In: Fales A, editor. SERS for Point-Of-care and Clinical Applications: Elsevier; 2022. p. 199-235.
183. Wang L, Liu W, Tang JW, Wang JJ, Liu QH, Wen PB, et al. Applications of Raman Spectroscopy in Bacterial Infections: Principles, Advantages, and Shortcomings. Front Microbiol. 2021;12:683580.
184. Breijyeh Z, Jubeh B, Karaman R. Resistance of Gram-Negative Bacteria to Current Antibacterial Agents and Approaches to Resolve It. Molecules. 2020;25(6).
185. Zgurskaya HI, Rybenkov VV. Permeability barriers of Gram-negative pathogens. Annals of the New York Academy of Sciences. 2020;1459(1):5-18.
186. Wiener MC, Horanyi PS. How hydrophobic molecules traverse the outer membranes of gram-negative bacteria. Proc Natl Acad Sci U S A. 2011;108(27):10929-30.
187. Nikaido H. Molecular basis of bacterial outer membrane permeability revisited. Microbiol Mol Biol Rev. 2003;67(4):593-656.
188. Liu B, Furevi A, Perepelov AV, Guo X, Cao H, Wang Q, et al. Structure and genetics of Escherichia coli O antigens. FEMS Microbiology Reviews. 2019;44(6):655-83.
189. Delcour AH. Outer membrane permeability and antibiotic resistance. Biochimica et Biophysica Acta (BBA) - Proteins and Proteomics. 2009;1794(5):808-16.
190. Pagnout C, Sohm B, Razafitianamaharavo A, Caillet C, Offroy M, Leduc M, et al. Pleiotropic effects of rfa-gene mutations on Escherichia coli envelope properties. Scientific Reports. 2019;9(1).
191. Yethon JA, Vinogradov E, Perry MB, Whitfield C. Mutation of the Lipopolysaccharide Core Glycosyltransferase Encoded by waaG Destabilizes the Outer Membrane of Escherichia coli by Interfering with Core Phosphorylation. Journal of Bacteriology. 2000;182(19):5620-3.
192. Mudapaka J, Taylor EA. Cloning and characterization of the Escherichia coli Heptosyltransferase III: Exploring substrate specificity in lipopolysaccharide core biosynthesis. FEBS Letters. 2015;589(13):1423-9.
193. Kneidinger B, Marolda C, Graninger M, Zamyatina A, McArthur F, Kosma P, et al. Biosynthesis pathway of ADP-L-glycero-beta-D-manno-heptose in Escherichia coli. J Bacteriol. 2002;184(2):363-9.
194. Taylor PL, Blakely KM, de Leon GP, Walker JR, McArthur F, Evdokimova E, et al. Structure and function of sedoheptulose-7-phosphate isomerase, a critical enzyme for

lipopolysaccharide biosynthesis and a target for antibiotic adjuvants. J Biol Chem. 2008;283(5):2835-45.
195. Grizot S, Salem M, Vongsouthi V, Durand L, Moreau F, Dohi H, et al. Structure of the Escherichia coli heptosyltransferase WaaC: binary complexes with ADP and ADP-2-deoxy-2-fluoro heptose. J Mol Biol. 2006;363(2):383-94.
196. Gurvic D, Zachariae U. Multidrug efflux in Gram-negative bacteria: structural modifications in active compounds leading to efflux pump avoidance. npj Antimicrobials and Resistance. 2024;2(1):6.
197. Touzé T, Eswaran J, Bokma E, Koronakis E, Hughes C, Koronakis V. Interactions underlying assembly of the Escherichia coli AcrAB–TolC multidrug efflux system. Molecular Microbiology. 2004;53(2):697-706.
198. Liu YF, Yan JJ, Lei HY, Teng CH, Wang MC, Tseng CC, et al. Loss of outer membrane protein C in Escherichia coli contributes to both antibiotic resistance and escaping antibody-dependent bactericidal activity. Infect Immun. 2012;80(5):1815-22.
199. Mager T, Braner M, Kubsch B, Hatahet L, Alkoby D, Rimon A, et al. Differential Effects of Mutations on the Transport Properties of the Na+/H+ Antiporter NhaA from Escherichia coli. Journal of Biological Chemistry. 2013;288(34):24666-75.
200. Palmer T, Berks BC. The twin-arginine translocation (Tat) protein export pathway. Nature Reviews Microbiology. 2012;10(7):483-96.
201. Zgurskaya HI, Nikaido H. AcrA is a highly asymmetric protein capable of spanning the periplasm11Edited by I. B. Holland. Journal of Molecular Biology. 1999;285(1):409-20.
202. Storz G, Tartaglia LA. OxyR: a regulator of antioxidant genes. J Nutr. 1992;122(3 Suppl):627-30.
203. Łyżeń R, Gawron G, Kadziński L, Banecki B. GSH Protects the Escherichia coli Cells from High Concentrations of Thymoquinone. Molecules. 2022;27(8):2546.
204. Benov L. CLY, Day B., Fridovich I. Copper, Zinc Superoxide Dismutase in Escherichia coli: Periplasmic Localization. Elsevier. 1995;319.
205. Singh R, Wiseman B, Deemagarn T, Jha V, Switala J, Loewen PC. Comparative study of catalase-peroxidases (KatGs). Archives of Biochemistry and Biophysics. 2008;471(2):207-14.
206. Ito R, Hayakawa H, Sekiguchi M, Ishibashi T. Multiple Enzyme Activities of Escherichia coli MutT Protein for Sanitization of DNA and RNA Precursor Pools. Biochemistry. 2005;44(17):6670-4.
207. Boiteux S, O'Connor TR, Lederer F, Gouyette A, Laval J. Homogeneous Escherichia coli FPG protein. A DNA glycosylase which excises imidazole ring-opened purines and nicks DNA at apurinic/apyrimidinic sites. J Biol Chem. 1990;265(7):3916-22.
208. Horii T, Ogawa T, Ogawa H. Organization of the recA gene of Escherichia coli. Proceedings of the National Academy of Sciences. 1980;77(1):313-7.
209. Soto SM. Role of efflux pumps in the antibiotic resistance of bacteria embedded in a biofilm. Virulence. 2013;4(3):223-9.
210. Tu WY, Pohl S, Summpunn P, Hering S, Kerstan S, Harwood CR. Comparative analysis of the responses of related pathogenic and environmental bacteria to oxidative stress. Microbiology. 2012;158(3):636-47.
211. Zhang J, Suo Y, Zhang D, Jin F, Zhao H, Shi C. Genetic and Virulent Difference Between Pigmented and Non-pigmented Staphylococcus aureus. Frontiers in Microbiology. 2018;9.

212. Liu CI, Liu GY, Song Y, Yin F, Hensler ME, Jeng WY, et al. A cholesterol biosynthesis inhibitor blocks Staphylococcus aureus virulence. Science. 2008;319(5868):1391-4.
213. Shui S, Zhao Z, Wang H, Conrad M, Liu G. Non-enzymatic lipid peroxidation initiated by photodynamic therapy drives a distinct ferroptosis-like cell death pathway. Redox Biology. 2021;45:102056.
214. Alvarez N, Sevilla A. Current Advances in Photodynamic Therapy (PDT) and the Future Potential of PDT-Combinatorial Cancer Therapies. Int J Mol Sci. 2024;25(2).
215. Kobayashi Y, Hayashi M, Yoshino F, Tamura M, Yoshida A, Ibi H, et al. Bactericidal effect of hydroxyl radicals generated from a low concentration hydrogen peroxide with ultrasound in endodontic treatment. J Clin Biochem Nutr. 2014;54(3):161-5.
216. Xu W, Dielubanza E, Maisel A, Leung K, Mustoe T, Hong S, et al. Staphylococcus aureus impairs cutaneous wound healing by activating the expression of a gap junction protein, connexin-43 in keratinocytes. Cellular and Molecular Life Sciences. 2021;78(3):935-47.
217. Kalyanaraman B, Dranka BP, Hardy M, Michalski R, Zielonka J. HPLC-based monitoring of products formed from hydroethidine-based fluorogenic probes--the ultimate approach for intra- and extracellular superoxide detection. Biochim Biophys Acta. 2014;1840(2):739-44.
218. Tomizawa S, Imai H, Tsukada S, Simizu T, Honda F, Nakamura M, et al. The detection and quantification of highly reactive oxygen species using the novel HPF fluorescence probe in a rat model of focal cerebral ischemia. Neuroscience Research. 2005;53(3):304-13.
219. Imlay JA. Diagnosing oxidative stress in bacteria: not as easy as you might think. Current Opinion in Microbiology. 2015;24:124-31.
220. Drummen GP, van Liebergen LC, Op den Kamp JA, Post JA. C11-BODIPY(581/591), an oxidation-sensitive fluorescent lipid peroxidation probe: (micro)spectroscopic characterization and validation of methodology. Free Radic Biol Med. 2002;33(4):473-90.
221. Levine RL, Wehr N, Williams JA, Stadtman ER, Shacter E. Determination of Carbonyl Groups in Oxidized Proteins. In: Walker JM, Keyse SM, editors. Stress Response: Methods and Protocols. Totowa, NJ: Humana Press; 2000. p. 15-24.
222. Vestby LK, Grønseth T, Simm R, Nesse LL. Bacterial Biofilm and its Role in the Pathogenesis of Disease. Antibiotics (Basel). 2020;9(2).
223. Costerton JW, Stewart PS, Greenberg EP. Bacterial biofilms: a common cause of persistent infections. Science. 1999;284(5418):1318-22.
224. Hall-Stoodley L, Stoodley P. Evolving concepts in biofilm infections. Cell Microbiol. 2009;11(7):1034-43.
225. Rocca DM, Silvero CM, Aiassa V, Cecilia Becerra M. Rapid and effective photodynamic treatment of biofilm infections using low doses of amoxicillin-coated gold nanoparticles. Photodiagnosis Photodyn Ther. 2020;31:101811.
226. Gygli SM, Borrell S, Trauner A, Gagneux S. Antimicrobial resistance in Mycobacterium tuberculosis: mechanistic and evolutionary perspectives. FEMS Microbiology Reviews. 2017;41(3):354-73.
227. Nimmo C, Millard J, Faulkner V, Monteserin J, Pugh H, Johnson EO. Evolution of Mycobacterium tuberculosis drug resistance in the genomic era. Front Cell Infect Microbiol. 2022;12:954074.
228. Shleeva M, Savitsky A, Kaprelyants A. Photoinactivation of mycobacteria to combat infection diseases: current state and perspectives. Appl Microbiol Biotechnol. 2021;105(10):4099-109.

229. Dutta AK, Choudhary E, Wang X, Záhorszka M, Forbak M, Lohner P, et al. Trehalose Conjugation Enhances Toxicity of Photosensitizers against Mycobacteria. ACS Cent Sci. 2019;5(4):644-50.